The investigation of exhaust control strategies and waste heat recovery practices of naturally-ventilated exhaust streams

THE INVESTIGATION OF EXHAUST CONTROL STRATEGIES AND WASTE HEAT RECOVERY PRACTICES OF NATURALLY-VENTILATED EXHAUST STREAMS

BY

JEFFREY GIRARD, B.Sc.

A THESIS

SUBMITTED TO THE DEPARTMENT OF MECHANICAL ENGINEERING

AND THE SCHOOL OF GRADUATE STUDIES

OF MCMASTER UNIVERSITY

IN PARTIAL FULFILMENT OF THE REQUIREMENTS

FOR THE DEGREE OF

MASTER OF APPLIED SCIENCE

Master of Applied Science (2016) McMaster University
(Mechanical Engineering) Hamilton, Ontario, Canada

TITLE:	The investigation of exhaust control strategies and waste heat recovery practices of naturally-ventilated exhaust streams
AUTHOR:	Jeffrey Girard B.Sc., (Mechanical Engineering) McMaster University, Hamilton, Canada
SUPERVISOR:	Dr. James Cotton
NUMBER OF PAGES:	xxi, 179

Abstract

Energy demands are projected to continue increasing over the next decade, which is prompting a change towards higher efficiencies and better utilization of the current energy supply. Thermal waste energy, a prominent inefficiency during any process, can be converted to electrical energy or re-purposed for low-grade energy needs, such as hot water and space heating/cooling. Naturally ventilated chimneys, driven by buoyancy differences between the exhaust gases and the surrounding air, prove to be a source of waste heat. The challenge of waste heat recovery from naturally ventilated exhaust networks is the reduction in buoyancy effects and increase in flow restrictions within the network. This research study will focus on understanding the effects of waste heat recovery and the associated exhaust control devices on the performance of a naturally ventilated exhaust network and the accompanying appliance(s).

To investigate the effects, a nodal network methodology using mass and energy conservation principles was adapted for exhaust networks to develop a one-dimensional computational model. In contrast to previous exhaust flow design methodologies, this method solves for the thermal input of the appliance and the associated flow rates, temperature, and pressures via the appliance set point temperature and exterior conditions, such as outside temperature and pressure. Using empirical correlations for heat transfer and pressure loss coefficients of appliance and exhaust

components, the computational model was validated through experimental testing of an exhaust network used in the development of a waste heat recovery system called TEG POWER (Thermal Electrical Generator Pizza Oven Waste Energy Recovery).

The experimental facility was constructed to investigate the exhaust network with and without the TEG POWER system, along with exhaust control devices. These devices included an exhaust throttling valve and a draft hood to induce dilution air into the chimney. To investigate the individual effects of the devices, experimental testing was conducted at an oven temperature of 300°F (148.9°C), 500°F (260°C), and 600°F (315.6°C) with varying degrees of throttling and/or dilution air. The mass flow measurements were calculated using an energy balance technique validated against a two-way energy balance and well-established heat transfer and pressure loss correlations of the heat exchanger. The experimental mass flow, temperature, and draft pressure results were compared against the respective computational predictions and found to be within a ±10% agreement.

The application of the exhaust control techniques with and without waste heat recovery is highly dependent on the objective(s), such as reducing natural gas consumption, and the constraint(s), such as a minimum chimney temperature, placed on the exhaust network design. Using the computational model, a design methodology was proposed to meet the objective(s) within the constraints of the exhaust network. To test the design methodology, a case study was performed with the objective to minimize oven natural gas consumption with a TEG POWER system in relation to a baseline appliance solely fitted with a draft hood. Within the constraints, the methodology was able to identify the appropriate degree of throttling and dilution air intake to minimize natural gas consumption.

With the inclusion of the TEG POWER system, the case study showed a potential reduction in natural gas consumption by up to 18% (1.7 L/min) and 13% (3 L/min) at 300 and 600°F oven operating temperatures, respectively. The implementation of the control technique allowed the oven to minimize the intake of dilution air by up to 70% and maintain operational stability during exterior fluctuations in temperature and pressure. The implementation of the waste heat recovery device captured up to 1.0 and 2.7 kW, or a natural gas equivalent of 1.9 and 5 L/min, at 300 and 600°F oven operating temperatures respectively. Implemented into the 8,000 pizza restaurants across Canada, the TEG POWER system would reduce total natural gas consumption by up to 65.5 million cubic meters, which is enough to heat 24,000 Canadian homes (Statistics Canada, 2011), and reduce CO_2 output by 112,000 metric tonnes.

Acknowledgements

I would like to extend my gratitude towards my supervisor and mentor, Dr. Jim Cotton, for providing the opportunity to work on the TEG POWER project. Thank you for your tutoring and support, but I would especially like to acknowledge your continued patience in allowing me the time to complete the writing of this thesis.

I would also like to thank Dr. Hossam Sadek for his support and his ability to provided a glimpse of reality when it was most needed.

To Raf, Yakoob, Mike, Corbin, and Donal who made working in the labs a joy and a pleasure. Thank you for your continued friendship and endless hours.

To all the past and present members of the TMRL reserach group, thank you for your support as I stand on the shoulders of giants.

I'd like to express my appreciation to the past and present departmental technicians, Ron, Mark, Michael, Jim, John, Joe, and Dan. Thank you for you support and the endless topics of conservation.

This work was made possible by the ingenuity Gerard Campeau at TEGTEC Corp. and the foresight of Pizza Pizza Ltd. Funding was partially provided by OCE and NSERC. Thank you for providing the resources to accomplish this project.

I would also like to thank my parents, Norm and Karen, for your support and continued dedication. They will finally get a graduation picture and I do understand

I went through an Undergraduate program. In addition, I'd like to thank all my friends and family for their support and well timed distractions.

Finally, to my best friend and better half Sepideh, thank you for staying up into the early hours of the morning to keep me company during unavoidable overnight tests, even when they were through proxy. Thank you for reviewing and re-reviewing numerous versions of this thesis. I cannot express the gratitude I feel for the time you've taken to support and "motivate" me. I'm seriously considering writing a book on the motivational tricks used. Thank you for being with me as you've been my source of energy.

Contents

List of Tables

List of Figures

Chapter 1

Introduction and Problem Statement

In 2010, 57% of the energy used in Canada for thermal processes was in the form of waste heat. This amounts to 1740 Peta Joules of waste heat generated across residential, commercial, and industrial sectors (CESAR, 2010). Additionally, Canada's energy consumption is projected to increase, on average, by 1.3% per year until 2035 (National Energy Board, 2014). Therefore, waste heat recovery is an attractive method of reducing energy consumption and relieving stress on current energy sources.

Presently waste heat recovery technologies have been well developed for the industrial sector, but little attention has been given to the commercial sector. This is attributed to a lower return on investment for recovering a relatively less abundant and lower grade thermal energy. For example, in 2010 the Canadian industrial sector produced 1100 Peta Joules of waste heat, the commercial sector produced 288 Peta Joules (CESAR, 2010). As the cost of energy and the interest in energy resiliency increases, more attention is being shifted towards developing waste heat recovery technologies for the commercial sector.

In the commercial sector, a significant source of waste heat comes from restaurants in the form of gas-fired appliances. In these appliances the thermal energy is "lost" through oven wall conduction losses, convection and radiation losses from opening doors, and exhaust gas heat losses (Energy Efficiency and Renewable Energy, 2004). Conduction losses are constantly occurring during operation and can be significantly reduced by properly insulating the appliance. Additionally, proper scheduling and an experienced operator can minimize heat losses when opening appliance doors. The previous sources of waste heat are dwarfed, by nearly an order of magnitude, in comparison to exhaust gas heat losses (Energy Efficiency and Renewable Energy, 2004).

During the combustion process the combustion gases act as a medium to transfer heat to the product in the appliance; which absorbs the thermal energy until it has reached a desired temperature. At this time the combustion gases still contain a substantial amount of thermal energy and are normally exhausted to the environment. Therefore, the major focus of this research is on waste heat recovery and reduction from the exhaust gases.

During any combustion process each fuel requires a minimum, or stoichiometric, amount of air to achieve complete combustion. A stoichiometric combustion process will produce the highest achievable temperatures and efficiencies for each respective fuel. The stoichiometric flame temperature is typically much higher than the appliance temperatures demanded by conventional cooking practices. To overcome this, excess air is used to dilute and lower the temperature of the combustion gases. Cooking appliances typically cannot control combustion air (or excess air) directly; rather a thermostat is used to regulate the supply of fuel and achieve the adequate air-to-fuel ratio to maintain a specified temperature.

Figure 1.1 illustrates the previously discussed relation between the combustion gas temperature and amount of excess air. The relationship can be observed at a fixed percentage of exhaust gas heat loss; following that as the exhaust air temperature increases, less excess air will be required to dilute and cool the combustion gases. In other words, higher exhaust gas temperatures will require lower air-to-fuel ratios. Unfortunately, the practice of introducing excess air does present the consequence that as the excess air increases, the percentage of recoverable energy decreases. Therefore waste heat recovery from gas-fired appliances is presented with two challenges: low quality thermal energy and marginal returns on thermal efficiencies as the exhaust temperature drops.

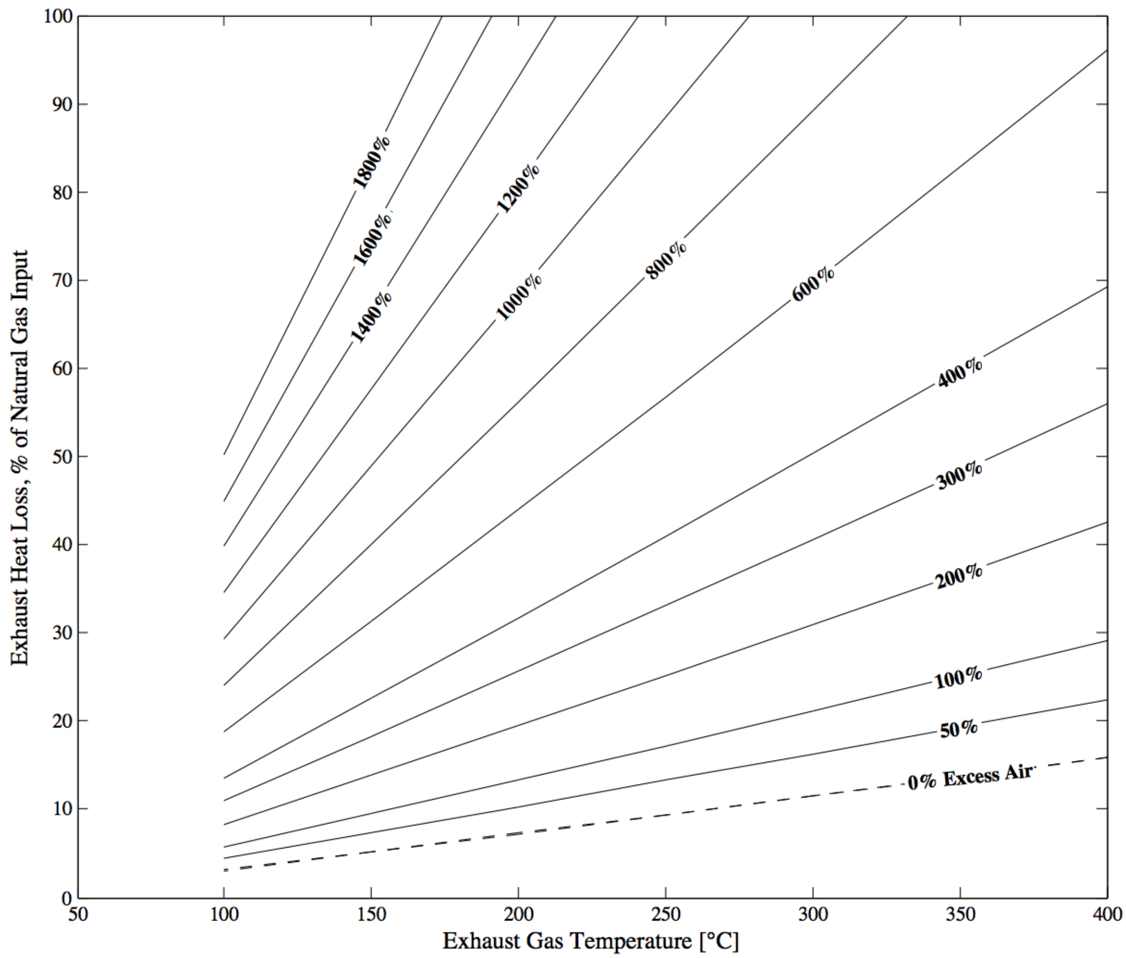

Figure 1.1: Relationship between exhaust heat losses and oven temperature under various amounts of excess air (adapted from Energy Efficiency and Renewable Energy (2004))

Excess air is a necessary component of any fuel-fired cooking process, but is simultaneously the largest cause for wasted thermal energy. As previously stated, the oven cannot directly control the amount of combustion air entering during operation. The amount of combustion air is rather a function of the draft condition, namely the static pressure difference between the chimney and atmosphere. This difference can be created by a combination of buoyancy effects and mechanical devices, such as fans and blowers. A draft condition driven solely by the buoyancy effects of the hot exhaust gases is called a natural draft. In combination with a natural draft, a mechanical device can be used to push or pull air into the combustion chamber and boost the draft. To further expand on natural draft, the chimney design and the temperature of the exhaust gases determine the draft condition and therefore the amount of combustion air. Additionally, a natural draft system is more prone to be affected by exterior conditions, such as outside temperature, pressure and wind conditions.

After investigating Figure 1.1, there exists two approaches to more effectively utilize and conserve thermal energy generated by a gas-fired appliance. The first approach is to reduce the exhaust gas heat losses by recovering additional thermal energy from the exhaust stream. A challenge of waste heat recovery from a natural draft exhaust stream is the reduction in the driving potential or exhaust temperature to drive the exhaust up the chimney. For example, cooler exhaust gases produce less draft and reduce exhaust flows, which lead to decreased performance of the heat recovery device. Alternatively, the second approach capitalizes on slowing the exhaust flow by adding a flow restriction or draft hood to lessen fuel consumption since maintaining the oven temperature requires a fixed air-to-fuel ratio. It was hypothesized that a combination of waste heat recovery and exhaust flow control techniques are needed to simultaneously conserve and effectively utilize the thermal energy generated by a gas-fired appliance. To test this hypothesis, additional information surrounding the techniques' effect on the flow dynamics of the exhaust stream must be gathered.

An understanding of the conventional flow dynamics of exhaust streams has been well developed and is practiced daily, with the design of chimneys everywhere. Traditionally, combustion ventilation design involves following protocols and guidelines outlined by the National Fire Protection Association (NFPA) and American Society of Heating, Refrigeration and Air-Conditioning Engineers (ASHRAE). Beyond protocols and guidelines, ventilation designers have two computational simulation software packages available: FLUESIM and Vent II. Despite being powerful analysis tools, the software packages do have limitations in respect to waste heat recovery applications and experimental validations (Rapp *et al.*, 2012). This knowledge gap plays a critical role in the available tools needed to develop and adopt waste heat recovery technologies and control strategies in naturally ventilated exhaust streams. Therefore, the goal of this research is to gain a better understanding of naturally driven exhaust stream dynamics for waste heat recovery and control techniques.

1.1 Objectives

The key objective of this thesis is to develop a one-dimensional computational model to investigate the effects of waste heat recovery and exhaust flow control on the flow dynamics of naturally ventilated exhaust streams. The model will be based on fundamental mass and energy conservation principals and validated using a full-scale ventilation system.

The effects of different flow control techniques, throttling and dilution air, are investigated along with understanding the functional strength of the respective techniques. This will provide a decision tool based on operational set points and measurable information, such as oven temperature; natural gas flow rate; and chimney temperature, to gauge the appropriateness of waste heat recovery technologies and exhaust control strategies.

1.2 Scope of Work

The purpose of this computational model is to act as an evaluation and design tool for designers of naturally ventilated exhaust systems for fuel-fired appliances. The evaluation aspect will focus on assessing the usefulness of a waste heat recovery system and exhaust control strategy. The design aspect will provide the necessary information to properly design heat transfer components encapsulated in waste heat recovery of naturally ventilated exhaust systems and provide insight into control algorithms for exhaust control strategies.

Along with acting as a stand-alone design tool, the model will also be integrated into a FORTRAN based waste heat recovery system model. The experimental validation component will provide accurate comparative measurements of exhaust velocities in various components of the ventilation system, along with respective pressures and temperatures. Overall, the experimental data will provide a range of operating points found typically in a restaurant setting to validate the computational model and better understand the intimate coupling between a naturally ventilated exhaust system and a waste heat recovery device.

Chapter 2

Literature Review

2.1 Introduction

This chapter outlines the current understanding of natural ventilation within exhaust systems. In relation to the current design methodology, a summary of the fundamental driving principles of exhaust systems will be reviewed. The relevant industrial standards will be discussed using supporting research studies. Using the fundamental principles as an evaluation framework, a review of the current exhaust system modeling methodologies will be completed and the shortcomings pertaining to waste heat recovery applications will be highlighted. Lastly, a building ventilation modeling techniques will be accessed by addressing the shortcomings of the previous methodologies.

2.2 Exhaust System Fundamentals

The function of an exhaust system is to safely vent exhaust gases from appliances to the exterior of the building. This is accomplished by generating a negative pressure differential between the exhaust system and the atmosphere, called draft pressure, to overcome frictional effects within the exhaust system and meet safety and cooking requirements. A summary of this concept can be mathematically represented as:

$$D_a = D_t - \Delta P_{loss} - D_{dp} + D_b \tag{2.1}$$

where

D_a is the available draft [Pa]

D_t is the theoretical draft (caused by buoyancy effects) [Pa]

ΔP_{loss} is the flow loss (caused by viscous effects) [Pa]

D_{dp} is the depressurization [Pa] (caused by wind and building HVAC systems)

D_b is the boost in static pressure produced by a fan [Pa]

2.2.1 Available Draft

The available draft (D_a) reflects the draft condition required at the exhaust outlet of the appliances for proper operation. According to Stone (1971), appliances can be divided into three categories based on their exhaust outlet draft condition. Figure 2.1 illustrates the general layout of the appliance and exhaust system along with the expected pressure profiles. These illustrations are not meant to be exhaustive, but to provide an overview of the exhaust system layouts.

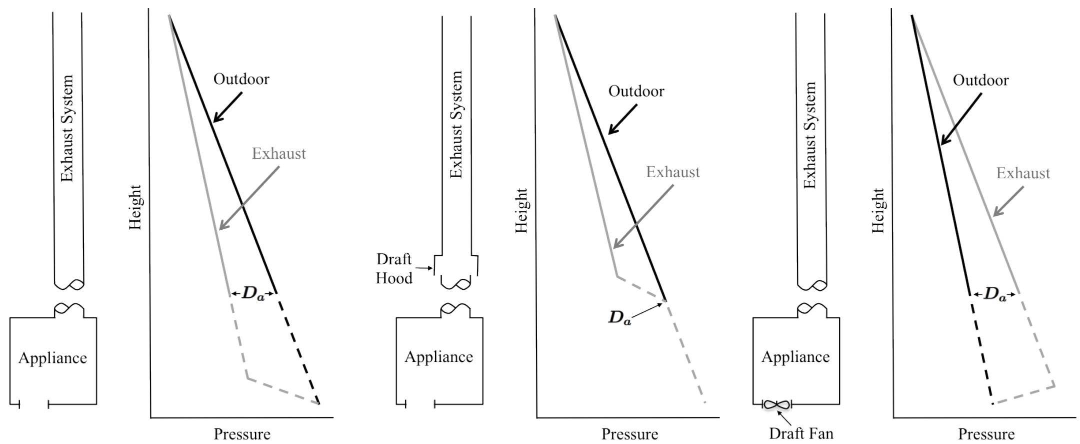

(a) $Da > 0$ (b) $Da = 0$ (c) $Da < 0$

Figure 2.1: General appliance and exhaust system categories (adapted from Stone (1971))

The three categories are as follows:

- $\boldsymbol{D_a > 0}$: The appliance requires a negative pressure (positive draft pressure) at the exhaust outlet of the appliance to induce air into the appliance. See Figure 2.1a for reference.

- $\boldsymbol{D_a = 0}$: The appliance operates with no draft at the exhaust outlet of the appliance. An appliance outfitted with a draft hood typically operates in this condition since a draft hood dilutes the combustion gases with conditioned air from the combustion appliance zone (CAZ) before entering the exhaust system. Any excess (or lack of) available draft (D_a) will be driven to zero by an increase (or decrease) in admission of conditioned air. See Figure 2.1b for reference. This condition will be the focal point of the upcoming discussion of current modeling techniques.

- $\boldsymbol{D_a < 0}$: The appliance produces a positive static pressure at the appliance exhaust outlet to push the exhaust gases to the outdoors with little or no help from the theoretical draft (D_t) generated by an exhaust system. This is typically accomplished by using a draft fan at the combustion air inlet of the appliance. See Figure 2.1c for reference.

2.2.2 Theoretical Draft

The theoretical draft (D_t), or stack effect, is the natural draft produced by the buoyancy effects of the hot gases in the exhaust system relative to the cooler gases in the surrounding atmosphere. A consequence of the stack effect is the neutral pressure level, which is an important concept in understanding the development of a pressure profile within an exhaust system. The neutral pressure level is not pivotal, but it allows the stack effect to be extended to more complex exhaust systems.

2.2.2.1 Stack Effect

The stack effect is well understood as the hydrostatic pressure differences between the hot exhaust gases and cool outside air. The hydrostatic pressure of air is a function of the density and the height relative to a reference point; which is calculated as:

$$P_s = P_r - \rho g H \tag{2.2}$$

where

P_s is the static pressure a distance (H) from the reference pressure [Pa]

P_r is the reference pressure [Pa]

ρ is the density of the fluid [kg/m^3]

g is the gravitational constant [m/s^2]

H is the vertical distance relative to a reference point [m]

The pressure difference between the top and bottom of the column is assumed negligible in relation to the atmospheric pressure. As a consequence, the atmospheric pressure is assumed to be constant along the length of the column.

The theoretical draft (D_t), or stack effect, is represented by subtracting the pressure difference between the inside and outside temperature air columns. This combination becomes:

$$D_t = (\rho_o - \rho_i)\, gH \tag{2.3}$$

where

ρ_o is the outside air density [kg/m^3]

ρ_i is the inside air density [kg/m^3]

A visualization of the stack effect can be found in Figure 2.2.

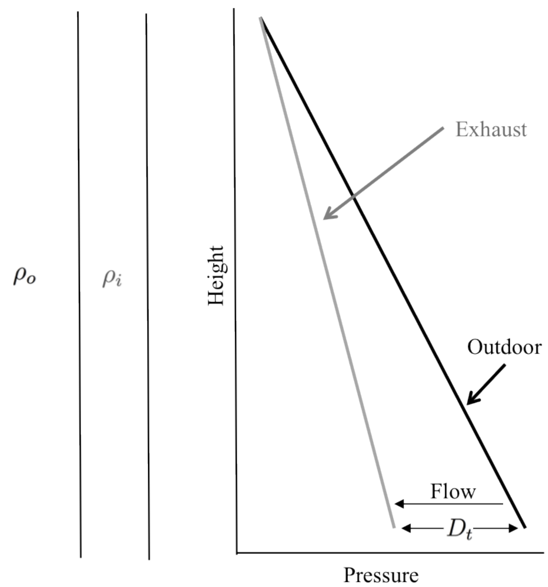

Figure 2.2: Pressure difference created by the stack effect with a reference point at the top of the column

A deeper analysis of the stack effect shows that as air enters the column, it will experience an acceleration via the pressure differential formed at the inlet. Once through the inlet, the inertia of the air will propel it through the exhaust system to the outlet, at which point flow inertia will be dissipated upon exiting the exhaust system. This process is illustrated in Figure 2.2 through the inability of the pressure differential to switch direction along the length of the column. The simplification that the inertial component is the sole contributor driving the air through the column restricts the stack effect concept from more complex exhaust systems. To extend the stack effect to more complex systems, the concept of a neutral pressure level (NPL) must be included.

2.2.2.2 Neutral Pressure Level

The neutral pressure level (NPL) was defined by Emswiler (1926) to be the height at which there is no pressure difference between air columns. Using this concept, Sherman (1991) found that a single zone volume with no internal flow resistances could be divided into two effective stacks of opposing pressure differences at the NPL. Figure 2.3 illustrates the application of the NPL in combination with the stack effect.

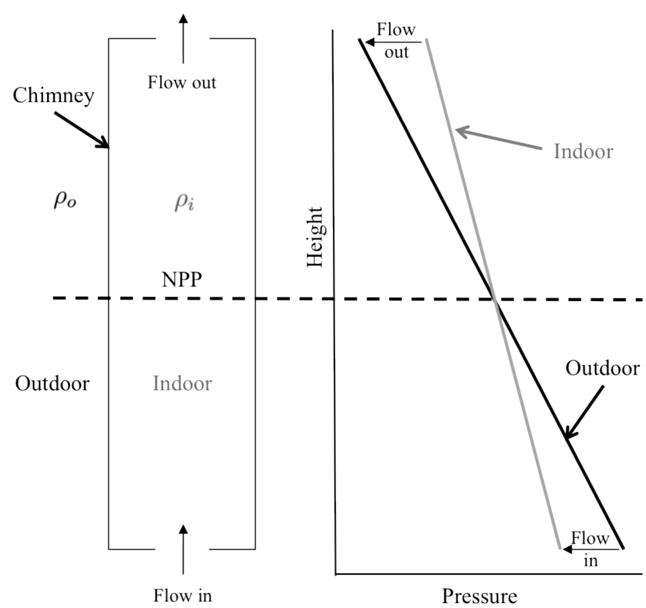

Figure 2.3: Neutral pressure plan within an air column

In this case, the indoor air is warmer than the outside air. The buoyancy effects causes the region below the NPL to depressurize and induces flow into the column. Above the NPL, the region is pressurized and outwards flow from the column is induced. Mathematically this is represented as:

$$\Delta P_{draft} = (\rho_o - \rho_i)\, g\, (H_{NPL} - H) \tag{2.4}$$

where

H_{NPL} is the height of the neutral pressure plane [m]

As indicated in Chapter 16 of the ASHRAE Handbook - Fundamentals, the location of the NPL is not fixed. In the event of a vertical exhaust stack, the NPL migrates to just above the straight outlet due to the inertial and frictional effects; which leads Equation 2.4 to simplify to Equation 2.3. This simplification is used extensively in past exhaust modeling methodologies.

This simplification neglects the fact that the NPL could be within the outlet due to the presence of an vent cap and that it is possible to have multiple NPL within a building envelop and exhaust systems. Extending this to exhaust systems, the NPL is influenced by flow resistances, vent orientation, and opening heights. The strength of the NPL concept is in the ability to predict the effects of multiple inlets and outlets at various heights. This allows for the determination of pressure profiles for complex systems, such as multiple appliances manifolded to a single exhaust vent.

The stack effect (Equation 2.3) and the neutral pressure level (Equation 2.4) describe the theoretical draft (D_t) to be a function of the exhaust temperature. Therefore heat transfer is an important consideration, which has been demonstrated with the introduction of a draft hood. A device, such as a draft hood, that mixes and subsequently cools the exhaust gases falls into the category of a direct contact heat exchanger. They are effective at controlling the theoretical draft (D_t) and subsequently the flow rate within the exhaust system. Another device which relies on this effect is a draft regulator. This device is mounted in a similar fashion has a draft hood, but will only actuate if the draft exceeds a specified threshold. In addition to direct heat exchangers, indirect heat exchangers also effect the draft in the identical manner except that the thermal energy is transferred to another fluid stream without mixing the exhaust with dilution air from the combustion appliance zone (CAZ). Other draft control strategies exist based on flow restriction and will discussed further in Section 2.2.3. Beyond control strategies, heat losses from the exhaust gases to the surroundings can be detrimental to the performance of the exhaust system and must be mitigated or accounted for.

2.2.3 Flow Losses

The flow losses (ΔP_{loss}) represent the frictional effects imposed on the flue gases by flow resistances through the exhaust system. The magnitude of the flow losses is a function of the exhaust velocity through a combination of the various chimney geometries (length and diameter), components (elbows, reductions, etc) and draft control devices.

Draft control is the act of modulating the draft pressure to control the exhaust flow. In Section 2.2.2, the draft control technique of manipulating the buoyancy effects has been introduced. The other draft control strategy is based on flow restrictions. The strategy utilizes an adjustable pressure drop across a device to modulate the exhaust flow rate. These types of devices include vent dampers and throttling valves.

2.2.4 Depressurization

Depressurization (D_{dp}) is the pressure reduction within the space surrounding the appliance, also called the combustion appliance zone (CAZ), relative to the surrounding atmospheric pressure. Depressurization may be caused by an unbalanced HVAC system and changes in surrounding atmospheric pressure and temperature due to weather patterns and seasons.

2.2.5 Boost

Boost (D_b) is the draft boost via a mechanical device, such as a fan or induction jet device. There exists two boost options: a positive static pressure (negative draft) boost using a forced-draft device at the inlet of the chimney, or a negative static pressure (positive draft) boost using an induced-draft device at the exit of the chimney.

2.3 Industrial Standards

2.3.1 Cooking Effluents Deposition

Effluent deposition within exhaust systems is a serious fire hazard and is a continuous challenge within the restaurant industry. Effluents generated during a cooking process can be observed as vapours and particles. Vapours condense into particles or onto a duct surface when the exhaust or surface temperature drops to or below the effluents' dew point temperature, respectively. The transportation and eventual deposition on the duct surfaces are via molecular and turbulent diffusion, thermophoresis, settling, and inertial effects (Kuehn *et al.*, 2001).

The National Fire Protection Association (NFPA) is the leading North American authority in fire protection. Municipal building codes across North America follow the guidelines and building standards outlined by NFPA. In relation to effluent deposition, the NFPA 96 standard states that a minimum exhaust velocity of 2.54 m/s (500 fpm) will deter excessive grease deposition in an exhaust system containing grease-laden vapours. The minimum velocity is rooted in an experimental study conducted by Kuehn *et al.* (2001) to investigate the reduction of the previously recommended minimum exhaust velocity of 7.62 m/s (1500 fpm). It was identified that the turbulent transportation effects diminish with the exhaust velocity in insulated ducts. In non-insulated ducts, the thermophoresis effects begin to increase the grease deposition rate on the duct walls with diminishing exhaust velocity. The transition between the turbulent and thermophoresis effects leads to a transition exhaust velocity of 5.1 m/s (1000fmp), where the grease deposition rate will be at a minimum.

NFPA 96 standard does not provide a minimum temperature, but further inspection of Kuehn *et al.* (2001) experimental study indicates that a minimum exhaust temperature of approximately 40°C was used. The importance of the ASHRAE funded study was the impact on energy savings observed when less conditioned air, from the CAZ, is used as combustion and dilution air to eventually be exhausted to the outdoors.

In accordance with this thesis, the minimum exhaust temperature is placed as a lower boundaries when minimizing the fuel and CAZ air consumption during operation of the appliances; thus maximizing the overall energy efficiency of the building and cooking process. The minimum exhaust velocity is of less importance as the exhaust from the interested cooking process is not considered grease-laden, but each process should be investigated to determine to application of the minimum exhaust velocity.

2.3.2 Vapour Condensation

Water vapour condensation within an exhaust system can lead to corrosion issues. Water vapour is produced during the combustion process and exhaust gases will retain the water vapour until the dew point temperature is reached. At which point, the vapour will condense and mix with the other gaseous compounds within the exhaust to form corrosive liquids such as carbonic acid.

According to (CSA B149.1-10) in Canada and (ANSI/NFPA 54 or ANSI/AGA Z223.1) in the United States, fuel-gas appliances are categorized by the tolerance of condensation within the exhaust system.

1. Category I appliances operate with negative vent static pressure and vent exhaust gas temperatures that avoids condensation within the exhaust system.

2. Category II appliances operate with a negative vent static pressure and vent exhaust gas temperatures that may produce excessive condensation within the exhaust system.

3. Category III appliances operate with a positive vent static pressure and vent exhaust gas temperatures that avoids condensation within the exhaust system.

4. Category IV appliances operate with a positive vent static pressure and vent exhaust gas temperatures that may produce excessive condensation within the exhaust system.

Based on the application under consideration in this thesis, the focus will be on Category I appliance with a draft hood or a no draft condition ($D_a = 0$). The introduction of dilution air will reduce the dew point temperature since it is proportional to the amount of water vapour contained in the air. In conjunction with the limiting temperature of 40°C via the NFPA 96 standard and strict compliance with CSA B149.1-10, the dew point temperature of the exhaust gases is low enough to not cause condensation within the exhaust system. An alternative approach is to use a dew point temperature as a minimum temperature boundary in the same regard as the effluent deposition temperature limit.

2.4 Modeling Methodologies

The basis of modeling an exhaust system is to balance the pressure differentials generated by buoyancy effects and mechanical devices with the pressure losses due to viscous effects, as outlined in Equation 2.1. This section will review the literature for models using different variations of this pressure balancing approach and provide an overview of tools available to ventilation designers.

2.4.1 Intake Coefficient Model

The simplest model was devised using the pressure inequality developed by the stack effect and, through Bernoulli's equation, equated to the pressure loss through the inlet of the exhaust stack. Once rearranged, the volumetric flow rate (Q) can be found using the following equation:

$$Q = CA\sqrt{2gH\left(\frac{T_i - T_o}{T_i}\right)} \tag{2.5}$$

where

C is the square root of the inlet loss coefficient ($\sqrt{K}$)

A is the cross sectional area of the vent stack [m^2]

T_i is the inside temperature [K]

T_o is the outside temperature [K]

This simplistic model is very effective at quickly predicting the performance of exhaust stacks at a uniform temperature with one inlet and outlet. The major disadvantages of this model is rooted in the lack of heat loss and system pressure loss analysis. The flow resistance at the inlet is assumed to be the dominant pressure loss in the exhaust; which limits the ability to analyze more complex exhaust systems containing horizontal vents, draft control equipment, and heat recovery devices.

2.4.2 General Chimney Design Method

In 1971, Stone developed a methodology to properly size exhaust systems with regards to the operating characteristics of the appliances. Using Equation 2.1, the methodology incorporated the effect of heat losses by using the mean exhaust gas temperature, based on empirical heat transfer formulations, to calculate the theoretical draft (D_t) via the stack effect phenomenon. The flow losses (ΔP_{loss}) are calculated using an appliance operating characteristic - such as the thermal input, excess air, and exhaust outlet temperature - and the velocity head method to better predict the flow resistance throughout the exhaust system. This method is the current semi-empirical vent sizing design tool for the exhaust ventilation industry and is featured in Chapter

34 of the ASHRAE Handbook - HVAC Systems and Equipment (SI).

The effectiveness of this method is proven by its widespread usage, but it is insufficient with respect to waste heat recovery from appliances with a draft hood and designed to vary the thermal input to maintain a constant temperature; such as gas-fired cooking appliances. The shortfall exists due to the inability to predict the mass flow through the appliance and the dilution air without a fixed thermal input specified by the appliance.

The importance of these mass flow predictions via draft conditions, rather than thermal inputs, becomes clear in the context of waste heat recovery and energy conservation. During waste heat recovery operation, the heat exchanger will be located in the hottest exhaust stream (namely the exhaust from the appliance) to capture the highest quality thermal energy. This will effect the draft condition of the appliance through thermal and viscous effects, which would not be captured if the thermal input was assumed to be fixed. The ability to predict the thermal input as a function of the draft condition provides an variable to minimize fuel consumption and help develop conservation strategies.

Beyond waste heat recovery, the method's semi-empirical heat loss approach include conduction losses through the chimney walls, but does not include air infiltration effects and vapour condensation. These limitations prompted the development of a numerical approach to better predict the effects of infiltration and condensation effects on the theoretical draft (D_t) of the exhaust system, which will be discussed in the following section (Section 2.4.3).

2.4.3 Vent II Software

Based on Section 2.1 and Stone's model, a numerical software was developed in 1986 by Rutz *et al.* (1992) to provide insight into transient effects during on/off cycling and steady operating performance for an exhaust system venting up to two gas-fired hot water heaters/furnaces. The software divided the exhaust system into two regions: vents connecting the appliance to the chimney, called connectors, and the chimney, called the common vent. The regions are further separated into component-based sections. This allows better prediction of the theoretical draft using:

$$D_t = \sum_{i=1}^{N} D_{t,i} \tag{2.6}$$

where

$D_{t,i}$ is the stack effect for that section [Pa]

subscript i is the section number

N is the total number of sections

The section based approach can also better predict consequences of infiltration and heat losses, along with mass and heat transfer due to vapour condensation.

The software was reportedly validated by the creators for common vent systems using venting guidelines for Category 1 appliances outlined in NFPA 54, but the cited validation reports are difficult to obtain (Rapp *et al.*, 2012). The exhaust ventilation industry has accepted the Vent II software as an appropriate engineering tool to generate the vent sizing tables for draft hood equipped and draft induced appliances

(Category 1) in the NFPA 54 industrial standard.

A study by Glanville *et al.* (2011) on the condensation rates of hot water fuel gases in masonry chimneys compared the Vent II software to a Fluent CFD model and experimental testing. The study found that the Vent II software could adequately predict condensation rates, but did not comment on the validity of the pressure and temperature predictions to experimental and numerical results. In another study by Rapp *et al.* (2013), Vent II had been found to adequately predict exhaust spillage into the CAZ due to depressurization in cold and mild outdoor temperature conditions, but not for hot conditions.

The advantages of the numerical approach is evident in the ability to include infiltration effects and most notably condensation effects, but the model still suffers with respect to determining the performance of waste heat recovery devices due to the input requirement of the appliance thermal input.

2.4.4 Nodal Network Model

Determining the mass flow of the dilution air and the exhaust through the appliance without using a fixed thermal input involves foregoing the simplifying assumption of no available draft at the draft hood and opting to consider the exhaust system plus the appliance as a continuous system.

A study by Andersen (2003) proposed a methodology for natural ventilation by thermal buoyancy using classical thermodynamic equations. The approach was applied to the simplest case of a room at a uniform temperature with two openings at different vertical heights, as seen in Figure 2.4.

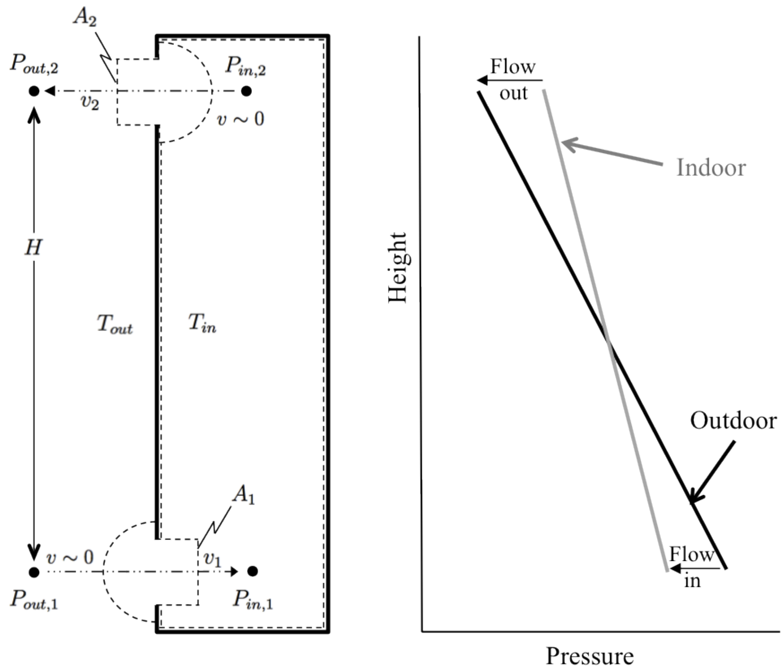

Figure 2.4: Control volumes of the flow sections except the outdoor control volume and the anticipated pressure profile (adapted from Andersen (2003))

The case was separated into four distinct sections - namely the inlet, outlet, room, outdoor sections - with defined control volumes and the associated boundaries. The control volumes forms a “piping loop” that can be analyzed by applying the mass and energy conservation principles across each control volume at the boundary nodes. Unlike the other modeling techniques, the nodal models inherently incorporate the NPL concept as seen in Figure 2.4. In addition, the fundamentals outlined in Equation 2.1 are still present within this methodology, but are no longer represented as individual contributors governing the natural ventilation phenomenon, but rather as interdependent variables.

The model developed by Andersen is considered a nodal network model. More advanced models in this category include Energy Plus, CONTAM, and ESP-r are currently used to model whole-building energy performance including natural ventilation via buoyancy effects. A study by Johnson *et al.* (2012) compared experimental data, collected by Li (2007), to the three nodal network models. The experimental data included six different cases of a full-size room with a vertical opening on a wall and a horizontal opening located on the ceiling. Case A, B, and C varied the area of the vertical opening and case D, E, and F varied the area of the horizontal opening. The temperature difference between the inside and outside was held nearly constant at around 7°C. It was found that when the flow through the openings were uni-directional, the models were able to predict the experimental airflow measurements to within an accuracy of 10%. In case F, the larger horizontal opening was found to have bi-directional flow causing the models to under predict the airflow by 50%. This shortfall is due the inability to account for the bi-directional flow within the one-dimensional environment of the model.

This methodology can be extended to exhaust systems by replacing the "room" with the exhaust system and introducing frictional effects due to the higher velocities within the section. The combustion air inlet and the dilution air inlet would be considered two inlets at different levels. The appliance would become the energy source providing a constant temperature to drive the buoyancy effects within the exhaust system. Therefore the nodal network methodology can be extended from natural ventilation in buildings to exhausts systems and address the thermal input requirement of past exhaust modeling techniques.

2.5 Summary

Current exhaust modeling techniques have been designed as a tool to size exhaust ducts as per the requirements of the appliance and not well adapted to investigate the performance of exhaust control strategies and waste heat recovery technologies. On the contrary, building ventilation modeling techniques have been shown to incorporate the necessary features to investigate these types of problems. The challenge in applying the current building ventilation modeling technique to an exhaust system analysis is the inability to account for higher frictional effects and heat losses, which are dominant factors in exhaust systems and a cornerstone of exhaust modeling techniques. To extend the advantage of the nodal network methodology from a building ventilation to an exhaust system analysis, the integration of the velocity head method and heat transfer techniques will be needed to account for the increased importance of frictional and heat loss effects.

Chapter 3

Naturally Driven Exhaust Model

3.1 Introduction

In this chapter, the solution methodology of naturally driven exhaust flow problems with a focus on waste heat recovery applications and exhaust control techniques will be presented; along with the application of the governing conservation principles; and the solution algorithm to obtain the operating parameters of an exhaust network. The solution methodology divides the exhaust system into component-based sections to allow for flexibility in adapting to any exhaust system. The governing principles of mass and energy conservation are applied to the discrete sections using a coordinate system based on flow direction. A discrete control volume approach, which is defined by the sections, formulate a system of linear equations to calculate the mass flow, temperature, and draft pressure at the respective nodes located on the faces of the control volumes. The initial and boundary conditions applicable to exhaust networks will be presented. The solution algorithm will outline the procedures and convergence criterion to solve the system of linear equations.

3.2 Solution Methodology

The solution methodology divides the naturally ventilated exhaust system into sections; which are based on the discrete components joined together to construct the exhaust system. This process is illustrated in Figure 3.1.

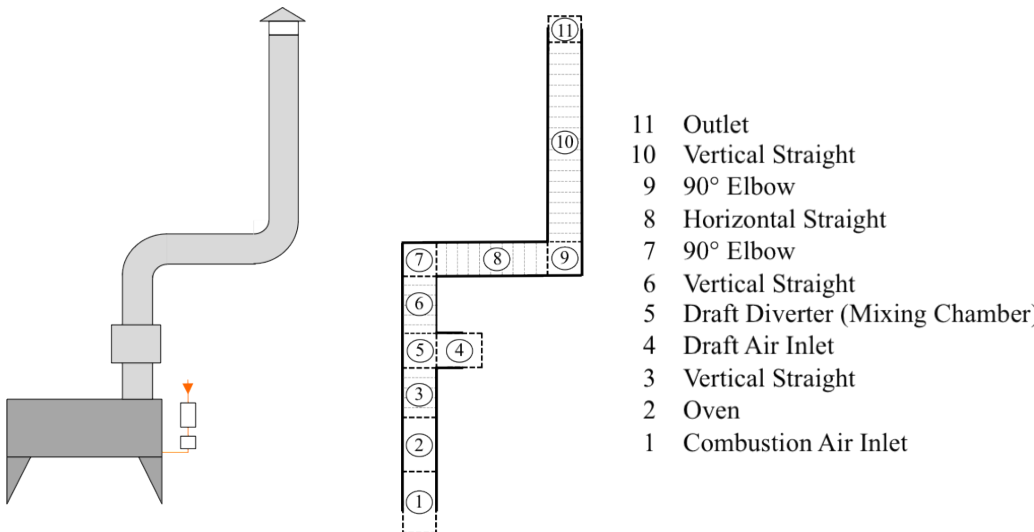

Figure 3.1: A visual representation of the exhaust system layout in relation to the solution methodology

The sections are open systems; which require the definition of two types of control volume boundaries. An opening boundary, which allows mass and energy into or out of the control volume, and a solid boundary, which allows only energy to across. This is illustrated in Figure 3.2.

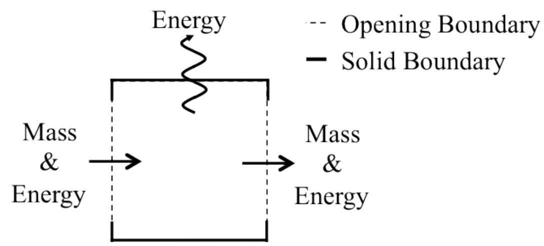

Figure 3.2: Definition of the control volume boundary types: open and solid

The sections are also grouped into two categories: flow paths and junctions. The flow paths contain sections with one inlet and outlet; examples include duct elbows and straight ducts. Furthermore, straight ducts are sub-divided into multiple sub-sections to better predict changes in pressure and thermal losses along the length of the duct. The governing fluid flow and energy transport principles are then tailored to the individual sections of the flow path and solved sequentially. This sequential technique entails the outputs (velocity, temperature, and pressure) of the previous section to be transferred to the inputs of the following section; which occurs at the openings of the control volumes. This is illustrated in Figure 3.3.

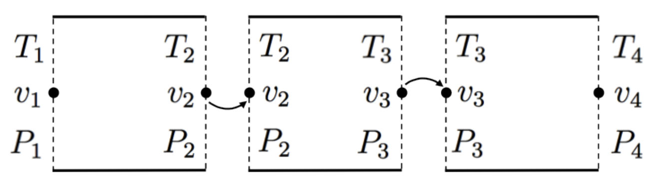

Figure 3.3: The transfer of operating parameters at the control volume boundaries

As opposed to flow paths, the junctions contain sections with multiple inlets and outlets; examples include draft hoods, exhaust manifolds, and infiltration or exfiltration points such as appliance doors. These sections must satisfy the mass and energy conditions outlined above; along with having a constant pressure at all inlets and outlets to satisfy the pressure loss condition. This is illustrated in Figure 3.4. The mechanical flow energy is neglected, which will be explained after investigating the governing equations further.

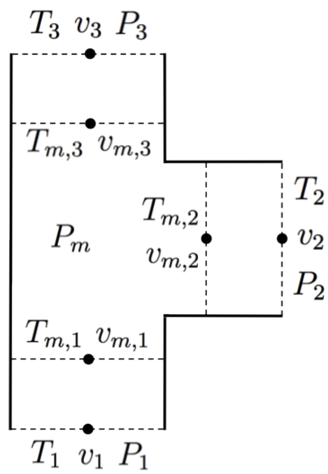

Figure 3.4: The application of the constant pressure condition on a junction-type section (draft hood)

3.3 Governing Equations

The physics of a naturally ventilated exhaust flow are fully described by the conservation of mass and energy principles. This section will outline the process of adapting the general conservation principles to a section-based methodology.

The fluctuating characteristics of the exhaust flow were identified to be 20 times faster relative to the reaction time of the appliance and exhaust network, which allowed the time domain to be ignored. The spacial characteristics adapted to a section-based approach require a directional definition of the open and solid boundaries, which will be presented in Section 3.4.1. The open boundaries are labeled as an inlet or outlet based on a positive (or negative) flow direction. The positive direction of flow for mass and energy is specified as flow from lower openings to the highest opening accessing the environment, as illustrated in Figure 3.5. As for a solid boundary, the positive flow direction defined for mechanical and thermal energy are entering and exiting the control volume, respectively. Using the temporal simplification and the coordinate system, the adaptation of the mass and energy conservation principles will be presented.

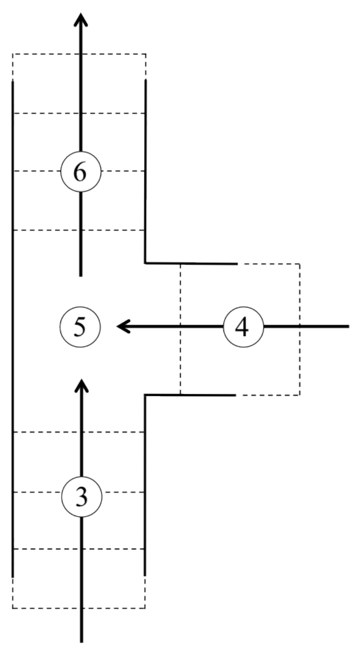

Figure 3.5: Positive flow direction of mass and energy transport as depicted by the arrows

3.3.1 Conservation of Mass

The general conservation of mass equation for steady state is:

$$\sum_{in} \dot{m} = \sum_{out} \dot{m} \tag{3.1}$$

The mass flow is also represented by:

$$\dot{m} = \rho v A \tag{3.2}$$

where

$\dot{m}$ is the mass flow [kg/s]

ρ is the density of the gas [kg/m^3]

v is the average gas velocity through the control volume cell wall [m/s]

A is the cross sectional of the control volume cell wall [m^2]

After substitution, the general conservation of mass equation becomes:

$$\sum_{in} \rho v A = \sum_{out} \rho v A \tag{3.3}$$

This general equation is then adapted to flow paths, which contain an inlet and outlet; and the junctions, which may contain multiple inlets and outlets. This is illustrated in Figure 3.6.

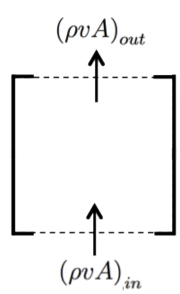

(a) Flow Path Control Volume

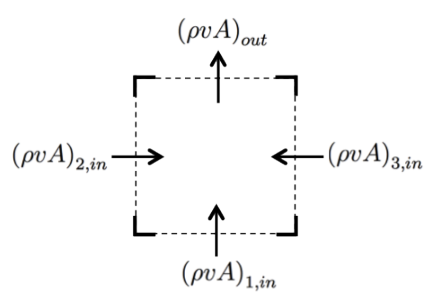

(b) Junction Control Volume

Figure 3.6: Mass conservation principle on control volumes

3.3.2 Conservation of Energy

The general conservation of energy equation for steady state is:

$$\dot{W}_{net} - \dot{Q}_{net} = \sum_{out} \dot{m} \left(u + \frac{P_T}{\rho} + \alpha \frac{v^2}{2} + gh \right) - \sum_{in} \dot{m} \left(u + \frac{P_T}{\rho} + \alpha \frac{v^2}{2} + gh \right) \quad (3.4)$$

where

$\dot{Q}_{net}$ is defined as the net thermal energy exiting the fixed control volume [W]

$\dot{W}_{net}$ is defined as the net work energy entering the fixed control volume [W]

u is the internal energy of the fluid [J/kg]

P_T is the thermodynamic pressure of the fluid [N/m^2]

α is the kinetic energy correction factor

$\frac{v^2}{2}$ is the kinetic energy [J/kg]

gh is the gravitational potential energy [J/kg]

As discussed in a future section (Section 3.4.3 and illustrated in Figure 3.1), the stability of the solution algorithm requires the temperature and velocity throughout the exhaust system to be fully solved during each iteration of the pressure profile solution. The current form of the conservation of energy equation requires the temperature, pressure, and velocity to be solved simultaneously. To allow an explicit solution, the energy equation can be divided into thermal and mechanical energy equations using the following assumptions:

1. Viscous dissipation is not a significant source of heat generation
2. Exhaust gases behave as an ideal gas

The thermal and mechanical equations are intimately coupled through the thermal energy term ($\dot{Q}_{net}$) and the flow energy term ($\frac{P}{\rho}$). The thermal energy term ($\dot{Q}_{net}$) is comprised of two sources: (1) the heat transferred through a solid boundary and (2) the heat generated by viscous dissipation. In this situation the viscous dissipation source can be neglected with respect to the thermal energy term, as it accounts for less than 0.1% of the total change in thermal energy. As discussed in Section 2.2.3, the viscous dissipation source contributes as a loss in pressure and cannot be neglected. Therefore, the heat transferred through the solid boundaries will be included in the thermal energy equation and the viscous dissipation will be included in the mechanical energy equation. The flow energy term ($\frac{P}{\rho}$) represents two forms of energy: (1) the energy of fluid expansion, and (2) the energy of a change in pressure. As pressure losses throughout the exhaust network contributed less than a 0.1% change in the absolute pressure of the fluid, the expansion of the exhaust gases become a function of temperature only and is described using the ideal gas equation.

$$\rho = \frac{P_{atm}}{RT} \tag{3.5}$$

P_{atm} is the atmospheric pressure [Pa]

R is the gas constant for air (287.058) [J/kgK]

The thermodynamic pressure is further separated into two parts: (1) a reference pressure term (P_{atm}) and (2) a dynamic pressure term (P) that is function of the flow path.

$$\frac{P_T}{\rho} = \frac{P_{atm}}{\rho} + \frac{P}{\rho} \tag{3.6}$$

As the fluid properties are solely a function of temperature, the reference pressure term (P_{atm}) of the flow energy is found in the thermal energy equation. As the kinetic energy is sensitive to changes in pressure, the dynamic pressure term (P) is found in the mechanical energy equation. The conservation of thermal energy equation is:

$$\dot{Q}_{thermal} = \sum_{in} \dot{m} \left(u + \frac{P_{atm}}{\rho} \right) - \sum_{out} \dot{m} \left(u + \frac{P_{atm}}{\rho} \right) \tag{3.7}$$

The reference pressure term (P_{atm}) also allows the introduction of the enthalpy equation referenced to a constant atmospheric pressure.

$$h = u + \frac{P_{atm}}{\rho} \tag{3.8}$$

Using the enthalpy equation, the conservation of thermal energy equation becomes:

$$\dot{Q}_{thermal} = \sum_{in} (\dot{m}h) - \sum_{out} (\dot{m}h) \tag{3.9}$$

This general equation is then adapted to flow paths, which contain an inlet and outlet; and the junctions, which may contain multiple inlets and outlets. This is illustrated in Figure 3.7.

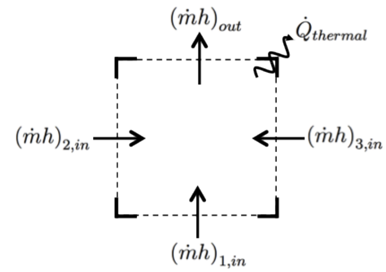

(a) Flow Path Control Volume (b) Junction Control Volume

Figure 3.7: Thermal energy conservation principle on control volumes

The conservation of mechanical energy equation is:

$$\dot{Q}_{frictional} + \dot{W} = \sum_{out} \dot{m}\left(\frac{P}{\rho} + \alpha\frac{v^2}{2} + gh\right) - \sum_{in} \dot{m}\left(\frac{P}{\rho} + \alpha\frac{v^2}{2} + gh\right) \tag{3.10}$$

As the viscous effects are neglected within a junction control since they are accounted for in the adjoining flow path control volumes, the adaption of the mechanical energy equation is depicted only for flow path control volumes as seen in Figure 3.8.

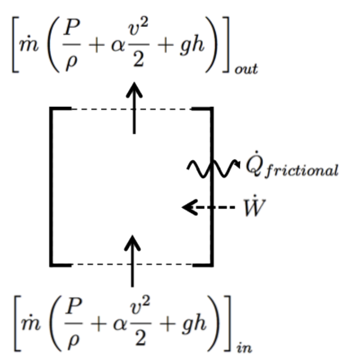

Figure 3.8: Mechanical energy conservation principle on a control volume cell

In control volume with a single inlet and outlet, the mechanical energy equation is divided by the mass flow term to further simplify the equation.

$$w_{net} - q_{frictional} = \left[\frac{P}{\rho} + \alpha\frac{v^2}{2} + gh\right]_{out} - \left[\frac{P}{\rho} + \alpha\frac{v^2}{2} + gh\right]_{in} \tag{3.11}$$

The viscous dissipation term ($q_{frictional}$) for the individual sections are represented empirically by major and minor energy losses. The major loss will be used for straight sections and the remaining sections will have a corresponding minor loss.

$$q_{frictional,major} = f\left(\frac{\Delta L}{D}\right)\frac{v^2}{2} \tag{3.12a}$$

$$q_{frictional,minor} = K\frac{v^2}{2} \tag{3.12b}$$

where

f is the friction coefficient of the straight duct

ΔL is the length of the control volume in the flow direction [m]

D is the inner diameter of the straight duct [m]

K is the loss coefficient of a section (heat exchanger, inlet, outlet, etc)

3.4 Solution of Governing Equations

The solution of a buoyancy driven flow commences with a pressure imbalance between two static columns of air at different temperatures. This pressure imbalance will naturally equalize by transforming the excess gravitational potential energy, or buoyancy potential, into kinetic energy within the smaller column. This transformation phenomenon is illustrated in Figure 3.9.

To avoid confusion, the smaller and larger column do not necessarily need to be "hot" and "cold" respectively. For example, the gas within the smaller column can be colder than the larger column, which will imply a reversal in the pressure inequality and lend itself directly to the reversal of the velocity component. However the interpretation of the column size is important, as this will establish the importance of the kinetic energy. For example, employing the conservation of mass, the velocity through a small column will be higher than through a large column of the same temperature. An alternative interpretation is as the column becomes larger, the velocity component becomes less important.

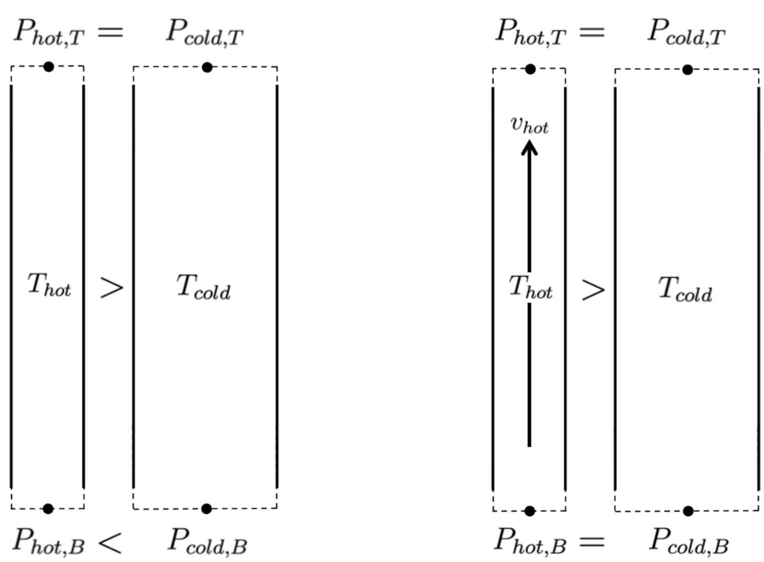

(a) Static pressure columns (b) Balanced pressure columns

Figure 3.9: Gravitational potential energy imbalance transformed into kinetic energy

The technique is extended to exhaust networks by recognizing the ducts as the smaller column transforming the buoyancy potential into kinetic energy; and the exterior environment as the larger static “cold” column. The understanding of the temperature and size effects of the column is critical in extending the technique to provide a simple, yet accurate solution of the velocities, pressures, and temperatures throughout an exhaust network.

The application of the technique begins with manipulating the governing equations to isolate the necessary variables. The initial and boundary conditions are then specified based on environmental and user defined inputs. A unique solution is pinpointed using a Gauss-Seidel iterative method based on a relative error convergence criteria.

3.4.1 Implementation of Governing Equations

As previously described the pressure is initially equal at the top of the column, causing the pressure imbalance to be established by evaluating the pressure profile from the top to bottom of the column. According to the coordinate system, the top down approach requires an unknown pressure at node (i) to be calculated based on a known pressure at node $(i+1)$. This unknown pressure variable is found using the conservation of mechanical energy principle (Equation 3.11).

$$P_i = \rho_i \left[\frac{P_{i+1}}{\rho_{i+1}} + \frac{\alpha \left(v_{i+1}^2 - v_i^2 \right)}{2} + g \left(h_{i+1} - h_i \right) + q_{frictional} - w_{net} \right] \tag{3.13}$$

Most of the terms in the pressure solution (Equation 3.13) are insensitive to flow direction, except for the frictional loss term ($q_{frictional}$). The current derivation of the frictional loss term (Equation 3.12) does not account for this sensitivity; which prompts the separation of the velocity component (v^2) into:

$$q_{frictional,major} = f \left(\frac{\Delta L}{D} \right) \frac{v|v|}{2} \tag{3.14a}$$

$$q_{frictional,minor} = K \frac{v|v|}{2} \tag{3.14b}$$

The minor loss coefficient (K) may also be dependent on flow direction. For example, if the section is a sudden expansion in the positive flow direction, then it will become a sudden contraction in the negative flow direction.

The pressure imbalance is established by sequentially solving for pressure along the length of the exhaust network and the corresponding exterior pressure. This is illustrated in Figure 3.10.

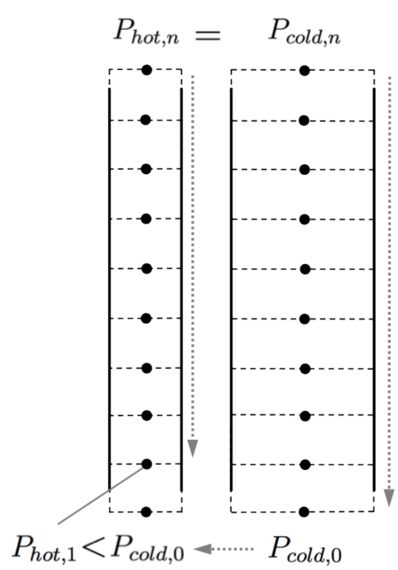

Figure 3.10: Illustration of the pressure solution algorithm

Once the pressure profiles and the subsequent imbalance are established, the velocity component is evaluated at the exhaust network inlet control volume. Using the conservation of mechanical energy (Equation 3.11), the unknown velocity at node $(i + 1)$ is isolated. Moreover, the directionality aspect of velocity requires that the magnitude and direction be calculated separately. The magnitude of velocity is:

$$|v_{i+1}| = \sqrt{\left|\frac{2}{\alpha}\left[\alpha\frac{v_i^2}{2} + \frac{P_i}{\rho_i} - \frac{P_{i+1}}{\rho_{i+1}} + g\left(h_i - h_{i+1}\right) - q_{frictional} + w_{net}\right]\right|} \tag{3.15a}$$

The direction of the velocity component is calculated based on the velocity:

$$\text{Flow Direction} = \frac{v_{i+1}}{|v_{i+1}|} \tag{3.15b}$$

The velocity calculated via the conservation of mechanical energy principle is applied to all exhaust network inlet control volumes based on the coordinate system. This is illustrated in Figure 3.11.

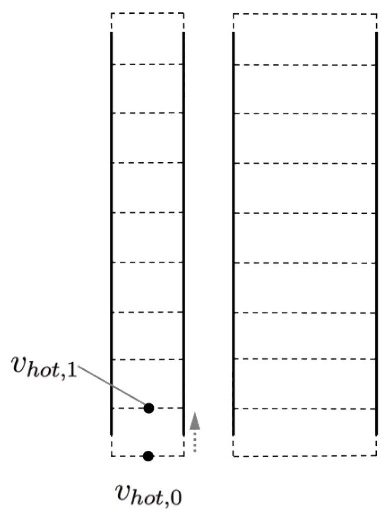

Figure 3.11: Illustration of the velocity solution algorithm at an exhaust inlet via the conservation of mechanical energy principle

Using the conservation of mass principle (Equation 3.3), the velocity exiting the inlet control volume is propagated to all remaining nodes throughout the exhaust network. As illustrated in Figure 3.12, this is accomplished by calculating the unknown velocity at node $(i+1)$ based on the known velocity at node (i) of the control volume. Therefore, the velocity magnitude is:

$$|v_{i+1}| = \left| \frac{\rho_i v_i A_i}{\rho_{i+1} A_{i+1}} \right| \tag{3.16a}$$

and the direction of the velocity component is:

$$\text{Flow Direction} = \frac{v_{i+1}}{|v_{i+1}|} \tag{3.16b}$$

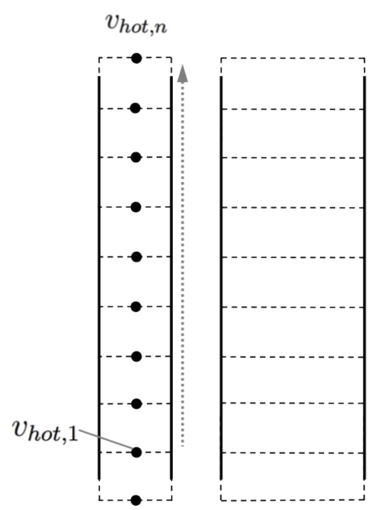

Figure 3.12: Illustration of the velocity solution algorithm via the conservation of mass principle

The buoyancy potential driving the velocity is determined by the density of the fluid; which is based solely on the temperature. The determination of temperature throughout the exhaust network is sensitive to the flow direction and the exterior conditions. This sensitivity is linked to the limiting ability of the thermal energy equation (Equation 3.7) to only support convective transportation of thermal energy;

which can only transport thermal energy in the direction of flow. This flow dependency is overcome by monitoring the flow direction, using Equation 3.15b and 3.16b, and solving the thermal energy equation in the direction of flow. In a positive flow direction, the enthalpy at node $(i + 1)$ is:

$$h_{i+1} = \frac{\dot{m}_i h_i - \dot{Q}_{thermal}}{\dot{m}_{i+1}} \tag{3.17a}$$

and in a negative flow direction, the enthalpy at node (i) is:

$$h_i = \frac{\dot{m}_{i+1} h_{i+1} + \dot{Q}_{thermal}}{\dot{m}_i} \tag{3.17b}$$

The corresponding temperature is deduced from well established enthalpy (h) relationships (Chase, 1998).

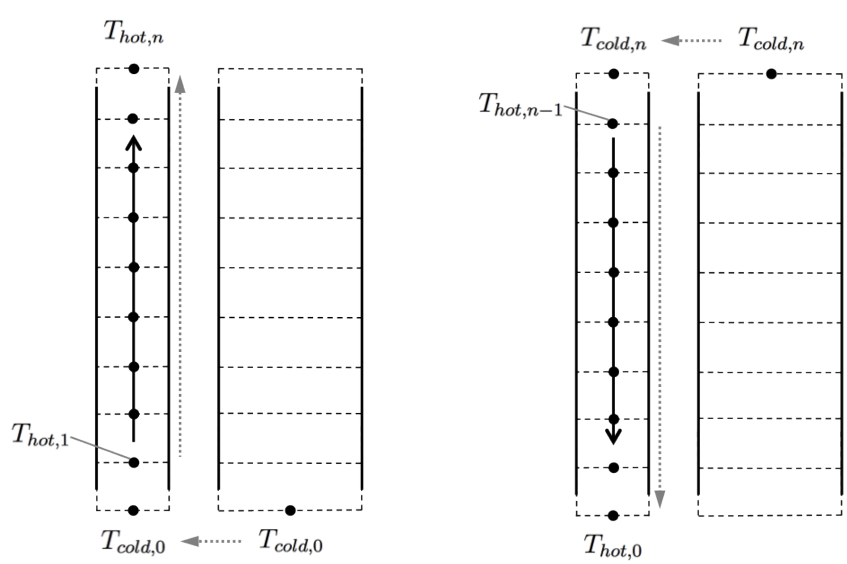

(a) Positive Flow Direction (b) Negative Flow Direction

Figure 3.13: Illustration of the temperature solution algorithm

In addition, the thermal energy entering or leaving the control volume will vary based on the section. The amount is calculated based on the following heat transfer equation:

$$Q_{thermal} = UA\left(T_{bulk} - T_{exterior}\right) \tag{3.18}$$

where

UA is the overall heat transfer coefficient for the sections [W/K]

T_{bulk} is the bulk temperate of the fluid or $\dfrac{T_i + T_{i+1}}{2}$ [K]

$T_{exterior}$ is the exterior temperature of the section [K]

Except for a heat exchanger control volume, which uses a logarithmic mean temperature difference (LMTD) approximation.

3.4.2 Initial and Boundary Conditions

The initial and boundary conditions are necessary components to solve the temperature, pressure, and velocity profiles using the governing equations. The initial conditions provides the exhaust network domain a starting condition. The velocity throughout the domain is set to zero and the pressure is set to a respective static pressure value. The temperature within the "small" and "large" columns are set to the respective user inputs values.

The boundary conditions confine the solution by upholding specific conditions. As shown in Figure 3.14, the boundary condition at the inlet and outlet of the exhaust network during a positive flow scenario are:

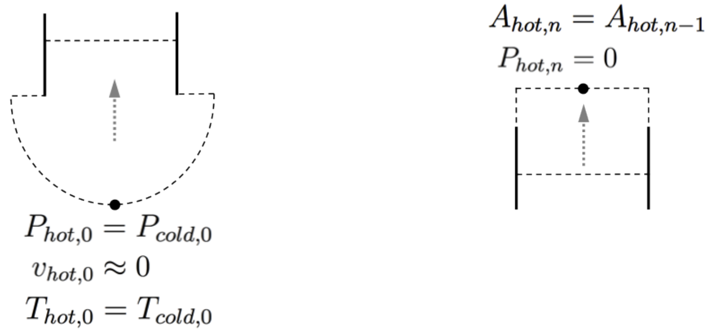

(a) Inlet (b) Outlet

Figure 3.14: Typical boundary conditions for positive flow direction

The basis of the velocity approximation assumes that the entrance area of the control volume is large and, according to the conservation of mass principle, requires the velocity to be nearly zero. The outlet boundary condition are approached in a similar manner. The kinetic energy of the fluid is not immediately dissipated upon exiting and is reflected in the extension of the flow area outside the exhaust network to capture the NPL above the outlet. Alternatively, a negative flow scenario will modify the boundary conditions of the inlet and outlet as shown in Figure 3.15.

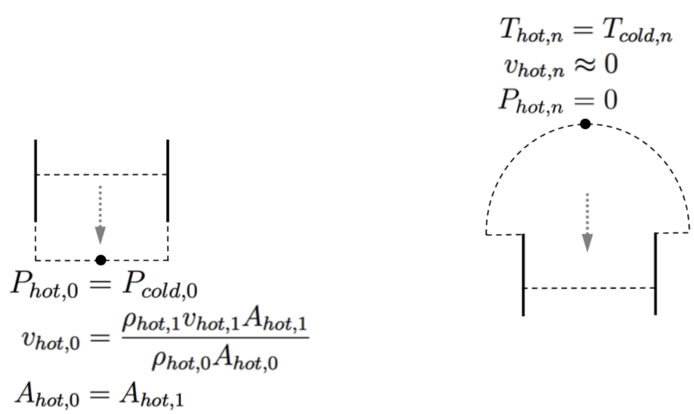

(a) Inlet (b) Outlet

Figure 3.15: Typical boundary conditions for negative flow direction

The inlet boundary conditions during a negative flow scenario adds a complication as the conservation of mass principle (Equation 3.16a) is not normally applied to an inlet control volume. Thus the mass conservation principle must be intrinsically upheld within the boundary condition in the event of a flow reversal.

The burner section supplies the thermal energy to the exhaust network at a constant pressure. The boundary conditions of the burner section are:

(a) Positive flow direction (b) Negative flow direction

Figure 3.16: Boundary conditions for burner section control volume

A boundary condition applied to the burner section specifies the "oven" temperature indicated by the user. Allowing the appliance thermal input to be a function of the draft condition. Similar to the other boundary conditions, the application is dependent on the flow direction.

3.4.3 Solution Algorithm

The solution algorithm utilizes a two-layer approach to maintain stability and maximize convergence. The two-layer approach consist of: (1) inducing a relaxed pressure profile throughout the exhaust domain and (2) solving the associated temperature and velocity profiles to convergence, then cycling back to induce a refined pressure profile until convergence. A depiction of the process is found in Figure 3.17. This algorithm forces the governing equations to be solved explicitly. The stability of convergence is not only a function of the solution order, but of the relative change within and between the temperature, velocity, and pressure profiles.

The primary method of limiting the relative change between profiles is under-relaxation (Versteeg and Malalasekera, 2007). It is applied during the updating stage of the temperature, velocity, and pressure profiles using the following equations:

$$T_i^k = (URF_T)T_i^* + (1 - URF_T)T_i^{k-1} \tag{3.19a}$$

$$v_i^k = (URF_V)v_i^* + (1 - URF_V)v_i^{k-1} \tag{3.19b}$$

$$P_i^k = (URF_P)P_i^* + (1 - URF_P)P_i^{k-1} \tag{3.19c}$$

where

URF is the under-relaxation factor [0-1]

k is the iteration number

The under-relaxation method allows the algorithm to gradually develop the pressure (loop 1) profile, while fully developing the temperature (loop 2) and velocity (loop 3) profiles during each successive iteration.

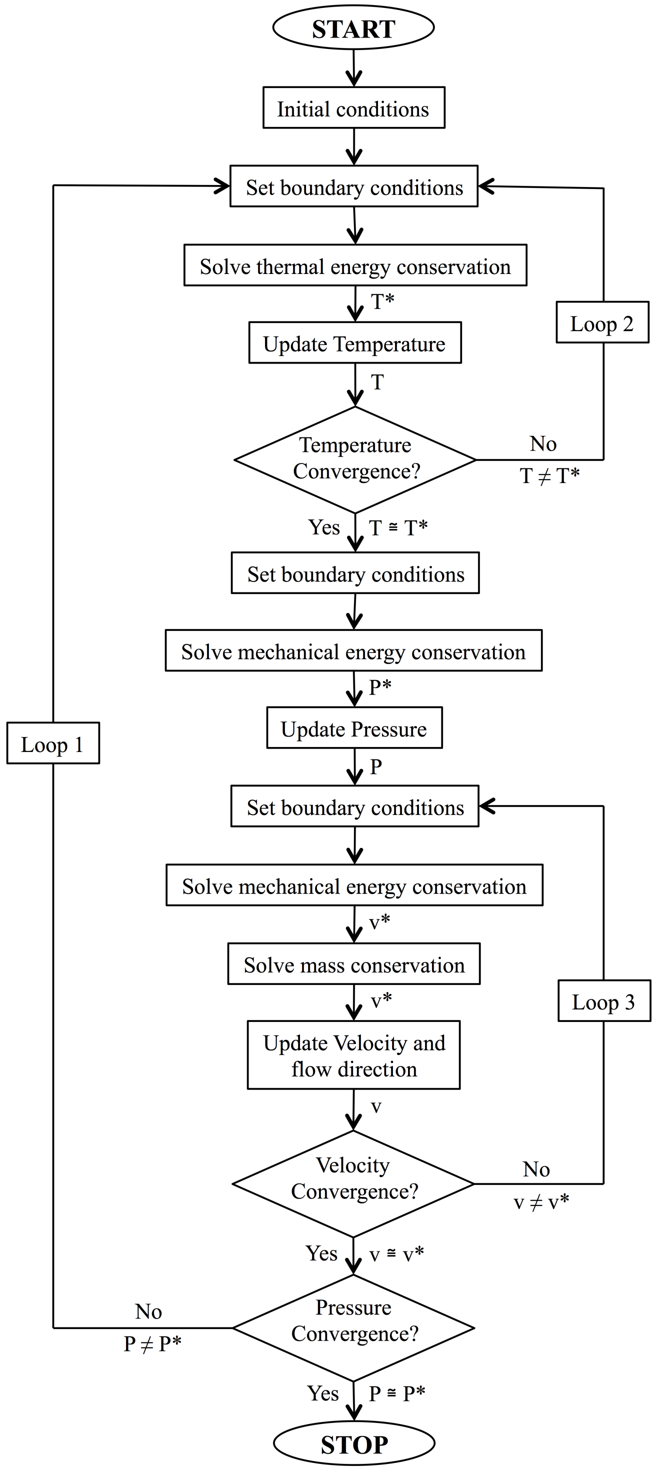

Figure 3.17: Solution algorithm

In addition, the under-relaxation method was implemented using a block correction approach. This involves calculating the entire profile and then applying the under-relaxation to each variable simultaneously. Without the block correction, the conservation laws would not be enforced since the under-relaxation would be applied sequentially and diminish the relative change between variables along the profile. The imbalance would subside over numerous iteration, but the gradually developing pressure profile would remain unstable due to the dependency of the temperature and velocity profiles.

The solution algorithm was verified using a simple investigation of a well-insulated pipe with the ability to maintain a constant air temperature within the pipe. The algorithm was found to agree with an analytical solution to within 1%.

3.4.4 Convergence Criteria

A convergence criteria provides a measurable output to gauge the adequacy of the solution and terminate the iterative process. The Gauss-Seidel iterative method is well adapted to using a residual convergence criterion, which is defined for temperature, velocity, and pressure as:

$$\delta_T = \sum_{i=1}^{n} \left| T_i^* - T_i^{k-1} \right| \tag{3.20a}$$

$$\delta_v = \sum_{i=1}^{n} \left| v_i^* - v_i^{k-1} \right| \tag{3.20b}$$

$$\delta_P = \sum_{i=1}^{n} \left| P_i^* - P_i^{k-1} \right| \tag{3.20c}$$

$$\tag{3.20d}$$

Within each loop, the (δ) must be less than 10^{-3} before the solution is considered complete. This convergence criteria was selected through a sensitivity analysis that showed any lower residual to require more time to converge and produced a change of less than 0.5% in the converged values of temperature, pressure, and mass flow.

The grid sensitivity within the straight section was also investigated as a function of the temperature differential across the control volume. It was found that a temperature difference of less than 1°C. Using an energy balance straight flow path control volume, the following criteria must be used to size length of the grid elements:

$$\Delta L = \frac{\dot{m}_{min} c_p R_{tot}}{(T_{max} - T_{amb})} \tag{3.21}$$

where

$\dot{m}_{max}$ is the minimum mass flow

c_p is the heat capacity of the exhaust

R_{tot} is the total resistance to heat transfer from the duct

$(T_{max} - T_{amb}$ is the maximum temperature difference between the exhasut gases and ambient

The investigated cases were found to be grid independent using a maximum grid element length of 10cm.

Chapter 4

Experimental Methodology

4.1 Introduction

An experimental facility was designed to validate the computational exhaust model. The validation involved accurately measuring the exhaust, dilution air, and exhaust mass flow rates, and the temperatures and pressures at key locations throughout the facility. Along with measuring mass flow rates and other exhaust parameters, the facility also monitors external conditions used as model input, which define exterior boundary and initial conditions. The facility has the capacity to simulate a wide range of conditions and allows for the evaluation of the model as an exhaust system design tool.

4.2 Experimental Facility

The experimental facility is composed of three major components: the oven, the chimney, and the exhaust control devices. The ability to simulate a wide range of conditions is attributed to the modular assembly of the exhaust control devices between the oven and chimney. Figure 4.1 depicts a conventional exhaust layout, which includes exhaust control devices such as a draft hood and throttling valve. Figure 4.2 depicts the proposed **T**hermal **E**lectric **G**enerator **P**izza **O**ven **W**aste **E**nergy **R**ecovery (TEG POWER) system integrated with the conventional exhaust layout. Figure 4.1 and 4.2 encapsulate the two experimental facility variations investigated in this study. Along with the components and the incorporated measurement equipment, the facility also has standalone measurement devices such as: a combustion gas analyzer, psychrometer, and weather station. All of which will be discussed in detail in later sections.

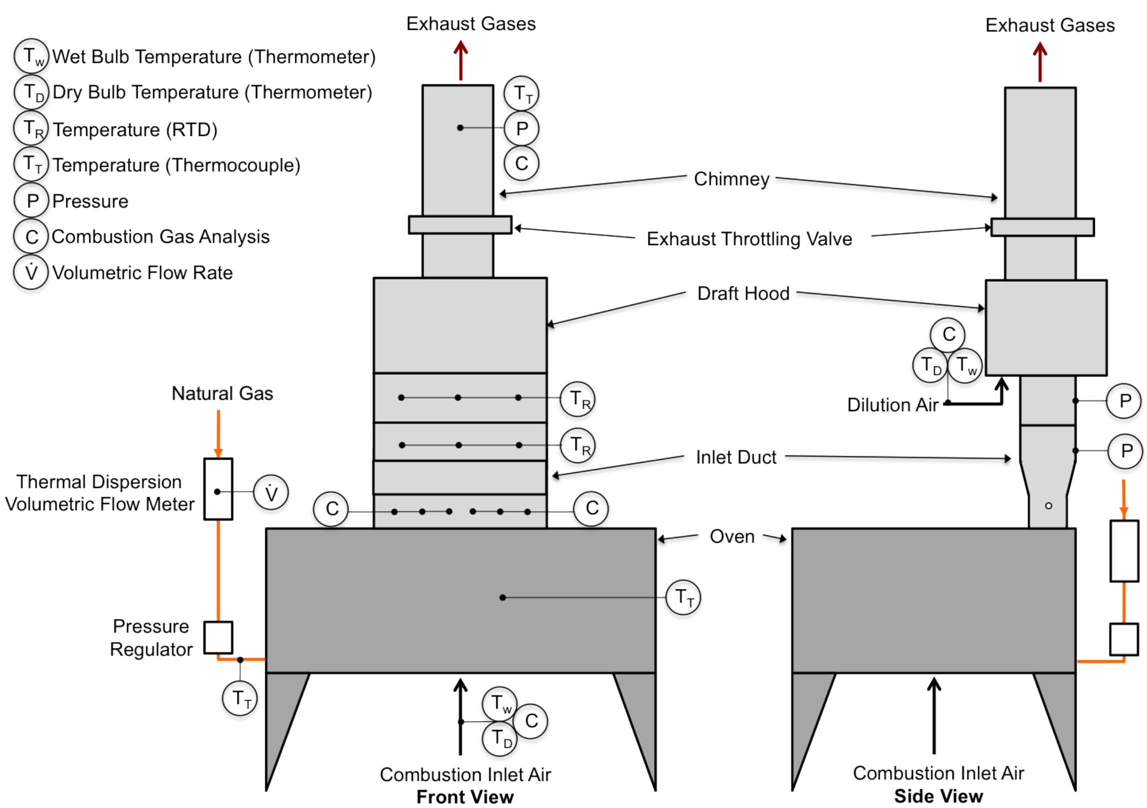

Figure 4.1: Schematic representation of the experimental facility without the TEG POWER system

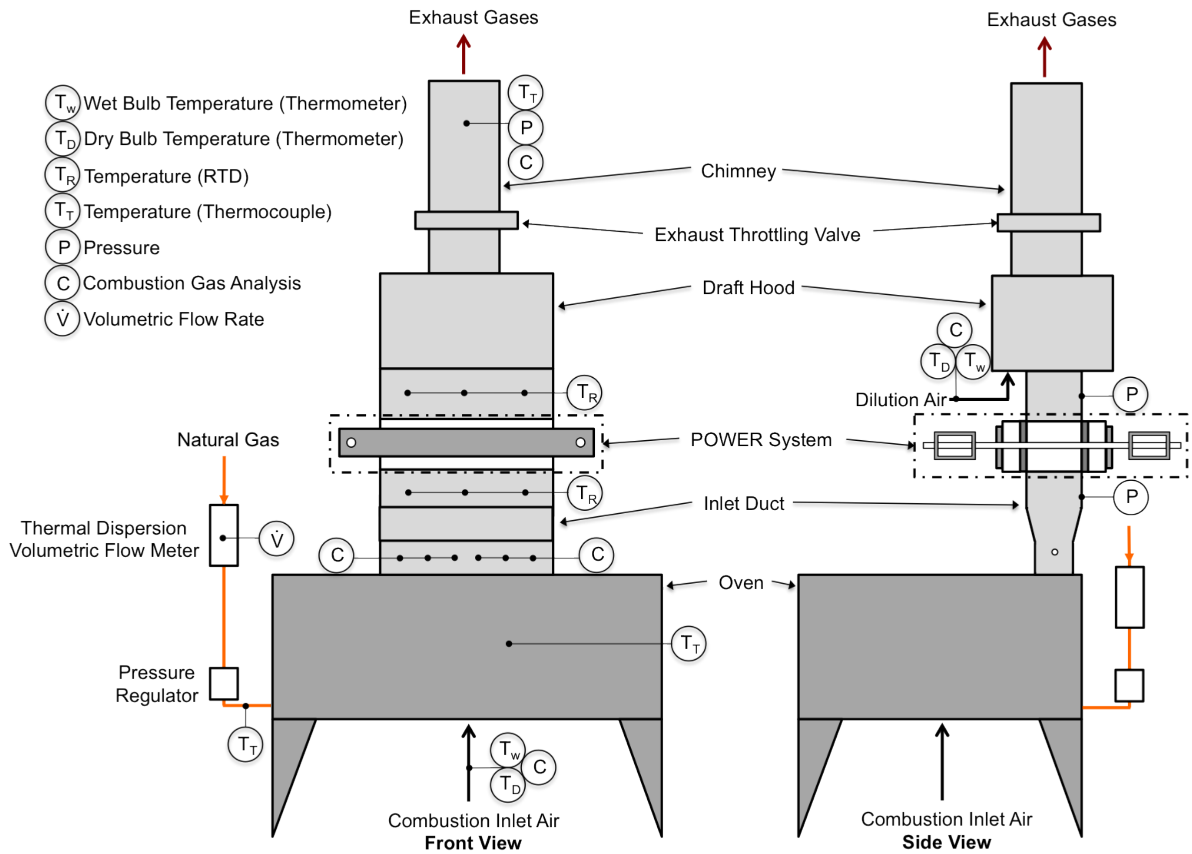

Figure 4.2: Schematic representation of experimental facility with the TEG POWER system

The operation of the facility begins with a mixture of combustion air and natural gas burning inside the oven to generate a source of heat. The thermal energy is transported via the hot exhaust gases into the chimney, where the control devices will partially remove the thermal and/or kinetic energy of the gas to regulate the flow. Within a conventional exhaust layout, the control methods include a direct heat exchanger, called a draft hood, that mixes conditioned ambient air from the room into the exhaust gases and an exhaust throttling valve that induces a pressure drop. With the inclusion of waste heat recovery, the TEG POWER system cools the exhaust gases. Beyond the control devices, the gases travel up the chimney to the exterior of the building.

4.2.1 Oven

A Blodgett 1048B natural gas-fired deck pizza oven is equipped with two 17.6kW (60,000 Btu/hr) barrel burners to provide the thermal energy input to the facility. The natural gas is supplied to the oven at an inlet pressure of 2.6kPa (10.5"W.C) and a thermal dispersion flow meter (McMillan 50D-13) and a surface mounted T-type thermocouple (Omega 5TV-TT-T-30-36) monitor the volumetric flow rate and temperature of the natural gas, respectively. The temperature of the oven is controlled using a modulating thermostat (Robert Shaw FD), which controls the amount of natural gas being mixed with the combustion air. The oven temperature is verified using an E-type thermocouple (Omega EMQSS-125U-24) placed beside the thermostats temperature sensing probe. Additionally, the chemical composition of the combustion air and exhaust gases are measured using a combustion gas analyzer discussed further in section 4.2.5.

4.2.2 TEG POWER Device

The prototype TEG POWER device can be separated into three components: the heat recovery device, the cooling loop, and the electronic DC load. Refer to Figure 4.3 for a schematic representation of the TEG POWER device.

The heat recovery device is comprised of an aluminum pin fin heat exchanger in contact with the exhaust gases. On the exhaust side, the exhaust gas draft pressures and temperatures at the inlet and outlet of the exhaust heat exchanger are measured using a differential pressure transducer (Fluke 922 Airflow Meter) and three inlet and three outlet platinum RTDs (Omega PRTF-11-2-100-1/8-3-E-BX), respectively. Refer to Figure 4.2 for measurement locations. Without the TEG POWER device, the pressure ports and six platium RTDs remain in place to measure the exhaust draft pressure and temperature exiting the oven as represented in Figure 4.1. The thermal energy harvested from the exhaust gases is then transferred to 48 thermoelectric generators (TEG Module TEG1-12610-5.1). The surface temperatures of the TEGs were measured using 16 T-type thermocouples (TMQSS-032U-6) distributed evenly on the exhaust (hot) heat exchanger and liquid (cold) heat exchanger sides of the TEGs. The liquid heat exchangers transfer the thermal energy via a cooling loop. A clamping mechanism is used to hold the device together and provides 18kN of force to minimize the thermal contact resistance between the individual components.

The cooling loop utilizes a chiller unit (Lytron RC045) to maintain the purified water entering the liquid heat exchanger at a constant temperature. A Coriolis effect mass flow meter (Endress+Hauser Proline Promass 80E) is used to accurately measure the mass flow rate of the coolant water. The temperatures and pressures at the inlet and outlet of the liquid heat exchanger were measured using calibrated thermocouples (Omega EMQSS-125U-6) and a pressure transducer (Validyne DP15, 34kPa diaphragm, Validyne CD23 signal conditioner), respectively. The water temperatures and mass flow rate were used to calculate the thermal energy being transferred to the water.

The electronic DC load (B&K Precision 8500) is a 300W programmable resistor used to apply a variable electrical load to the TEG POWER system and record electrical power output of the thermoelectric generators.

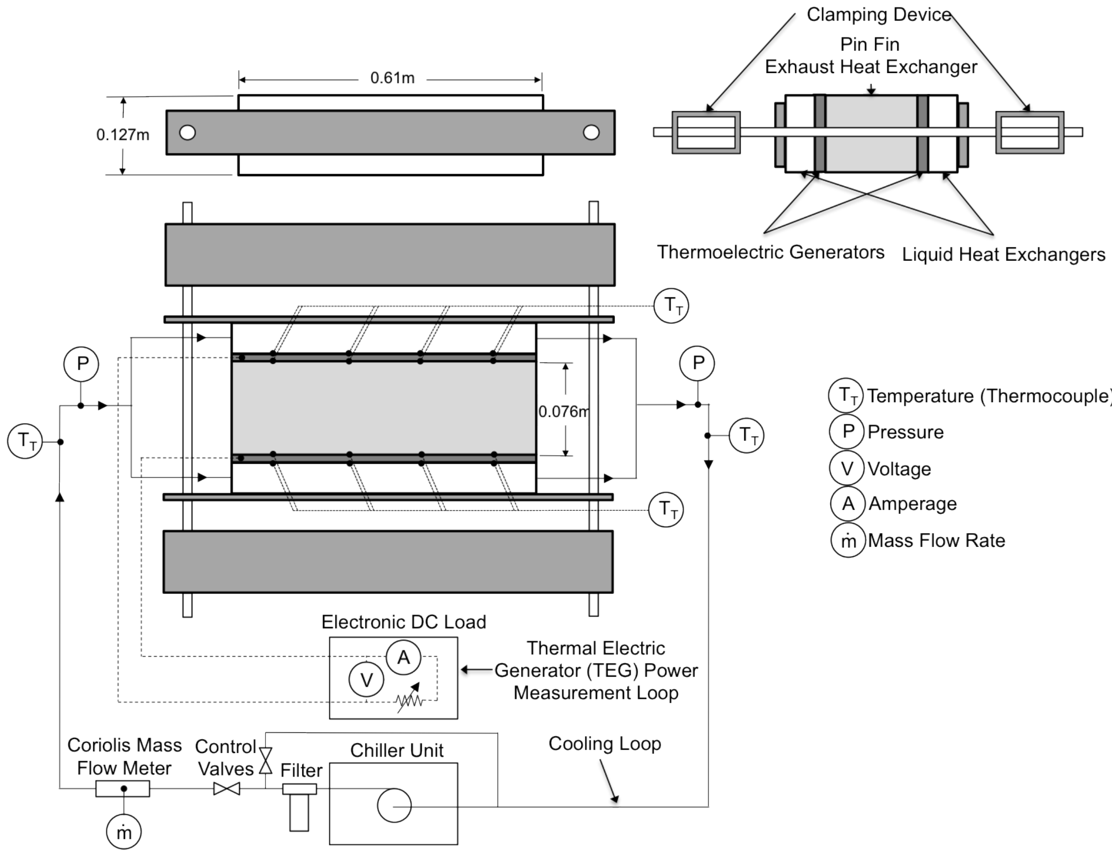

Figure 4.3: Schematic representation of the TEG POWER system

4.2.3 Draft Hood and Exhaust Throttling Valve

The draft hood is located downstream of the oven, as illustrated in Figure 4.1 and 4.2, and acts as a mixing chamber. It allows appliance exhaust gases and dilution air (conditioned ambient room air) to enter separately from the bottom and the diluted exhaust mixture exits from the top vent. Refer to Figure 4.4 for a schematic of the draft hood. Dilution air baffles were installed to avoid interference between re-circulation of cold dilution air and the hot exhaust temperature measurements at the exit of the TEG POWER device. The dilution air inlet was fitted with removable baffles to vary the amount of dilution air entering the draft hood from no dilution air to a maximum based on the operating conditions and the geometry of a standard draft hood design. The baffles were comprised of six equally sized rectangular plates (three on each side of the draft hood) to reduce the flow area into the draft hood. The reduction in flow area causes a large resistance to dilution air from entering the draft hood.

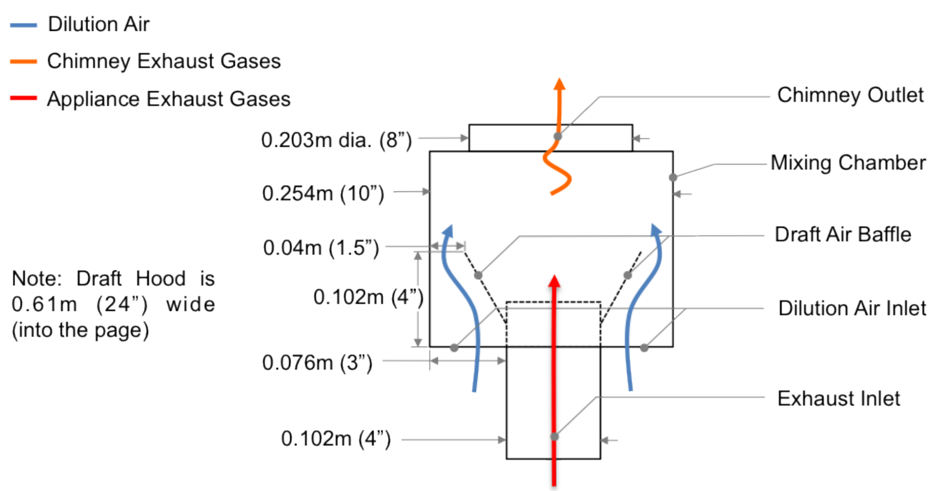

Figure 4.4: Schematic of the draft hood showing key dimensions

The exhaust throttling valve is located downstream of the draft hood, as illustrated in Figure 4.1 and 4.2, and is a manually actuated sealed guillotine valve (Duct Incorporated Style 172) with a position indicator graduated with 10% increments from 0% to 100% closed valve. The positioning system allows different exhaust flow restrictions to be accurately investigated based on the position of the valve. A pressure transducer (Fluke 922 Airflow Meter) is used to measure the pressure differential across the damper valve.

4.2.4 Chimney Layout

The insulated chimney is composed of two differently sized ducts. The vertical section is a 0.254m (10") stainless B-vent chimney (ICC Chimney Company). The connection between the oven and the vertical chimney is a 0.203m (8") stainless exhaust ductwork insulated with 0.05m (2") of fiberglass insulation surrounded with an aluminum wrap. Refer to Figure 4.5 and Figure 4.6 for a schematic representation with dimensions of the chimney layout and other components.

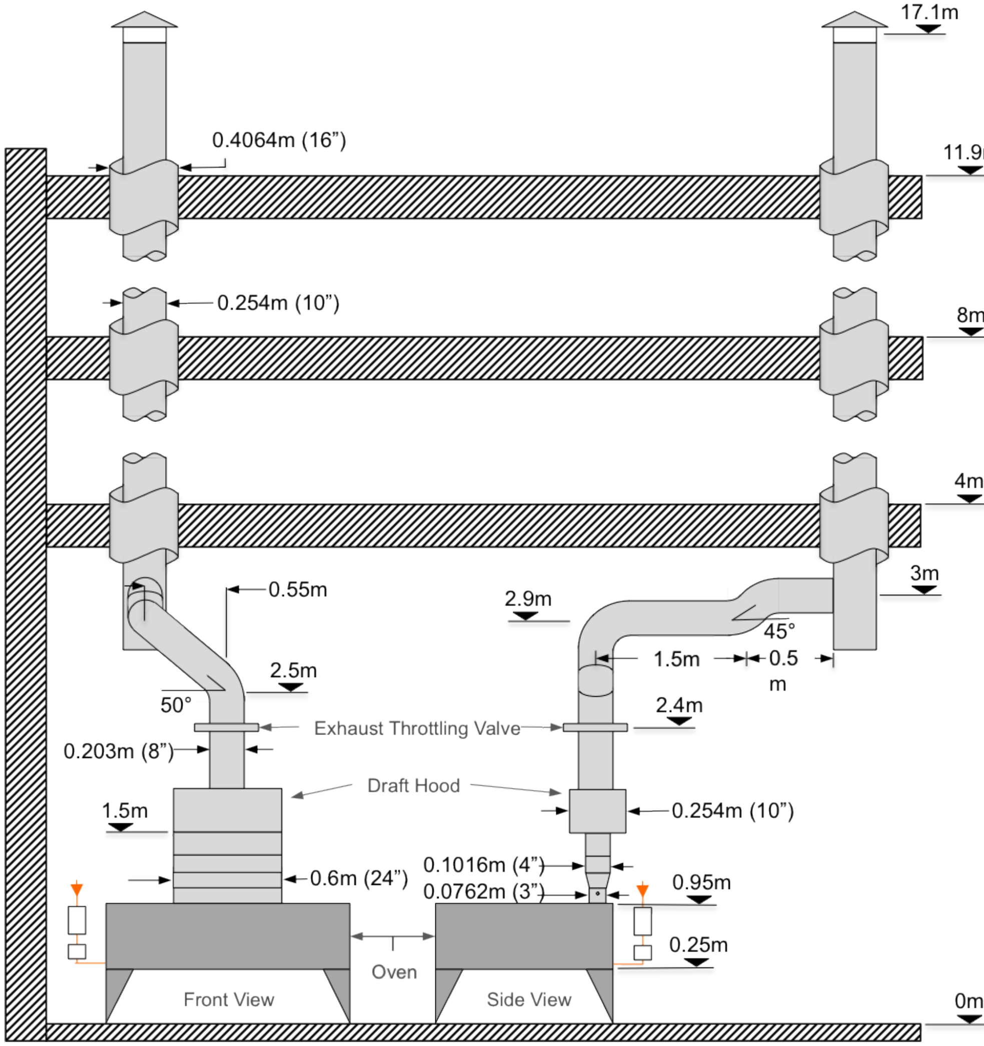

Figure 4.5: Schematic representation of the chimney layout without TEG POWER

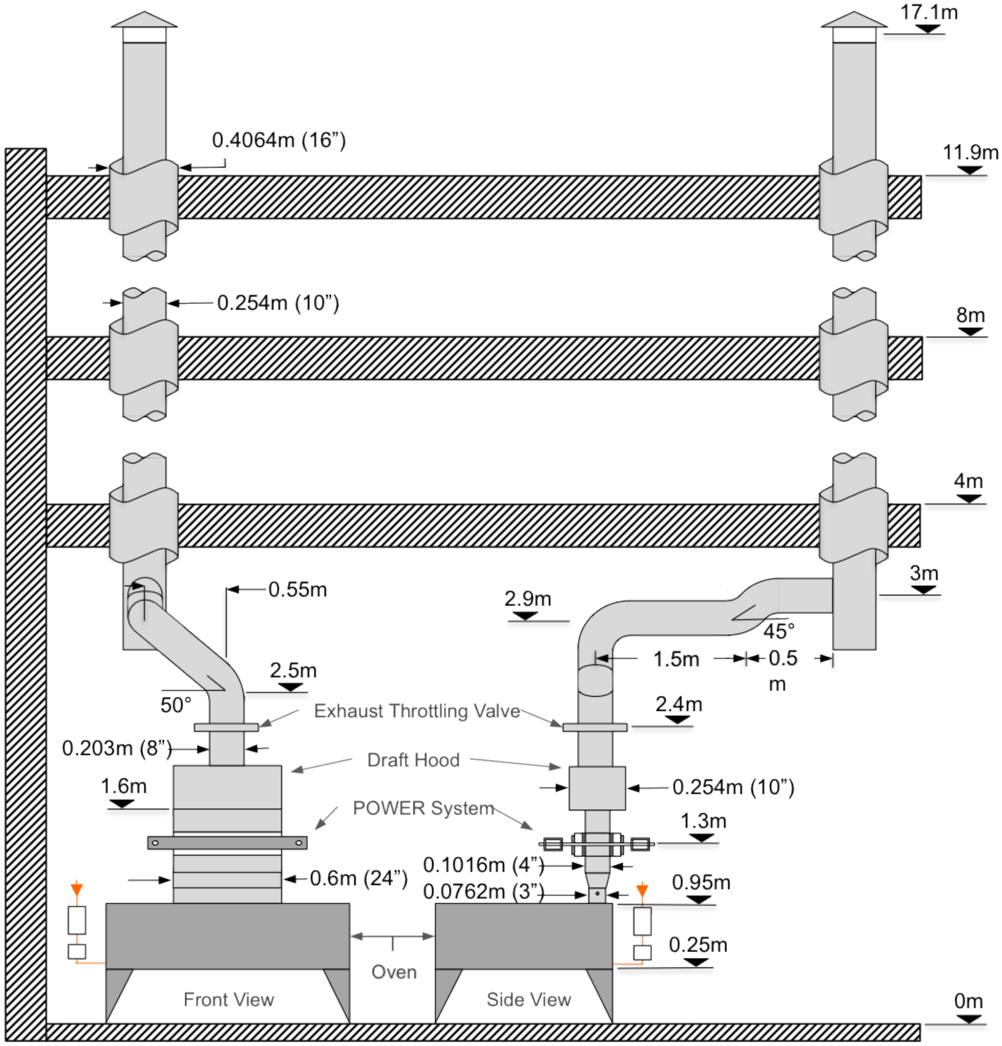

Figure 4.6: Schematic representation of the chimney layout with TEG POWER

4.2.5 External Measurement Equipment

An E-Instruments 8500 combustion analyzer was used to measure the chemical composition of the exhaust gases, combustion air, and dilution air. The exhaust gases were measured at six locations across the exhaust outlet of the oven and a single location in the chimney. The combustion and dilution air were monitored at a single location under the oven and at the dilution air inlet, respectively. See Figure 4.1 and Figure 4.2 for approximate locations. The gas analyzer was able to measure the concentrations of the chemical compounds outlined in Table 4.1. Using the chemical composition data, the exhaust and dilution air mass flow rates were calculated.

Table 4.1: E-8500 chemical measurement capabilities

Compound	CO_2	CO	O_2	NO	NO_2	SO_2	CH_4
Measurement Units	% vol	ppm	% vol	ppm	ppm	ppm	% vol

The humidity and temperature of the combustion and dilution air were measured using a psychrometer. The psychrometer utilized two thermometers mounted on a wooden stand and a DC fan blowing air over the thermometer bulbs. A cotton wick was wrapped around the wet-bulb thermometer and dipped in purified water. The wet and dry-bulb temperatures were read and the humidity was calculated using a psychometric humidity relationship (Wexler, 1976).

A pressure transducer (Omega PX653-0.1D5V) was used to measure the room pressure. It was found that the building HVAC system pressurizes the room during the day. During the evening and night, the room would be at a positive or negative pressure relative to the exterior conditions based on the building supply fan schedule.

The McMaster weather station (McMaster University, 2014) located on the roof of the John Hodgins Engineering (JHE) building near the chimney outlet was used to record outside temperature, atmospheric pressure, and humidity readings necessary for the computational model. Additionally, the wind speed was monitored and testing only occurred when speeds were less than 5km/h. This allowed for parametric isolation of the outside temperature effects on the exhaust mass flow rate.

4.2.6 Data Acquisition System

A National Instruments 8-slot USB chassis (NI cDAQ-9178) was equipped with:

- 16-Channel Thermocouple Input Module (NI 9213) (1200S/s 24-Bit)
- 4-Channel Thermocouple Input Module (I 9211) (14S/s 24-Bit)
- 4-Channel Universal Analog Input Module (NI 9219) (100S/s/ch 24-Bit)
- 4-Channel 100 RTD Input Module (NI 9217) (400S/s 24-Bit)
- 4-Channel 100 RTD Input Module (NI 9217) (400S/s 24-Bit)

A dedicated Data Processing Computer (Dell) was used to display and record the raw data from the DAQ via a National Instruments Labview 11 software package. The ability to display real-time data was crucial in determining the steady state condition to begin recording.

4.3 Experimental Procedures

The investigation into the exhaust draft performance was split into the following categories:

- Typical exhaust system
- Heat recovery system

The experimental procedures of each respective category differed slightly and will be discussed in the following sections, but it is important to highlight that each category was studied at a steady state condition. Due to the importance of this condition, a steady state definition was investigated. This investigation provided the insight into identifying when steady state was reached; namely if the fluctuations of the natural gas flow rate and oven temperature were less than 0.1 L/min and 0.5°C, respectively, for a period of more than 30 minutes. From start-up, this process normally required a minimum of 5 hours and another 2 hours between tests within a test matrix. The steady state values were obtained by averaging 60 samples over a minute. All the values from the standalone external measurement equipment were documented. Using the respective calibration curves and data reducing calculations, the post-processing of the recorded data, from external measurement devices and DAQ, was completed via Microsoft EXCEL.

4.3.1 Typical Exhaust System

The typical exhaust system measurements provided a baseline of the chimney performance. At this stage of the study the effects of the active exhaust control devices (draft hood and exhaust damper valve) independent of the TEG POWER system were investigated

The initial oven start-up procedures were followed, which are outlined below:

1. The outdoor air louver was opened to aid in equalizing the pressure between the room and the exterior of the building
2. The exhaust damper was fully opened and the draft hood was sealed to accommodate the testing matrix

3. The natural gas supply was turned on and the oven pilot light was lit.
4. The initial measurement values are recorded for comparison purposes between initial and steady state conditions
5. The oven temperature was set to 150°C (300°F) and the main gas valve was opened
6. The facility was allowed to reach steady state

Once the facility reached steady state, all the parameters listed in Table 4.2 are recorded as stated previously.

Table 4.2: Experimentally measured parameters for the typical exhaust system

Symbol	Measurement
C_{ex-i}	Oven outlet exhaust chemical composition at location 1-6
$C_{chimney}$	Chimney inlet exhaust chemical composition
C_{air}	Combustion air chemical composition
$C_{dilution}$	Dilution air chemical composition
T_{ex-i}	Oven outlet exhaust temperature at location 1-6
T_{oven}	Oven temperature at thermostat probe
$T_{chimney}$	Chimney inlet temperature
$T_{air,wb}$	Combustion air wet bulb temperature
$T_{air,db}$	Combustion air dry bulb temperature
$T_{dilution,wb}$	Dilution air wet bulb temperature
$T_{dilution,db}$	Dilution air dry bulb temperature
P_{ex}	Oven outlet draft pressure
P_{hood}	Draft hood draft pressure
$P_{chimney}$	Chimney inlet draft pressure
$T_{outdoor}$	Outdoor air temperature
$\phi_{outdoor}$	Outdoor air relative humidity
P_{atm}	Outdoor atmospheric pressure
V_{wind}	Outdoor wind speed
D_{wind}	Outdoor wind direction
P_{room}	Differential pressure between the room and outside
$\dot{V}_{NG}$	Natural gas volumetric flow rate
T_{NG}	Natural Gas inlet temperature

After which, the exhaust damper and/or the draft hood are adjusted appropriately to the conditions of the test matrix displayed in Table 4.3.

Table 4.3: Typical exhaust system test matrix

Test#	1	2	3	4	5	6	7	8	9
Draft hood	0%	0%	0%	0%	17%	17%	33%	50%	100%
Throttling Valve	0%	50%	60%	70%	0%	50%	0%	0%	0%

After the text matrix has been completed, the oven temperature is raised to 260°C (500°F) and the test matrix is repeated. This procedure is repeated for a final oven temperature of 315°C (600°F). Once the test matrix is repeated at the specified oven temperature set points, the gas supply is shutoff and the oven is allowed to cool back to room temperature and the louver is shut.

4.3.2 Heat Recovery System

The heat recovery system test procedure was developed to investigate the draft performance and controllability with the presence of the TEG POWER system. The initial start-up procedures are similar to previous list, but with the added component of a coolant loop. The start-up procedures were followed and are outlined below:

1. The coolant loop was turned on and the coolant outlet temperature and flow rate were set to 16°C and 0.07 kg/s (1.1 gpm), respectively
2. The air in the coolant loop is bled from the system
3. The outdoor air louver was opened to aid in equalizing the pressure between the room and the exterior of the building
4. The exhaust damper was fully opened and the draft hood was sealed to accommodate the testing matrix
5. The natural gas supply was turned on and the oven pilot light was lit

6. The initial measurement values are recorded for comparison purposes between initial and steady state conditions
7. The oven temperature was set to 150°C (300°F) and the main gas valve was opened
8. The facility was allowed to reach steady state

Once the facility reached steady state, the steady state values listed in Table 4.4 are recorded in the same manner as the previous procedures.

Table 4.4: Experimentally measured parameters for the heat recovery system

Symbol	Measurement
C_{ex-i}	Oven outlet exhaust chemical composition at location 1-6
$C_{chimney}$	Chimney inlet exhaust chemical composition
C_{air}	Combustion air chemical composition
$C_{dilution}$	Dilution air chemical composition
$T_{HX\ in-i}$	Heat exchanger inlet exhaust temperature at location 1-3
$T_{HX\ out-i}$	Heat exchanger outlet exhaust temperature at location 1-3
$T_{TEG,hot-i}$	Heat exchanger outlet exhaust temperature at location 1-8
$T_{TEG,cold-i}$	Heat exchanger outlet exhaust temperature at location 1-8
T_{oven}	Oven temperature at thermostat probe
$T_{chimney}$	Chimney inlet temperature
$T_{air,wb}$	Combustion air wet bulb temperature
$T_{air,db}$	Combustion air dry bulb temperature
$T_{dilution,wb}$	Dilution air wet bulb temperature
$T_{dilution,db}$	Dilution air dry bulb temperature
$P_{HX,inlet}$	Heat exchanger inlet draft pressure
$P_{HX,outlet}$	Heat exchanger outlet draft pressure
$P_{chimney}$	Chimney inlet draft pressure
$T_{outdoor}$	Outdoor air temperature
$\phi_{outdoor}$	Outdoor air relative humidity
P_{atm}	Outdoor atmospheric pressure
V_{wind}	Outdoor wind speed
D_{wind}	Outdoor wind direction
P_{room}	Differential pressure between the room and outside
$\dot{V}_{NG}$	Natural gas volumetric flow rate
T_{NG}	Natural Gas inlet temperature
$T_{water\ in}$	Coolant water inlet temperature
$T_{water\ out}$	Coolant water inlet temperature
$\dot{m}_{water}$	Coolant water mass flow rate
ΔP_{HX}	Differential pressure across coolant heat exchangers

The damper and/or the draft dilution are adjusted appropriately to cycle through the respective test matrix, which is displayed in Table 4.5.

Table 4.5: Heat recovery system test matrix

Test#	1	2	3	4	5	6	7
Draft hood	0%	0%	0%	0%	17%	17%	33%
Throttling Valve	0%	50%	60%	70%	0%	50%	0%

After the text matrix has been completed, the oven temperature is raised to 260°C (500°F), then to 315°C (600°F), while cycling through the text matrix for each temperature. Once the test matrix is cycled through, the gas supply is shutoff and the oven is allowed to cool back to room temperature and the louver is shut.

4.4 Data Reduction

Using mass and energy balance approach, the performance of the appliance and exhaust system can be quantified. The performance aspects includes mass and energy flow characteristics, thermal losses, and various mass flow rates throughout the exhaust system. In addition, the accompanying pressure loss coefficients for the exhaust components are calculated using the respective mass flow rates.

4.4.1 Mass Flow Analysis

The measurement of the mass flow through the various exhaust network components required the determination of an appropriate measurement technique, which was evaluated using the following criteria:

- Measures mass flow through various appliances and exhaust duct geometries,
- Allows for changes in bulk temperature and composition of the fluid
- Negligible pressure drop as to not affect the draft condition

Traditional measurement techniques were investigated such as ultrasonics, anemometry, static/dynamic pressure relationships, and combustion mass balance. Unfortunately, these techniques were found to require unattainable development lengths and incredibly sensitive pressure transducers, be sensitive to temperature changes and composition, cause excessive pressure drops, or have poor sensitivity at low CO_2 concentrations. Despite these shortfalls a pitot tube was used during preliminary experimentation, but it was unable to calculate an average flow through each respective duct since the velocity profile were found to vary with time and have a skewed parabolic profile with inaccurate velocity measurements. A conventional combustion mass balance was performed to find that the low concentration levels of CO_2 in the combustion exhaust and chimney gases produced maximum relative errors of 152% in CO_2 concentration levels and 68% in the exhaust mass flow ($\dot{m}_{exhaust}$) calculations. It is recommended that the combustion mass balance technique only be used with CO_2 sensors with an accuracy greater than 0.01% vol. due low levels of CO_2 (<1.5% vol.) caused by the high volume of excess air to meet the cooking requirements.

Once abandoning more conventional techniques, the combustion energy balance approach was investigated and implemented as outlined in Section 4.4 for the appliance (combustion chamber) and the draft hood. Using the conservation of mass and energy principles, the chemical concentrations and thermal characteristics can be used to determine exhaust gas and air flow characteristics. By simultaneously solving the coupled equations, this approach provided an non-invasive measurement methodology to investigate the performance of the appliance and exhaust system.

4.4.1.1 Combustion Chamber

The combustion chamber mass flow analysis begins with the formulation of the conversion of chemical compounds based on a pseudo complete combustion process. Through testing, the formulation of the exhaust gases must include unburnt fuel (CH_4) within the exhaust gases due to the relatively high concentrations detected during low temperature tests and an exclusion of CO, NO_x, and SO_x since the concentrations were found to be negligible. The molar concentrations of the chemical compounds constituting the respective gases are outlined in Table 4.6.

Table 4.6: Chemical composition of the reactants and products during the combustion process

Nomenclature (i or j)	1	2	3	4	5
Natural Gas	CH_4	CO_2	C_2H_6	C_3H_8	N_2
Combustion air	O_2	N_2	–	–	–
Exhaust Gases	CO_2	O_2	N_2	CH_4	–

The chemical composition of the natural gas was referenced from the gas utility supplier (Union Gas, 2014). The chemical composition of the combustion air and exhaust gases were outputted by the E-8500 combustion analyzer. The exhaust gases were measured at six equally spaced locations across the outlet of the oven and at a single location in the chimney, which allowed for an average exhaust composition to be calculated using:

$$C_{avg,j} = \frac{1}{7}\sum_{k=1}^{7} C_{j-k} \tag{4.1}$$

where subscript (k) denotes the measurement position. The positioning follows the numbering scheme listed in Figure 4.5 and the chimney location is denoted as the 7$^{\text{th}}$ measurement.

The N_2 concentration for the combustion air can not be measured directly using the combustion analyzer and were therefore calculated based on the remaining volume. This is illustrated through equation 4.2.

$$C_{N_2} = 100\% - \sum_{i=1}^{M}[C_i] \tag{4.2}$$

The mole balance of the chemical equation describing the combustion process is represented as:

$$\sum_{i=1}^{N}[N_i]_{NG} + (EX+1)(a_{th})\sum_{j=1}^{N}[N_j]_{air} + cH_2O \Longleftrightarrow \sum_{j=1}^{N}[N_j]_{exhaust} + (c+f)H_2O \tag{4.3}$$

where

$$\sum_{i=1}^{N}[N_i]_{NG} = \sum_{i=1}^{N}[C_i]_{NG}$$
$$\sum_{j=1}^{N}[N_j]_{air} = [C_{O_2}]_{air} + [C_{N_2}]_{air}$$
$$\sum_{j=1}^{N}[N_j]_{exhaust} = dCO_2 + eN_2 + (EX)(a_{th})[C_{O_2} + C_{N_2}]_{air} + gCH_4$$

and

EX is the amount of excess air within the combustion process

a_{th} is the amount of theoritical air

To clarify, the term $N_{i\,or\,j}$ describes the number of moles of the respective compound and encompasses $C_{i\,or\,j}$, which is a concentration measurement. The composition of the exhaust gases is unknown and is solved based on the composition of the natural gas and combustion air, along with the measured concentration of unburnt fuel (g) within the exhaust gases. Based on the exhaust concentration ($[C_{CH_4}]_{exhaust}$), the moles of unburnt fuel is described by:

$$g = \frac{[C_{CH_4}]_{exhaust}\Big(c + f + d + e + (EX)(a_{th})[C_{N_2} + C_{O_2}]_{air}\Big)}{1 - [C_{CH_4}]_{exhaust}} \tag{4.4}$$

Next, the variables (a_{th}, d, e, f) are described through a stoichiometric analysis to remove the effects of excess air and moisture within the combustion air.

$$\sum_{i=1}^{N}[C_i]_{NG} + (a_{th})[C_{O_2} + C_{N_2}]_{air} \iff dCO_2 + eN_2 + fH_2O + gCH_4 \tag{4.5}$$

Once the stochiometric combustion equation is balanced correctly, the unknown variable (c) denoting the moisture found in the combustion air can be calculated. The ability to independently solve for variable (c) stems from the assumption that the moisture entering through the combustion air will not react to form other chemical compounds, but will simply add to the moisture leaving in the exhaust gases. To begin this analysis, the relative humidity of the combustion air must be calculated by inputting the wet bulb ($\mathrm{T_{air,wb}}$) and dry bulb ($\mathrm{T_{air,db}}$) temperature into the following equation (Parish and Putnam, 1977):

$$\phi(T_{air,db}, T_{air,wb}, P_{atm}) = \frac{10^{-\left(23.5518+\left[\frac{-2937.4}{T_{air,db}+273}\right]\right)}}{(T_{air,db}+273)^{-4.9283}}\left[\frac{10^{\left(23.5518+\left[\frac{-2937.4}{T_{air,wb}+273}\right]\right)}}{(T_{air,wb}+273)^{4.9283}}\right.$$
$$\left. - (6.6\times10^{-4} + (7.57\times10^{-7})T_{air,wb})P_{atm}(T_{air,db} - T_{air,wb})\right] \tag{4.6}$$

The vapour pressure of the moisture in the air is estimated by first calculating the saturation pressure of water at the dry bulb temperature ($\mathrm{T_{air,db}}$) using the following equation (Wexler, 1976):

$$log_e(P_{sat,water}) = \sum_{i=0}^{3} c_i(T_{air,db} + 273.15)^{i-1} + c_4 log_e(T_{air,db} + 273.15) \tag{4.7}$$

where

$$c_0 = -0.60436117 \times 10^4 \quad c_1 = 0.189318833 \times 10^2$$
$$c_2 = -0.28238594 \times 10^{-1} \quad c_3 = 0.17241129 \times 10^{-4}$$
$$c_4 = 0.2858487 \times 10^1$$

The multiplication of the relative humidity (ϕ) and the saturation pressure of water ($P_{\mathrm{sat,water}}$) reveals the vapour pressure of the moisture in the air.

$$P_{v,air} = \phi P_{sat,water} \tag{4.8}$$

The molar quantity of moisture in the combustion air, or variable (c), is solved using an ideal gas relationship between the pressure and molar ratios illustrated by equation 4.9.

$$c = \frac{\frac{P_{v,air}}{P_{atm}} N_{tot,air}}{1 - \frac{P_{v,air}}{P_{atm}}} \tag{4.9}$$

where ($N_{\mathrm{tot,air}}$) is the total amount of moles of combustion air involved in the combustion process including the moisture content. In this case, the total number of moles of combustion air ($N_{tot,air}$) also depends on the amount of excess air. Which is determined via the percentage of excess air (EX) needed to satisfy the experimentally measured temperature characteristics of the oven using the conservation of energy principle. To finalize the calculations, the molar quantity of moisture in the combustion air (c) is added to the moisture generated by the combustion process (f).

$$\sum_{i=1}^{N}[N_i\Delta\bar{h}_i]_{NG} + \sum_{j=1}^{N}[N_j\Delta\bar{h}_j]_{air} + (c)\Delta\bar{h}_{H_2O,air} = \sum_{j=1}^{N}[N_j\Delta\bar{h}_j]_{exhaust} + (c+f)\Delta\bar{h}_{H_2O,exhaust} + Q_{loss,oven} \quad (4.10)$$

where

$$\sum_{i=1}^{N}[N_i\Delta\bar{h}_i]_{NG} = \sum_{i=1}^{N}[C_i\Delta\bar{h}_i]_{NG}$$

$$\sum_{j=1}^{N}[N_j\Delta\bar{h}_j]_{air} = (EX+1)\,(a_{th})\left[C_{O_2}\Delta\bar{h}_{O_2} + C_{N_2}\Delta\bar{h}_{N_2}\right]_{air}$$

$$\sum_{j=1}^{N}[N_j\Delta\bar{h}_j]_{exhaust} = d\,\Delta\bar{h}_{CO_2} + \Big(e + (EX)(a_{th})[C_{N_2}]_{air}\Big)\Delta\bar{h}_{N_2} + \Big((EX)(a_{th})[C_{O_2}]_{air}\Big)\Delta\bar{h}_{O_2} + g\,\Delta\bar{h}_{CH_4}$$

and

$\Delta\bar{h} = \bar{h}^{\circ} + \bar{h}_T - \bar{h}_{ref}$ is the enthalpy of the element [J/mol]

$\bar{h}^{\circ}$ is the enthalpy of formation [J/mol]

$\bar{h}_T$ is the enthalpy at the fluid temperature [J/mol]

$\bar{h}_{ref}$ is the reference enthalpy at 298K [J/mol]

$Q_{loss,oven}$ is the oven thermal losses [J/kg of NG]

The enthalpy values were estimated using a linear approximation through enthalpy data for the respective chemicals from the JANAF property tables (Chase, 1998). The thermal loss of the oven ($Q_{loss,oven}$) was calculated based on an overall heat transfer coefficient and the operating temperatures. An arithmetic mean was used to average the exhaust gas temperatures since the exhaust gases exiting the oven were measured at various location across the duct.

$$Q_{loss,oven} = UA\frac{(T_{oven} - T_{air,db}) - (T_{ex,inlet} - T_{air,db})}{ln(\frac{T_{oven} - T_{air,db}}{T_{ex,inlet} - T_{air,db}})} \tag{4.11}$$

The overall heat transfer coefficient (UA) is estimated using a transient lumped sum system analysis based on oven cool down experiments collected by Hirmiz (2014). A detailed recording of the analysis can be found in Appendix B.

The evaluation of the unknown variables (a_{th}, c, d, e, f, g) and the amount of excess air (EX) must employ a simultaneous iterative solution of Equation 4.4, 4.5, and 4.10. Once convergence is achieved, the outline combustion parameters based on molar concentrations and thermal characteristics are calculated. These parameters include:

- Air-to-fuel ratio (AF)
- Exhaust-to-fuel ratio (EF)
- Exhaust Dew Point Temperature

The air-to-fuel ratio was calculated by dividing the masses (in kg) of the combustion air, including the moisture, with the natural gas using the following equation:

$$AF = \frac{(EX+1)(a_{th})\sum_{j=1}^{N}[N_jM_j]_{air} + (c)M_{H_2O}}{\sum_{i=1}^{N}[C_iM_i]_{NG}} \tag{4.12}$$

where the (M) represents the molar mass (kg/kmol) of the respective element.

The exhaust-to-fuel ratio was calculated using the following equation:

$$EF = \frac{\sum_{j=1}^{N}[N_j M_j]_{exhaust} + (c+f)M_{H_2O}}{\sum_{i=1}^{N}[C_i M_i]_{NG}} \tag{4.13}$$

The dew point temperature (T_{dew}) of the exhaust is defined as the water saturation temperature at the partial pressure of the water vapour (P_v) in the exhaust. The partial pressure (P_v) is estimated using the same ideal gas relationship used in equation 4.9.

$$P_v = \frac{N_v}{N_{tot}} P_{atm} \tag{4.14}$$

where

$$N_v = \frac{c+f}{x}$$

The dew point temperature was found by rearranging the Clausius-Clapeyron equation and using JANAF steam tables (Chase, 1998).

$$T_{dew} = \frac{1}{\left(\frac{R_{v,water}}{\Delta h_{fg}}\right) log_e \left(\frac{P_v}{P_{sat@T}}\right) + \frac{1}{T}} - 273.15 \tag{4.15}$$

where

$R_{v,water}$ is the gas constant of water vapour [kJ/kgK]

Δh_{fg} is the latent heat of vaporization [kJ/kg]

T is the known calibration temperature from the steam tables [K]

$P_{sat@T}$ is the known saturation pressure at temperature T [kPa]

4.4.1.2 Draft Hood

An energy balance approach was used to determine the mixing occurring between the entering exhaust ($\dot{m}_{exhaust}$) and dilution air ($\dot{m}_{dilution}$) and exiting chimney ($\dot{m}_{chimney}$) mass flows. Similar to the combustion chamber, the analysis begins with the formulation of the molar balance within the draft hood.

$$\sum_{i=1}^{N}[N_i]_{exhaust} + (c+f)H_2O_{exhaust} + (DA)\sum_{j=1}^{N}[N_j]_{air} + hH_2O_{air} \Longleftrightarrow \sum_{j=1}^{N}[N_j]_{chimney} + (c+f+h)H_2O_{chimney} \quad (4.16)$$

where

$$\sum_{j=1}^{N}[N_j]_{chimney} = \sum_{j=1}^{N}[N_j]_{exhaust} + (DA)\sum_{j=1}^{N}[N_j]_{air}$$

Using the conservation of energy, the amount of draft air (DA) can be determined.

$$\sum_{i=1}^{N}[N_i\Delta\bar{h}_i]_{exhaust} + (c+f)\Delta\bar{h}_{H_2O,exhaust} + (DA)\sum_{j=1}^{N}[N_j\Delta\bar{h}_j]_{air} + h\Delta\bar{h}_{H_2O,air}$$
$$\Longleftrightarrow \sum_{j=1}^{N}[N_j\Delta\bar{h}_j]_{chimney} + (c+f+h)\Delta\bar{h}_{H_2O,chimney} + Q_{loss,hood} \quad (4.17)$$

The thermal losses ($Q_{loss,hood}$) are calculated using heat transfer coefficients (UA) based on empirical formulation and a logarithmic temperature difference ($LMTD$) between the exhaust gases and the surroundings, which is described in Appendix B.

Using a similar approach to the combustion chamber analysis, the parameters listed below can be calculated.

- Dilution air-to-exhaust ratio (DAE)
- Chimney-to-exhaust ratio (CE)
- Chimney Dew Point Temperature

The dilution air-to-exhaust ratio is:

$$DAE = \frac{(DA)\sum_{j=1}^{N}[N_jM_j]_{air} + (h)M_{H_2O}}{\sum_{i=1}^{N}[C_iM_i]_{exhaust} + (c+f)M_{H_2O}} \quad (4.18)$$

The chimney-to-exhaust ratio:

$$CE = \frac{\sum_{i=1}^{N}[N_iM_i]_{exhaust} + (c+f)M_{H_2O}}{\sum_{j=1}^{N}[C_jM_j]_{chimney} + (c+f+h)M_{H_2O}} \quad (4.19)$$

4.4.2 Heat Exchanger Performance

Using the TEG POWER device, depicted in Figure 4.2, the thermal energy extracted from the exhaust stream into the coolant water was calculated using the following equation:

$$Q_{water} = \dot{m}_{water} c_{p,water} (T_{waterout} - T_{waterin}) \tag{4.20}$$

The specific heat capacity of water ($c_{p,water}$) is based on the average temperature of the coolant water.

The exhaust heat exchanger heat transfer coefficient ($\bar{h}_{ex}$) was determined using the temperature difference between the bulk exhaust gas temperature (T_{bulk}) and the hot side surface temperature of the TEGs (T_{TEGhot}), as per the studies conducted by Zukauskas and Ulinskas (1985) and Kays and London (1954).

$$\eta_{fin} \bar{h}_{ex} = \frac{Q_{water}/A_{ex}}{T_{bulk} - T_{TEG,hot}} \tag{4.21}$$

where

η_{fin} is the fin efficiency [%]

A_{ex} is the exhaust heat exchanger heat transfer area [m^2]

4.4.3 Mass Flow Rate

The mass flows throughout the experimental facility are categorized into:

- Combustion chamber mass flow ($\dot{m}_{chamber}$)
- Exhaust mass flow ($\dot{m}_{exhaust}$)
- Exfiltration mass flow ($\dot{m}_{exfiltration}$)
- Dilution air mass flow ($\dot{m}_{dilution}$)
- Chimney mass flow ($\dot{m}_{chimney}$)

4.4.3.1 Combustion Chamber

The combustion chamber ($\dot{m}_{chamber}$) was calculated using the combustion chamber mass and energy balance adapted from Section 4.4.1.1.

The combustion analysis focus on using the respective exhaust-to-fuel ratio to calculate the exhaust flow rate ($\dot{m}_{chamber}$). Obtaining the exhaust mass flow rate begins with calculating the gas constant of the natural gas based on the chemical composition found in Table 4.6.

$$R_{NG} = R_u \sum_{i=1}^{N} \frac{f_i}{M_i} \tag{4.22}$$

where

f_i is the mass fraction of the chemical compounds

M_i is the molecular mass of the chemical compounds

R_u is the universal gas constant [8.314462 kJ/kmolK]

Once the gas constant was estimated, the natural gas mass flow rate was calculated based on the ideal gas law involving the natural gas volumetric flow rate, gas constant, and absolute pressure and temperature.

$$\dot{m}_{NG} = \frac{P_{NG}\dot{V}_{NG}}{R_{NG}T_{NG}} \tag{4.23}$$

where

P_{NG} is the absolute pressure of the natural gas [kPa]

$\dot{V}_{NG}$ is the volumetric flow rate of natural gas [m^3/s]

R_{NG} is the gas constant of natural gas [kJ/kgK]

T_{NG} is the absolute temperature of the natural gas [K]

The exhaust mass flow rate through the combustion chamber ($\dot{m}_{chamber}$) was then calculated by multiplying the natural gas mass flow rate ($\dot{m}_{NG}$) and the exhaust-to-fuel ratio.

$$\dot{m}_{chamber} = EF \times \dot{m}_{NG} \tag{4.24}$$

4.4.3.2 Exhaust

In the presence of the TEG POWER system, the exhaust mass flow through the exhaust outlet ($\dot{m}_{exhaust}$) was calculated via an energy balance of the heat transfer between the exhaust gases and the coolant flowing through the TEG POWER system. This technique is called the waste energy balance approach adapted from Section

4.4.2.

$$\dot{m}_{exhaust} = \frac{Q_{water}}{h_{ex,inlet} - h_{ex,outlet}} \tag{4.25}$$

where

$h_{ex,inlet}$ is the enthalpy of the appliance exhaust gases [kJ/kg]

$h_{ex,outlet}$ is the enthalpy of the exhaust gases exiting TEG POWER [kJ/kg]

The enthalpies were calculated using the composition of the exhaust gases and the arithmetic average of the inlet ($T_{ex,inlet}$) and outlet ($T_{ex,outlet}$) temperatures of the exhaust gases.

In the absence of the TEG POWER system, the exhaust mass flow was calculated by subtracting an estimated exfiltration mass flow ($\dot{m}_{exfiltration}$) from the combustion chamber mass flow ($\dot{m}_{chamber}$). This is referred to as the adjusted combustion chamber energy balance.

$$\dot{m}_{exhaust} = \dot{m}_{chamber} - \dot{m}_{exfiltration} \tag{4.26}$$

The calculated and estimated exfiltration mass flow will be described next.

4.4.3.3 Exfiltration

The exfiltration mass flow ($\dot{m}_{exfiltration}$) is an alternate path for the exhaust gases to escape from the appliance to the surrounding, primarily through the appliance door. It was quantified by comparing the exhaust mass flow calculated via the combustion chamber analysis and the waste energy balance techniques. The combustion mass and energy balance provide a method of measuring the exhaust flow generated by the combustion process, which is a combination of the exhaust gases exfiltrating from the appliance and the exhaust gases traveling up the chimney. The waste energy balance provides a method of measuring the exhaust traveling up the chimney, solely. Therefore the exfiltration mass flow can be calculated by subtracting the exhaust mass flows, as follows.

$$\dot{m}_{exfiltration} = \dot{m}_{chamber} - \dot{m}_{exhaust} \tag{4.27}$$

In the event that the TEG POWER system is not present to measure the exhaust mass flow ($\dot{m}_{exhaust}$), as in Section 4.3.1, the estimated exfiltration mass flow was calculated as a function of the pressure at the exhaust outlet of the appliance (P_{ex}). The empirical relationship of the calculated exfiltration and the measured draft pressure ($P_{HX,inlet}$) during the experiments outlined in Section 4.3.2 were best described by an exponential function of the form:

$$\dot{m}_{exfiltration} = \alpha e^{\beta(P_{ex})} \tag{4.28}$$

where the values α and β will be investigated and presented in Chapter 5.

4.4.3.4 Dilution and Chimney

The dilution mass flow ($\dot{m}_{dilution}$) and the chimney mass flow ($\dot{m}_{chimney}$) were calculated via the draft hood mass and energy balance based on Section 4.4.1.2.

The dilution air mass flow can be calculated by multiplying the dilution air-to-exhaust ratio by the exhaust mass flow.

$$\dot{m}_{dilution} = DAE \times \dot{m}_{exhaust} \tag{4.29}$$

and the chimney mass flow ($\dot{m}_{chimney}$) is calculated similarly.

$$\dot{m}_{chimney} = CE \times \dot{m}_{exhaust} \tag{4.30}$$

4.4.4 Fluid Flow Parameters

The fluid flow parameters consist of the loss coefficients (K) associated with the exhaust components, namely the appliance, the TEG POWER device, and the exhaust damper valve.

The primary pressure drop along the exhaust ventilation path through the appliance is estimated to begin downstream of the cooking chamber, after the exfiltration of exhaust gases, as the geometry of the ventilation path becomes constrictive and forms sharp turns; which eventually transform into the rectangular outlet exhaust duct. The loss coefficient associated with the appliance was estimated via a rearrangement of the mechanical energy balance across the device using the exhaust mass flow ($\dot{m}_{exhaust}$). The pressure differential is measured as the draft pressure exiting the appliance and thus requires the subtraction of pressure loss effects that are not inclusive to the appliance ventilation flow path. The effective loss coefficient for the appliance is presented below in Equation 4.31a.

$$K_{oven} = \frac{\left[\Delta P_{ex} + (\rho_{out} - \rho_{oven})g\Delta h - (1 + K_{oven,inlet})\right]\dfrac{\dot{m}^2_{chamber}}{2\rho_{out}A^2_{oven,inlet}}}{\dfrac{2\rho_{oven}A^2_{oven}}{\dot{m}_{exhaust}}} - (1 - \sigma + K_{oven,outlet})\frac{\rho_{oven}}{\rho_{oven,outlet}} \quad (4.31a)$$

where

ρ_{out} is the inlet combustion air density [kg/m^3]

ρ_{oven} is the exhaust density in the oven [kg/m^3]

$\rho_{oven,outlet}$ is the exhaust density at the oven outlet [kg/m^3]

σ is the flow area ratio between the outlet duct and oven ($\mathrm{A_{outlet}/A_{oven}}$)

ΔP_{ex} is the draft pressure at the outlet of the oven [Pa]

$K_{oven,inlet}$ is the oven inlet loss coefficient

$K_{oven,outlet}$ is the oven outlet duct loss coefficient

Δh is the height difference between the measurement point and the air intake [m]

The loss coefficient associated with the hot heat exchanger in the TEG POWER device was estimated via a rearrangement of the momentum and mechanical energy balance across the device. This method provides the ability to isolate the viscous effects caused by the heat exchanger core from the entrance and exit effects and the pressure recovery due to the fluid deceleration during exhaust gas cooling. A more detailed reconstruction of the method can be found in Appendix C. Ultimately, the effective loss coefficient for the hot heat exchanger is presented below.

$$K_{HX} = \left[\frac{2\rho_{inlet}(P_{HX,inlet} - P_{HX,outlet})}{\left(\frac{\dot{m}_{exhaust}}{A_{HX}}\right)^2} - \left(1 + \sigma^2\right)\left(\frac{\rho_{inlet}}{\rho_{outlet}} - 1\right)\right] \frac{\rho_{HX}}{\rho_{inlet}} \tag{4.31b}$$

where

ρ_{inlet} is the exhaust density at the heat exchanger inlet [kg/m^3]

ρ_{outlet} is the exhaust density at the heat exchanger outlet [kg/m^3]

ρ_{HX} is the mean exhaust density within the heat exchanger [kg/m^3]

σ is the area ratio ($\mathrm{A_{HX}/A}$)

A_{HX} is the minimum flow area of the heat exchanger [m^2]

A is the frontal flow area of the inlet or outlet duct [m^2]

$\dot{m}_{exhaust}$ is the exhaust mass flow rate [kg/s]

$P_{HX,inlet}$ is the draft pressure at the inlet of the heat exchanger [Pa]

$P_{HX,outlet}$ is the draft pressure at the outlet of the heat exchanger [Pa]

The loss coefficient of the exhaust throttling valve is calculated using the same method.

$$K_{TH} = \frac{2(P_{draft} - P_{chimney})\rho_{chimney}}{\left(\frac{\dot{m}_{chimney}}{A_{chimney}}\right)^2} \tag{4.31c}$$

where

$\rho_{chimney}$ is the exhaust density at the inlet of the chimney [kg/m^3]

$A_{chimney}$ is the frontal flow area of the chimney [m^2]

$\dot{m}_{chimney}$ is the chimney mass flow rate [kg/s]

P_{draft} is the draft pressure at the inlet of the throttling valve [Pa]

$P_{chimney}$ is the draft pressure at the inlet of the chimney [Pa]

4.5 Uncertainty Analysis

An uncertainty anaylsis of the experimentally measured variables was conducted as per the guidelines of Figliola and Beasley (2010). The uncertainty (δx_i) of any measurement is grouped into two categories: precision (P_i) and bias (B_i) uncertainties. These two uncertainties were combined using the *root-sum-squared (RSS) method* to quantify the total uncertainty surrounding the respective measurement.

$$\delta x_i = \sqrt{P_i^2 + B_i^2} \tag{4.32}$$

The bias uncertainties for flow meters, combustion analyzers, RTDs, secondary thermocouples and pressure transducers were cited from manufacturer data. The coolant water thermocouples and pressure transducer were calculated based on calibration. The precision uncertainties were based on a 95% confidence interval surrounding 60 experimental measurements at a sampling rate of 1 s/sec using the DAQ system. The one-minute collection time proved to sufficiently encapsulate the random fluctuations during steady experimental operating conditions. A summary of the measurement devices and the associated total uncertainties can be found in Table 4.7 and Table 4.8. Further detail in the uncertainty calculations can be found in Appendix A.

The propagation of the uncertainty of the independent variables into the calculated or dependent variables was conducted the Monte Carlo method. The basic approach defines a probability density function ($p(x_i)$) for each independent variables (x_i). The dependent variables (f), a function of the independent variables (x_i), is calculated repeatedly using probable values of the independent variables based on the probability density functions. After numerous iterations, the method will have generated a large enough sample to perform a statistical analysis. The convergence of this numerical technique is achieved when the standard deviation of the calculated variable (f) changes less than 1%.

The advantage of the Monte Carlo method over the traditional uncertainty propagation methods is the ability to identify deviation from the typically assumed normal distribution. This deviation is caused by large uncertainty values in the independent variables and bounded measurement values, which were present in this analysis. Therefore, the average measurement value was represented using the median, rather than the mean, due to the skewness of the distributions. Furthermore, all uncertainties are represented as a 95% confidence interval. Table 4.9 to Table 4.12 summarize the uncertainties of calculated parameters.

It should be noted that a few stated relative uncertainties of key parameters are large, but do not a large impact on the overall analysis. The large relative uncertainties will translate to small absolute uncertainties. This will be discussed in detail within Section 4.6.

Table 4.7: Total uncertainty of measured parameters for the combustion analysis

Measurement	Device	Total Uncertainty	
		Maximum Absolute	Relative
Oven Temperature	Omega E-type Thermocouple	±0.5°C	max (@156°C) = ±0.32% min (@312°C) = ±0.17%
Chimney Temperature	Omega T-type Thermocouple	±0.89°C	max (@48°C) = ±1.10% min (@249°C) = ±0.22%
Natural Gas Volumetric Flow Rate	McMillan 50D-13 Thermal Dispersion Flow Meter	±1.7 L/min	max (@11 L/min) = ±15.4% min (@39.4 L/min) = ±4.32%
Draft Pressure	Fluke 922 Airflow Meter	±1.54 Pa	max (@2 Pa) = ±51.2% min (@56 Pa) = ±2.7%
Atmospheric Pressure	Model 61205 R.M. Young Barometric Pressure Sensor	±0.042 kPa	±0.04%
Wet and Dry Bulb Temperature	Thermometer	±0.5°C	±2.38%
Room Depressurization	Omega PX653-0.1D5V Pressure Transducer	±0.6 Pa	±20.4%
O_2 Concentration	E-Instruments 8500 combustion analyzer	±0.12% vol.	max (@18% vol.) = ±0.67% min (@20.7% vol.) = ±0.54%
CO Concentration		±0.74 ppm	max (@2ppm) = ±35.6% min (@40ppm) = ±4.2%
CO_2 Concentration		±0.3% vol.	max (@0.2% vol.) = ±152.2% min (@1.1% vol.) = ±28.0%
NO Concentration		±0.54 ppm	max (@1ppm) = ±35.6% min (@6ppm) = ±10.9%
NO_2 Concentration		±0.5 ppm	
SO_2 Concentration		±0.5 ppm	
CH_4 Concentration		±0.007% vol.	max (@0.01% vol.) = ±70.8% min (@0.12% vol.) = ±5.2%

Table 4.8: Total uncertainty of measured parameters for the TEG POWER system analysis

Measurement	Device	Total Uncertainty	
		Maximum Absolute	Relative
Water Temperature (Calibrated)	Omega T-type Thermocouple	±0.13°C	max (@15.7°C) = ±0.8% min (@30°C) = ±0.39%
Water Mass Flow Rate	Endress+Hauser Proline Promass 80E Mass Flow Meter	±0.0003 kg/s	±0.48%
Exhaust Temperature	Omega 100ohm Platinum RTDs	±1.9°C	max (@89.7°C) = ±1.19% min (@284.2°C) = ±0.66%

Table 4.9: Uncertainty of mass flow parameters with TEG POWER system

Mass Flow Type		Minimum and Maximum Relative Uncertainty		
		300F	500F	600F
Combustion Chamber	min	±16.3% (0.008kg/s)	±10.7% (0.006kg/s)	±9.2% (0.005kg/s)
	max	±22.6% (0.01kg/s)	±11.6% (0.006kg/s)	±10.3% (0.005kg/s)
Exhaust (Waste Energy)	min	±3.3% (0.001kg/s)	±2.2% (0.0007kg/s)	±1.9% (0.0007kg/s)
	max	±3.7% (0.002kg/s)	±2.6% (0.002kg/s)	±2.5% (0.001kg/s)
Exfiltration	min	±44.7% (0.006kg/s)	±29.8% (0.004kg/s)	±24.7% (0.003kg/s)
	max	±109.7% (0.007kg/s)	±133.1% (0.004kg/s)	±157.5% (0.004kg/s)
Dilution Air	min	±6.1% (0.002kg/s)	±3.8% (0.001kg/s)	±3.5% (0.001kg/s)
	max	±8.0% (0.004kg/s)	±5.0% (0.003kg/s)	±5.0% (0.003kg/s)
Chimney	min	±4.6% (0.003kg/s)	±3.0% (0.002kg/s)	±2.7% (0.002kg/s)
	max	±6.1% (0.005kg/s)	±3.9% (0.003kg/s)	±4.2% (0.004kg/s)

Table 4.10: Uncertainty of mass flow parameters without TEG POWER system

Mass Flow Type		Minimum and Maximum Relative Uncertainty		
		300F	500F	600F
Combustion Chamber	min	±9.4% (0.007kg/s)	±5.2% (0.004kg/s)	±4.4% (0.004kg/s)
	max	±17.4% (0.007kg/s)	±11.5% (0.005kg/s)	±9.3% (0.004kg/s)
Adjusted Combustion Chamber	min	±9.9% (0.007kg/s)	±5.2% (0.004kg/s)	±4.5% (0.004kg/s)
	max	±27.3% (0.002kg/s)	±17.4% (0.005kg/s)	±13.7% (0.004kg/s)
Exfiltration*	min	±12.6% (0.0016kg/s)	±13.0% (0.0015kg/s)	±13.2% (0.0015kg/s)
	max	±39.5% (0.0006kg/s)	±60.2% (0.0002kg/s)	±66.5% (0.0002kg/s)
Dilution Air	min	±14.9% (0.006kg/s)	±8.8% (0.004kg/s)	±7.0% (0.004kg/s)
	max	±29.6% (0.0013kg/s)	±18.4% (0.01kg/s)	±14.2% (0.008kg/s)
Chimney	min	±13.8% (0.012kg/s)	±8.3% (0.008kg/s)	±6.8% (0.007kg/s)
	max	±28.0% (0.012kg/s)	±18.0% (0.0015kg/s)	±13.9% (0.012kg/s)

*Calculated using the exponential relationship between the mean exfiltration mass flow and the draft pressure

Table 4.11: Total uncertainty of heat transfer coefficients

Device	Maximum Relative Uncertainty
Oven	±1%
Heat Exchanger	±3.4%

Table 4.12: Total uncertainty of loss coefficient

Device		Maximum Relative Uncertainty
Oven		±32.0%
Heat Exchanger		±35.6%
Throttling Valve	0%	±400.0%
	50%	±49.7%
	60%	±31.9%
	70%	±23.8%

4.6 Mass Flow Measurement and Exhaust Component Parameters

The mass flows throughout the exhaust system are important in providing accurate data to develop loss coefficients relationships, heat transfer coefficient correlations, and as points of validation - beyond pressure and temperature - for the numerical model. This section will present a comparison to validate the exhaust mass flow measurement methodologies, along with a comparison of the associated pressure loss and heat transfer coefficients against well-established empirical correlations. The combination of these comparisons will provide strong evidence towards the validity of the mass flow measurement techniques and the associated measurement uncertainty. The heat transfer and pressure drop correlations using the calculated mass flows for the oven and throttling valve will also be presented and uncertainties discussed.

4.6.1 Exhaust Mass Flow Comparison

The mass and energy analysis on the combustion chamber and the waste heat recovery device allows the measurement of the exhaust mass flow ($\dot{m}_{exhaust}$) via two different techniques. These techniques are:

- Combustion Energy Balance (Section 4.4.1.1)
- Thermal Energy Extraction or Waste Energy Balance (Section 4.4.2)

To validate the accuracy of the measurement techniques, a comparison was conducted and is presented in Figures 4.7, 4.8, and 4.9. Refer to Section 4.3.2 for description of the test matrix setpoints. The information provided by the comparison will then be extended to the testing without the waste heat recovery system.

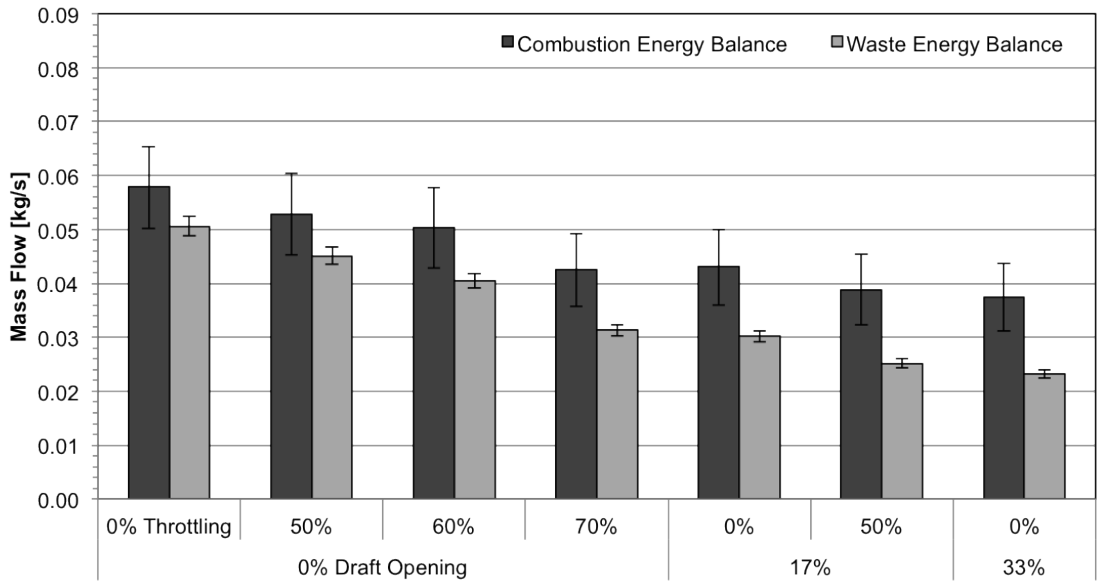

Figure 4.7: Comparison of exhaust mass flow techniques for oven temperature of 300°F with TEG POWER system

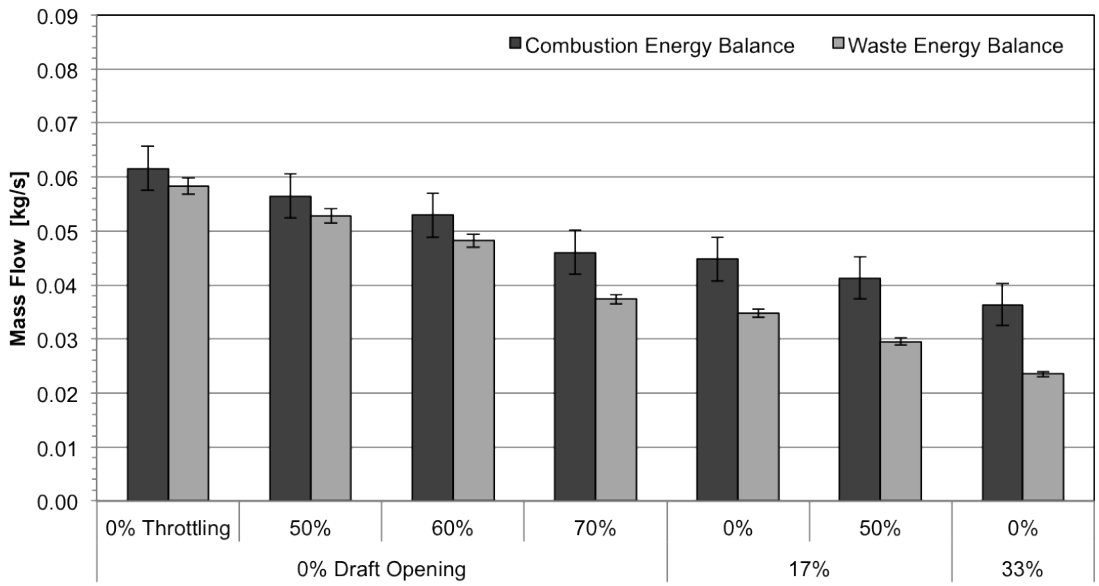

Figure 4.8: Comparison of exhaust mass flow techniques for oven temperature of 500°F with TEG POWER system

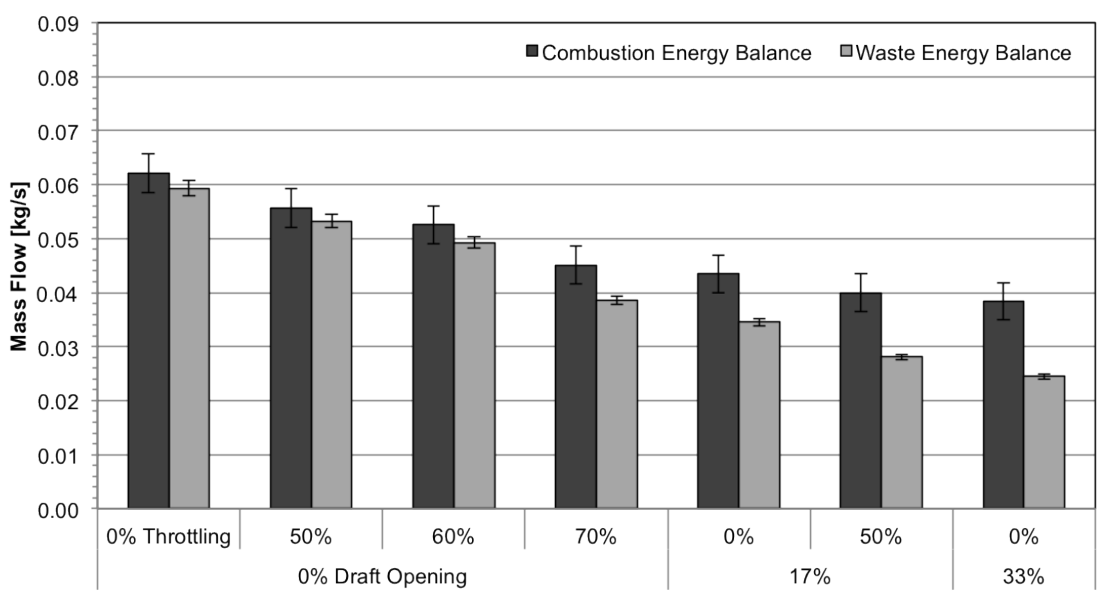

Figure 4.9: Comparison of exhaust mass flow techniques for oven temperature of 600°F with TEG POWER system

The comparison shows that the techniques provide little consensus on the true value of the exhaust flow. The large discrepancies were found to be due to the exfiltration (leakage) from the oven door, which typically occurs during normal operation of the oven. The combustion energy balance provide a method of measuring the exhaust flow generated by the combustion process; which is a combination of the exhaust gases exfiltrating from the oven door and the exhaust gases traveling up the chimney. The waste energy balance provides a method of measuring the exhaust traveling up the chimney, solely. It was hypothesized that the tendency for exfiltration is related to the draft pressure generated within the appliance by the exhaust system or chimney. Meaning that the larger the draft generated by the chimney, indicated by the negative pressure at the exhaust outlet of the oven, the less exhaust that will exfiltrate from the oven door.

In an attempt to validate this hypothesis, all tests were found to show a degree of exfiltration from the oven door through a smoke test. A comparison of the combustion energy and waste energy balance techniques indicate the presence of exfiltration during all tests and agrees with the direct observations of exfiltration via the smoke tests. Without conducting a test that eliminates exfiltration, the accuracy of the hypothesis can be validated by observing a high temperature range test with full chimney draft. As seen in Figure 4.15 and Figure 4.16, the 0% throttling and draft opening case provide a situation with little exfiltration, as per smoke testing, that show a convergence within 10% of the mean value measure by the two techniques.

With the established confidence that the combustion energy and waste energy balance are providing accurate measurements, the exfiltration can be deduced via the difference between the two techniques, as shown in Section 4.4.3.3. Using the draft pressure at the heat exchanger inlet ($P_{HX,inlet}$) and the exfiltration flow, a relationship was identified and presented in Figure 4.10.

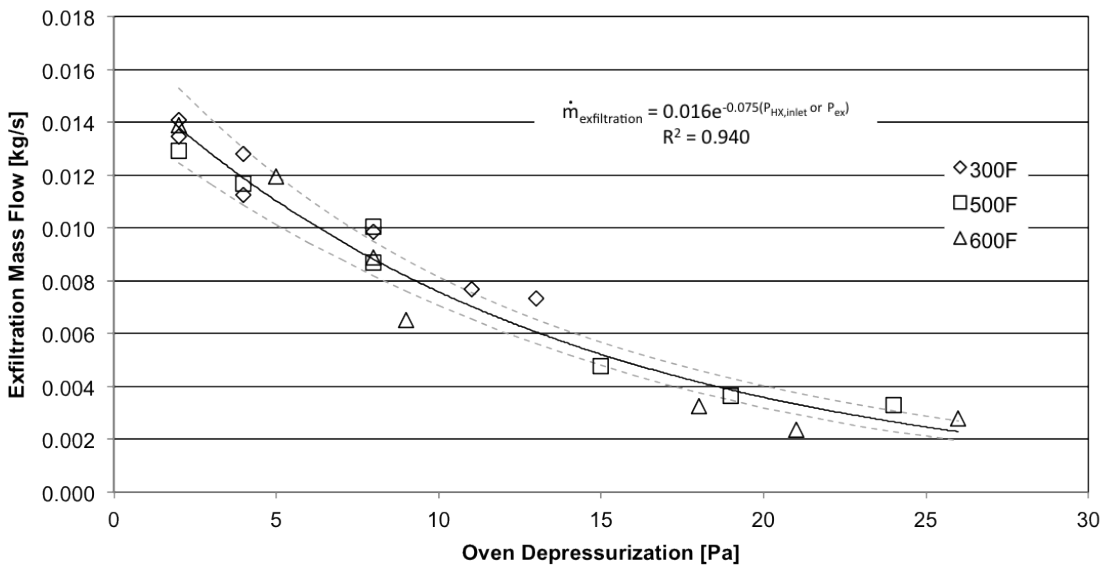

Figure 4.10: Relationship between the draft condition or oven depressurization and the mean exfiltration mass flow from the oven (with 95% CI uncertainty boundaries)

An exponential relationship was fitted between the exfiltration mass flow and the draft pressure. The trend indicated that has the oven becomes more depressurized, due to the draft generated by the chimney, the exfiltration mass flow can be seen to approach zero asymptotically. Alternatively as the oven becomes less depressurized, the exfiltration mass flow increases as the drive for the exhaust gases to enter the chimney diminishes and the path of least resistance becomes the oven door. Essentially, the path through the oven door can be thought of as a short secondary chimney competing with the primary exhaust system. Therefore, the tendency for exfiltration is amplified as the appliance becomes less depressurized, which is observed as the chimney draft is reduced via draft control devices, waste heat recovery device, or a reduction in the oven setpoint temperature.

As seen in Table 4.9, the relative uncertainty of the individual exfiltration values can be large. This is due to the values of exfiltration mass flow and the relatively large uncertainty in the mass flow values calculated via the combustion energy balance and waste energy balance. This is further pronounced when the exfiltration is small, as in the 0% throttling and draft opening tests at 600°F. Using the median values of the calculated exfiltration rates, the uncertainty of the oven draft pressure relationship was found to be lower. Applying the exfiltration relationship to the experimental facility without the waste heat recovery device, the uncertainty of the low draft pressure conditions contributed to a large uncertainty of these exfiltration rate calculations found in Table 4.10. Though the relative uncertainties are large, the absolute uncertainty of these values is very similar to the absolute uncertainty of the exhaust mass flow measurements.

Based on this analysis, the exhaust mass flow traveling up the chimney can be predicted using the combustion energy balance technique in conjunction with the exfiltration relationship, as presented in Equation 4.26 within Section 4.4.3.2. This technique will be used to measure the mass flows in the absence of the waste energy balance technique. Figure 4.11, 4.12, and 4.13 extends the analysis to the operation without a waste heat recovery device and illustrate the exhaust mass flow ($\dot{m}_{exhaust}$) as predicted by the combustion energy balance technique with and without an adjustment from the exfiltration relationship. Refer to Section 4.3.1 for description of the test matrix setpoints.

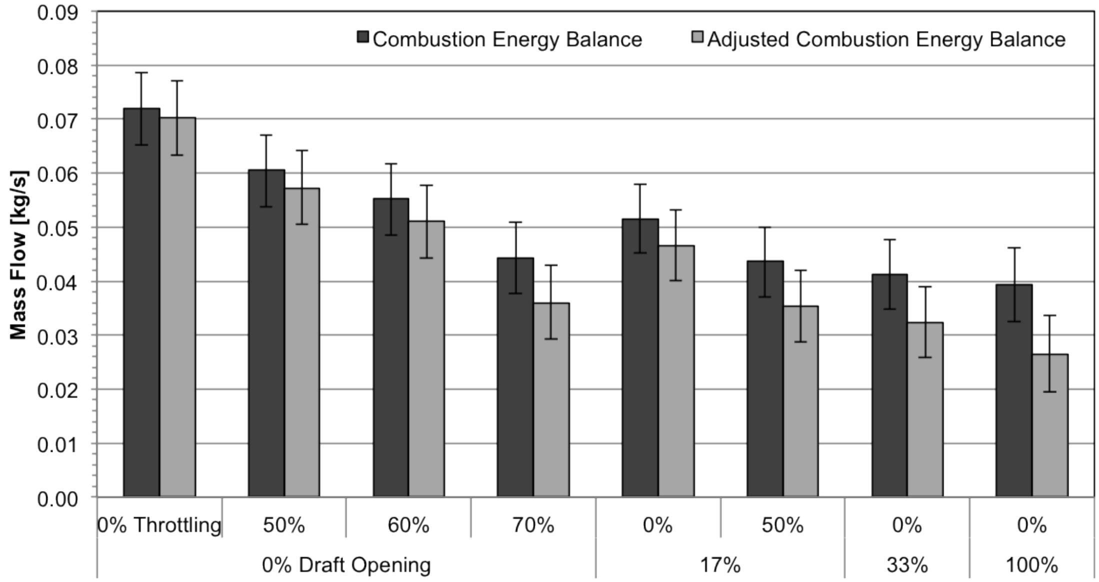

Figure 4.11: Comparison of exhaust mass flow techniques for oven temperature of 300°F without TEG POWER system

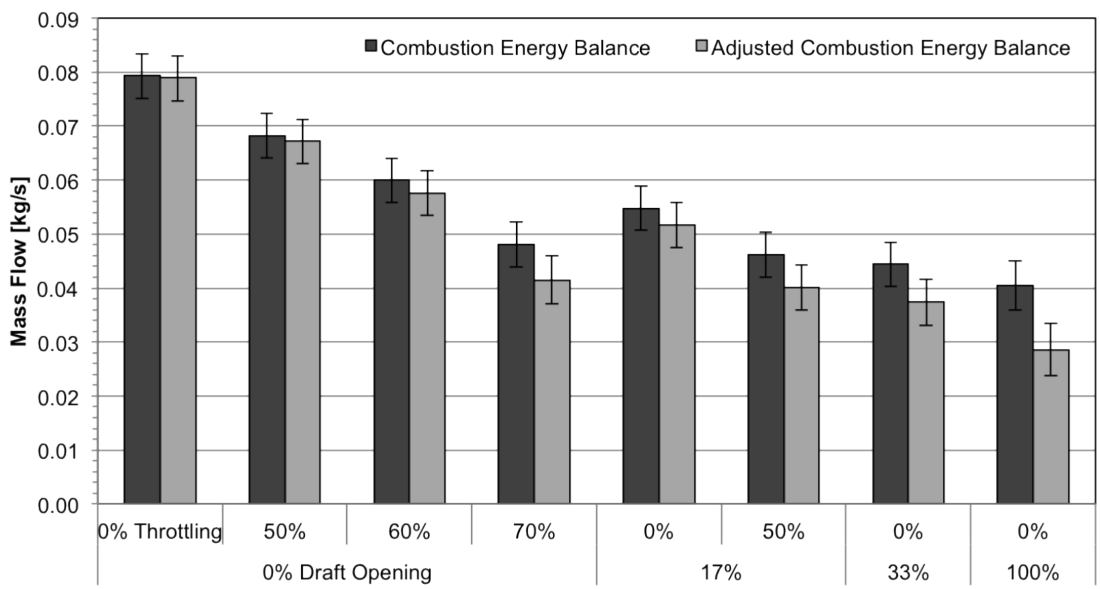

Figure 4.12: Comparison of exhaust mass flow techniques for oven temperature of 500°F without TEG POWER system

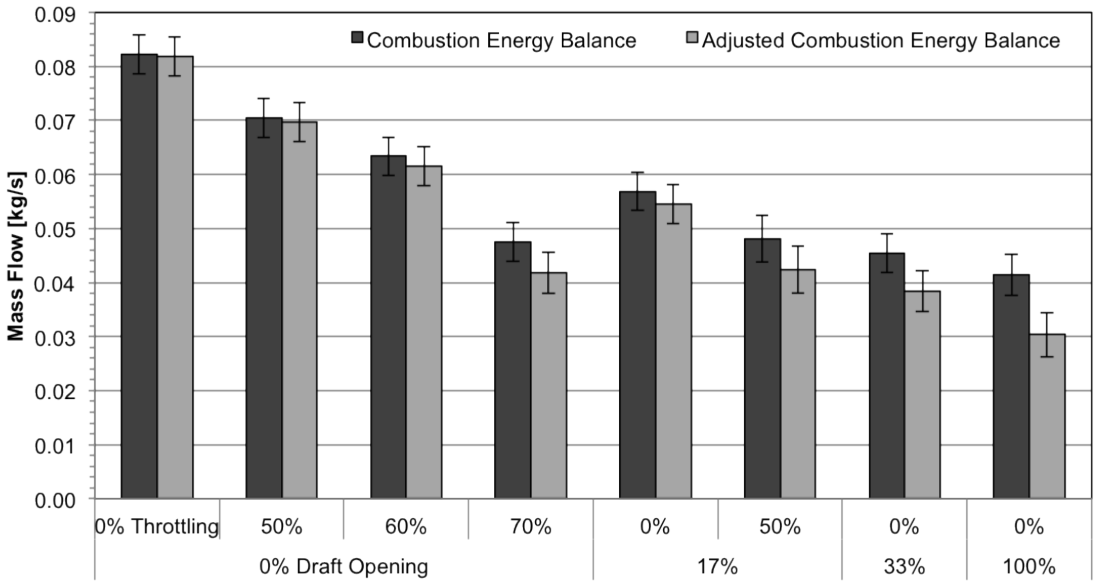

Figure 4.13: Comparison of exhaust mass flow techniques for oven temperature of 600°F without TEG POWER system

In the absence of the waste heat recovery device, the exhaust flows follow a similar trend but with an overall larger mass flow in all cases and a reduced amount of exfiltration. This was expected as the absence of the waste heat recovery device allows a higher draft inside the oven to develop, thus increasing the exhaust mass flow through the chimney and reducing exfiltration. Using these techniques to determine the exhaust mass flow, the flow and heat transfer characteristics of the TEG POWER device and throttling valve can be determined along with validation points of the mass flow output from the model.

4.6.2 Dilution and Chimney Mass Flow Comparison

The draft hood is viewed as a mixing chamber; which is characterized as two streams ($\dot{m}_{exhaust}$ and $\dot{m}_{dilution}$) entering at different temperatures and mixing to form a third stream ($\dot{m}_{chimney}$) with a mixed temperature. The dilution air ($\dot{m}_{dilution}$) and chimney ($\dot{m}_{chimney}$) mass flow are illustrated for all the draft hood scenarios in Figure 4.14, 4.15, and 4.16. Refer to both Section 4.3.1 and 4.3.2 for descriptions of the test matrix setpoints for the draft hood scenarios with and without the waste heat recovery system (TEG POWER).

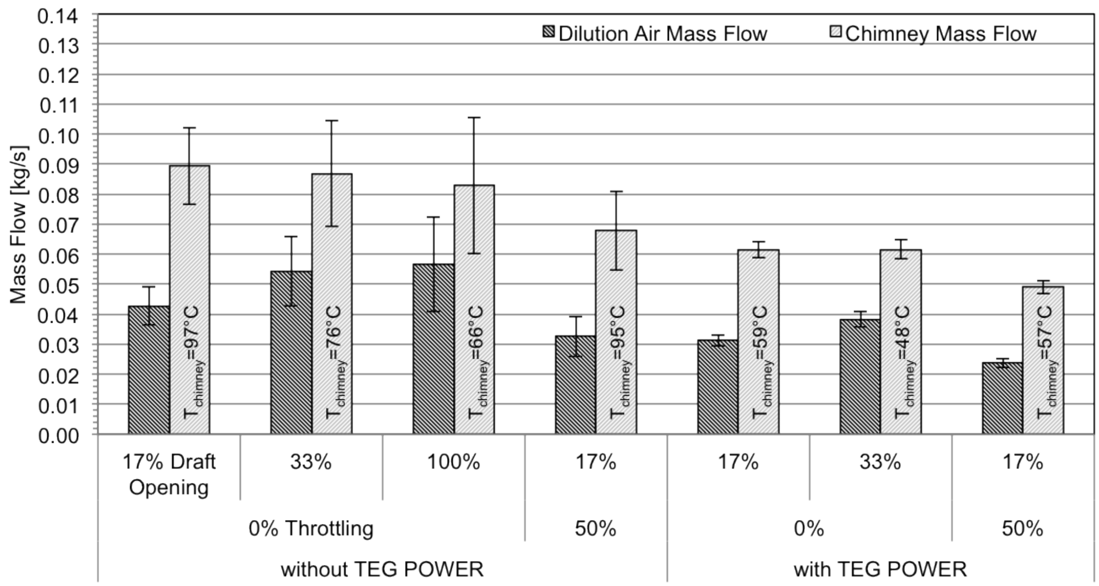

Figure 4.14: Dilution air and chimney mass flow for oven temperature of 300°F

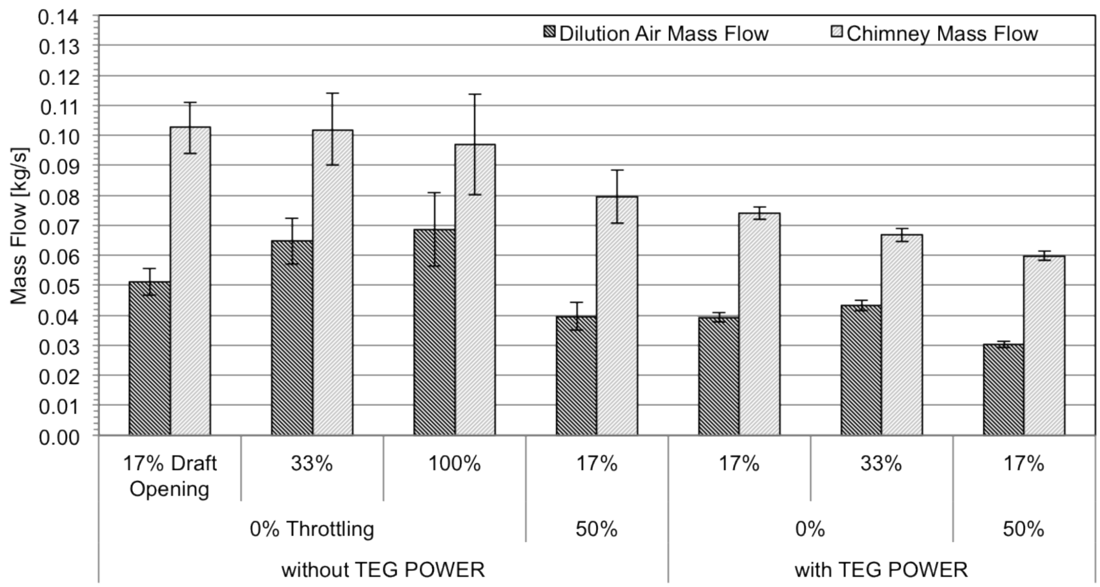

Figure 4.15: Dilution air and chimney mass flow for oven temperature of 500°F

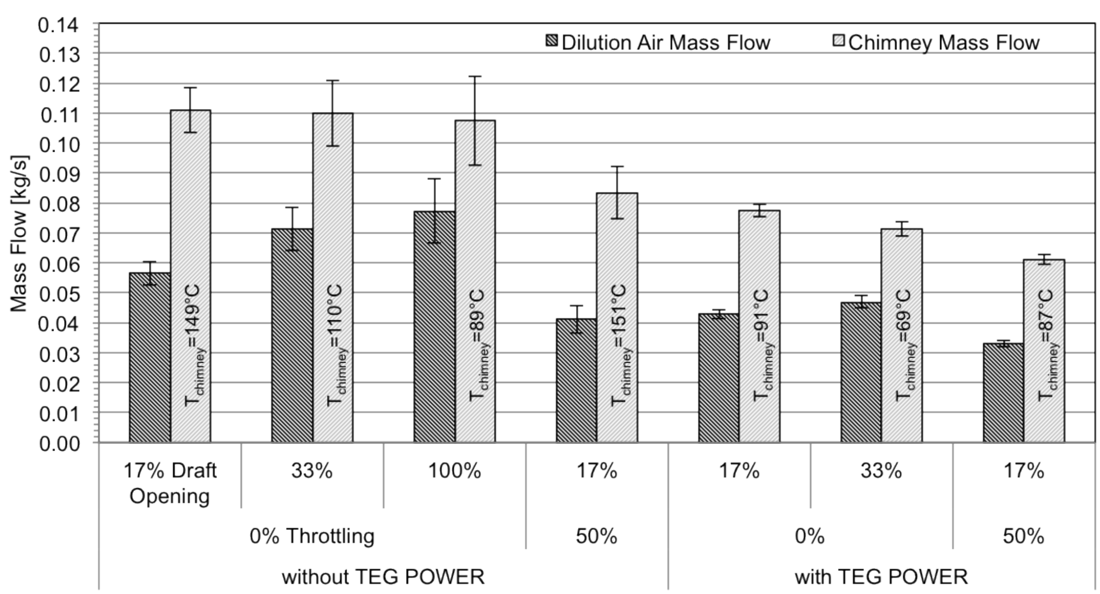

Figure 4.16: Dilution air and chimney mass flow for oven temperature of 600°F

4.6.3 Heat Transfer and Pressure Loss Parameters

To accurately predict the mass flow, temperature, and pressure within the exhaust network, the numerical model required a set of parameters detailing the thermal and flow behaviours of the appliance and the exhaust components. For common components, such as elbows and straight ducts, these parameters are sourced from established relationships found in engineering handbooks, which are presented in Appendix B and C. For more specialized components, such as the appliance or flow control devices, these parameters were established through experimental studies. In addition, the experimental studies of the heat transfer and pressure loss parameters for the waste heat recovery device will be presented against empirical correlations.

4.6.3.1 Heat Transfer

The focus of this section is to present the heat transfer characteristics of the major components dominating the thermal energy transfer within the exhaust network. These components include the oven and the waste heat recovery device.

Oven Starting with oven, the overall heat transfer coefficient (UA_{oven}) was determined through a transient analysis of a set of cool down experiments. With an uncertainty of less than 1%, the overall heat transfer coefficient for the oven (UA_{oven}) was found to be 3.71 W/K, which is outlined in Appendix B.

Waste Heat Recovery Device The exhaust heat transfer coefficient (h_{ex}) of the waste heat recovery device was quantified using Equation 4.21. As the experiments were conducted at various oven temperatures and exhaust mass flow rates, the effects of these variables on the exhaust heat transfer coefficient was captured in the form of a Nusselt versus Reynolds number relationship and presented in Figure 4.17. The Reynolds number is defined specifically for a pin-fin heat exchanger:

$$Re_{HX} = \frac{\rho_{HX} V_{max} D}{\mu_{HX}} \tag{4.33}$$

where

ρ_{HX} is the mean exhaust density within the heat exchanger [kg/m^3]

V_{max} is the maximum velocity through the heat exchanger [m/s]

μ_{HX} is the mean dynamic viscosity of the exhaust gases [kg/ms]

And the accompanying Nusselt number is defined as:

$$Nu_{HX} = \frac{h_{ex} D}{k_{HX}} \tag{4.34}$$

where

D is the pin diameter [m]

k_{HX} is the bulk thermal conductivity of exhaust gases [W/mK]

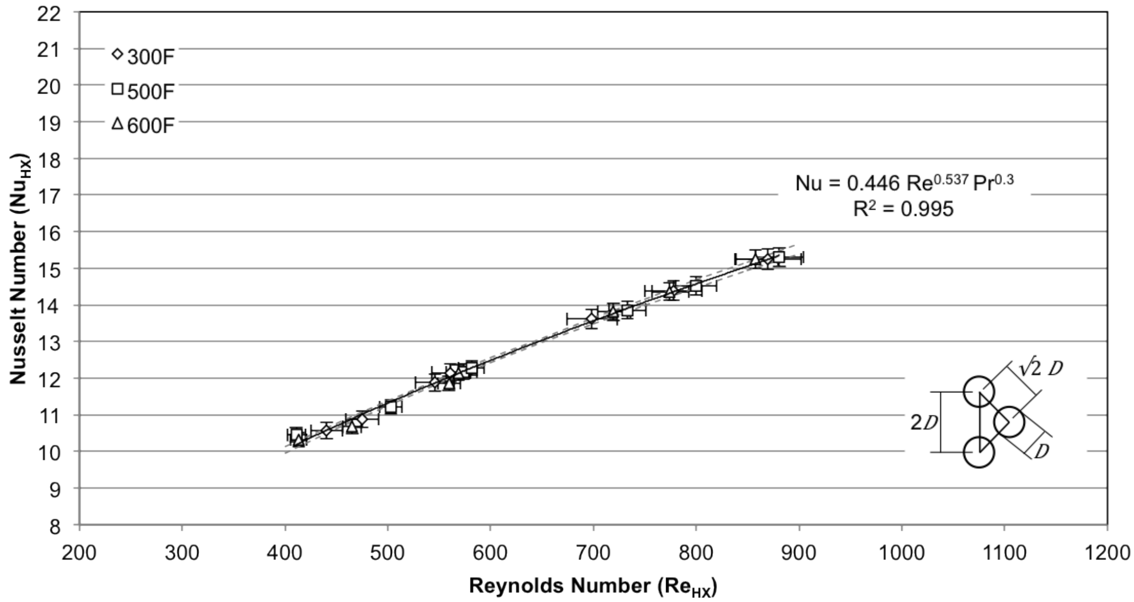

Figure 4.17: Nusselt number of the exhaust heat exchanger (Nu_{HX}) at various Reynolds numbers (Re_{HX})

A positive power relationship between the flow (Reynolds number) and the ability to transfer heat (Nusselt number) was observed with an uncertainty of less than 1%. The additional turbulence and accompanying disturbances in the thermal gradient between the exhaust gases and exhaust heat exchanger lead to higher rates of heat transfer. Beyond this trend, the relationship was validated against a set of experimental correlations developed by Zukauskas and Ulinskas (1985) over a wide range of Reynolds numbers and data sets collected and analyzed by Kays and London (1954).

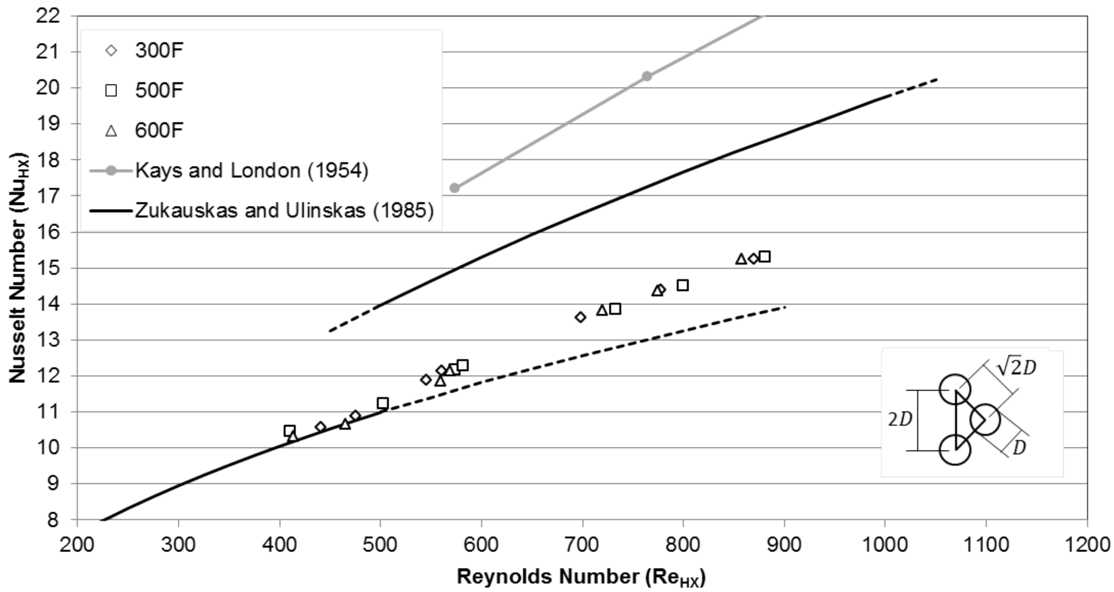

Figure 4.18: Nusselt number comparison using well-established heat transfer relationships for tube banks

It should be noted that the transitional flow regime begins at a Reynolds number of 100 and extends to about 10,000, as per Kakaç *et al.* (1983). Variations between the data sets can be explained by the sensitivity between surface characteristics of the heat exchanger and the transition from laminar to turbulent flow. Encompassing the inherent variability of the transitional flow regime, Figure 4.18 shows poor agreement with the established correlations developed by Zukauskas for Reynolds number of 500 to 1000 and a similar situation is observed with the Kays and London data set. The Zakauskas correlation for Reynolds number between 100 to 500 was extended (represented as a dotted line) to higher Reynolds numbers to show a good agreement with the correlation beyond the applicable range with a trend towards the higher Reynolds number correlation. The agreement between the experimental and empirical correlations further validates the mass flow measurement methodologies.

4.6.3.2 Pressure Loss

The focus of this section is to present the pressure drop characteristics of the major components dominating the mechanical energy conversions within the exhaust network. These components include the oven, heat recovery device, and the throttling valve. The minor components, such as straight duct and elbows, are sourced from engineering handbooks and presented in Appendix C.

Oven The sharp turns and constrictions of the exhaust ventilation path through the appliance presents a major flow restriction to the exhaust network. To simplify the analysis, Equation 4.31a found in Section 4.4.4 aggregates the turns and constrictions into a single oven loss coefficient (K_{oven}). The exhasut flow through the oven is represented as a Reynolds number (R_{oven}), which is calculated by:

$$Re_{oven} = \frac{\rho_{oven} V_{oven} D_h}{\mu_{oven}} \tag{4.35}$$

where

V_{oven} is the oven outlet exhaust velocity [m/s]

D_h is the hydraulic diameter of the oven exhaust outlet [m]

μ_{oven} is the mean dynamic viscosity of the oven exhaust gases [kg/ms]

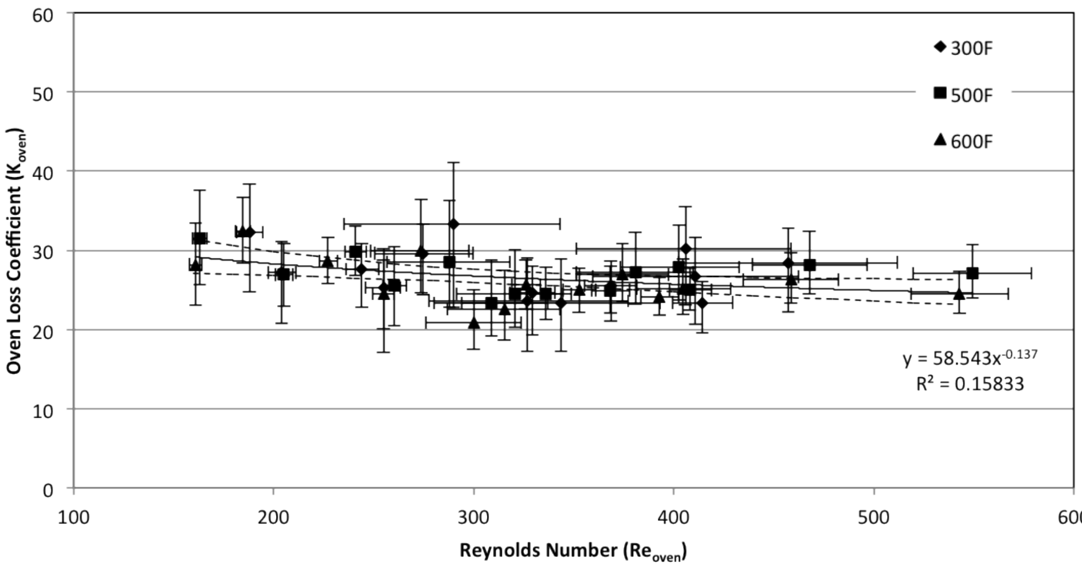

Figure 4.19: Loss coefficient for the oven (K_{oven}) at various Reynolds numbers (Re_{oven})

As observed in Figure 4.19, the loss coefficient is nearly independent of Reynolds number over the range. The uncertainty of the measurements of the Reynolds number is due to the uncertainty in the exhaust mass flow measurement, which is expected. The uncertainty in the loss coefficient is a combination of the uncertainty in the exhaust mass flow and the outlet draft pressure measurement. It should be noted that the oven loss coefficient correlation using the median values was found to have a maximum uncertainty of 7.7%.

Waste Heat Recovery Device The waste heat recovery device is a variable source of pressure drop within the exhaust network due to the unique ability to decelerate the exhaust flow during the cooling process. To adequately characterize the pressure drop variability, the total pressure drop was divided into four parts as described in Section 4.4.4 and Appendix C. The factor influencing the variability caused by the flow deceleration is the rate of heat transfer, which can fluctuate substantially due to a number of factors including the temperature of the coolant used to transport the heat from the exhaust gases to a thermal storage tank. To isolate the effects of fluid deceleration from the viscous losses (K_{HX}), an experiment was conducted to remove the cooling component of the heat exchanger and solely investigate the viscous effects contributing the pressure drop. Using Equation 4.31b, the experiments with and without cooling at 300°F, 500°F and 600°F were compared and presented in Figure 4.20.

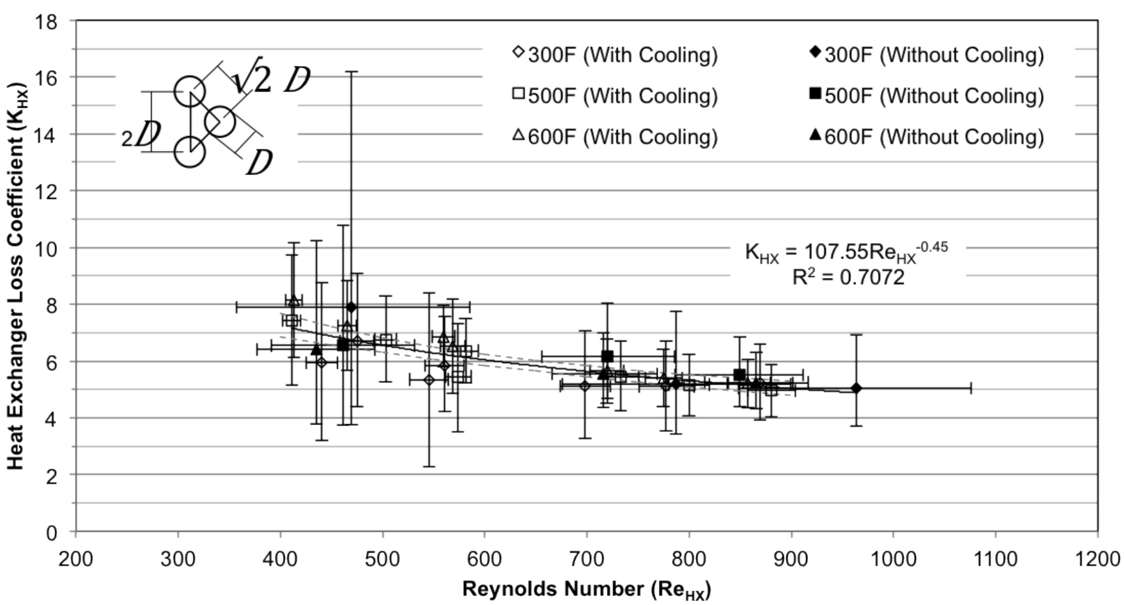

Figure 4.20: Loss coefficient for the exhaust heat exchanger (K_{HX}) at various Reynolds numbers (Re_{HX})

As shown, the loss coefficient (K_{HX}) forms a negative power relationship with Reynolds number with an uncertainty of 5%. This relationship is most likely due to the increased angle of separation of the fluid around the circumference of the tubes causing less form drag on the acting tube and wake effects on the subsequent tubes.

Beyond the trend the two experiments have collapsed on to each other, thus showing that the calculated loss coefficient (K_{HX}) has been isolated from the deceleration effects occurring when heat is transferred from the exhaust gases. The uncertainty of the individual loss coefficient measurements are linked to the uncertainty of the pressure differential measurement. To verify the calculated values, the loss coefficient was compared to the well-documented pressure loss correlations by Zukauskas and Ulinskas (1985) and Kays and London (1954).

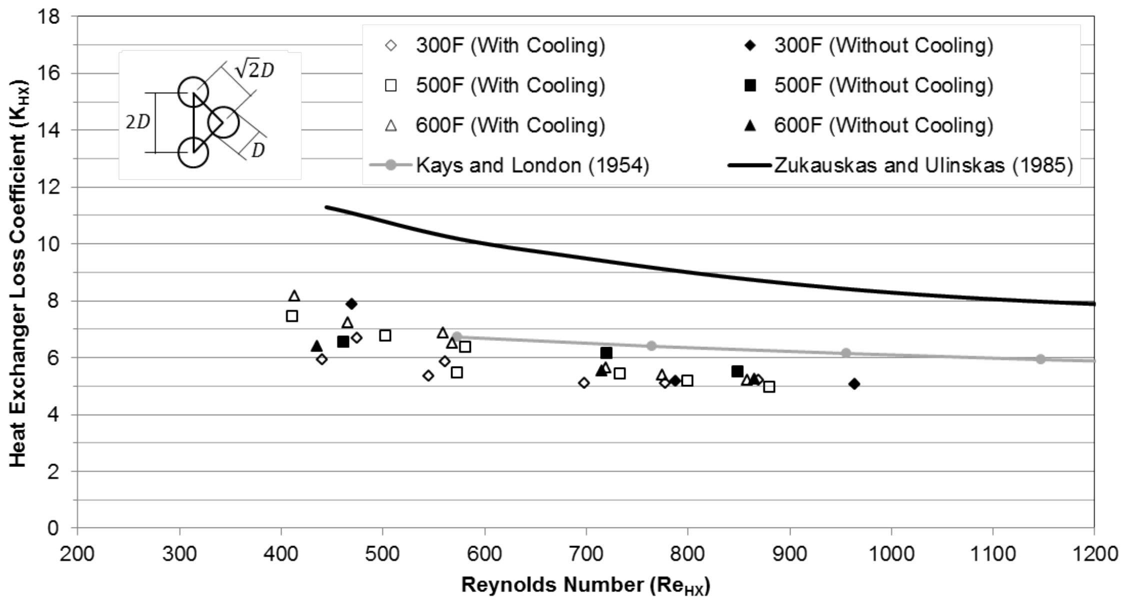

Figure 4.21: Loss coefficient comparison using well-established pressure loss relationships for tube banks

The calculated loss coefficient shows good agreement with Kay and London, but a 20% difference exists with the data presented by Zukauskas and Ulinskas. An analysis conducted by Beale (1993) has shown discrepancies of over-prediction in the Zukauskas loss coefficient curves, particularly in the interested Reynolds number range. This agreement further validates the mass flow measurement methodologies.

Throttling Valve The throttling valve is used to control the exhaust flow rate by applying a sudden pressure drop. By measuring the exhaust flow rate and the pressure drop across the valve, a loss coefficient (K_{TH}) can be calculated for tested valve positions. The loss coefficient is calculated using Equation 4.31c in Section 4.4.4. The exhaust flow is also represented as a Reynolds number (R_{TH}), which is calculated by:

$$Re_{HX} = \frac{\rho_{chimney} V_{chimney} D}{\mu_{chimney}} \tag{4.36}$$

where

$V_{chimney}$ is the exhaust velocity within the chimney [m/s]

D is the inner diameter of the chimney [m]

$\mu_{chimney}$ is the mean dynamic viscosity of the chimney exhaust gases [kg/ms]

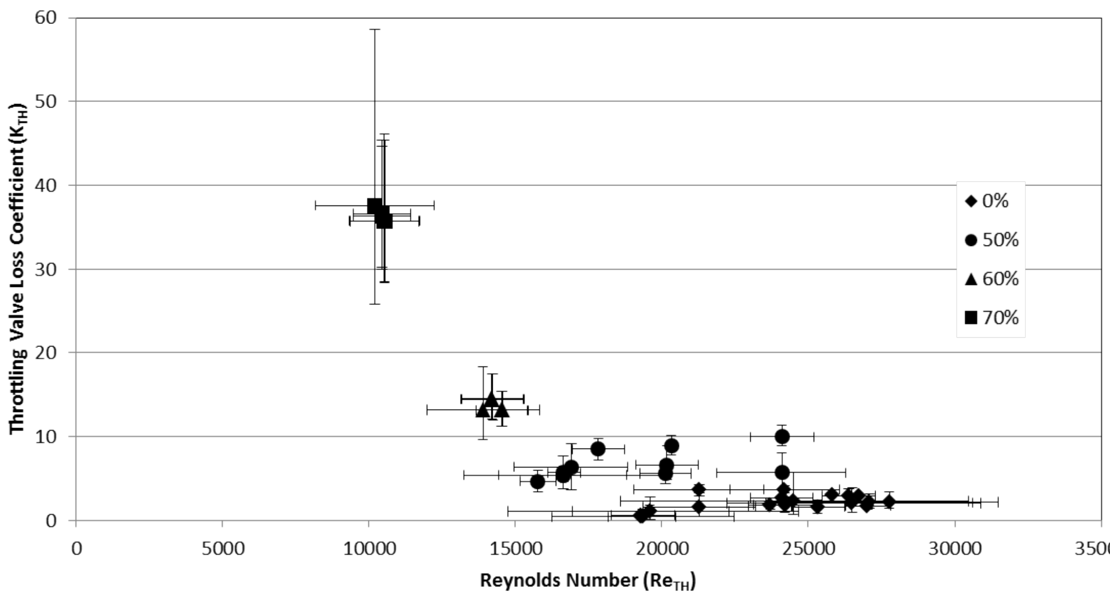

Figure 4.22: Loss coefficient for the throttling valve (K_{TH}) at various Reynolds numbers (Re_{TH})

As observed in Figure 4.22, the loss coefficients for the lower valve positions were found to be nearly independent of Reynolds number. Unfortunately, the experimental facility limited the investigation of a similar relationship with higher valve positions. Within the range of interest, it is expected that the higher valve positions will possess a similar relationship of Reynolds number independence and that for the purposes of this investigation the loss coefficients are independent of Reynolds number. It was also noticed that the sensitivity of the throttling valve is focused in the higher valve positions; which is typical of shutoff type valves. In terms of valve selection, better exhaust control valves should be considered. The relative uncertainty of the loss coefficients, particularly the 0% closed position, is primarily due to the uncertainties of the pressure differential measurements relative to the near zero pressure differential. Table 4.13 summarizes the average loss coefficient for each respective valve position.

Table 4.13: Average loss coefficient at specified throttling valve position

Valve Position	**Loss Coefficient (K_{TH})**
0%	0.7
50%	5.4
60%	13.7
70%	36.4

Chapter 5

Results and Discussion

This chapter will outline the validation and functionality of a naturally ventilated exhaust model using the flow, temperature, and pressure measurements discussed previously. For model validation, the experimental results were used to investigate the presence of a waste heat recovery device and draft control devices, along with an operational baseline to access the effectiveness (i.e natural gas conservation) of the devices. This entailed the investigation of scenarios with and without a waste heat recovery device, and various degrees of dilution air and flow restrictions. The model validity will be presented with a comparison to the experimental results. Lastly, a design application of the model will be outlined and discussed.

5.1 Model Validation

The numerical model was developed to predict the mass flows and temperature and pressure profiles throughout the various components of an exhaust system. To model the exhaust system accurately, the heat transfer and pressure loss aspects of various components, including the waste heat recovery device, were characterized. Using these experimentally determined heat transfer and pressure loss coefficients, the model was compared to experimental mass flow, temperature, and pressure results over the wide array of situations outlined above. The comparison provided a validation of the numerical model and builds confidence in the utility as a design tool.

5.1.1 Mass Flow Comparison

This section will compare experimental and computational flue gas mass flow results, along with a discussion of any discrepancies. As highlighted in Section 4.4.3, the flow through the exhaust network is a combination of three mass flows:

- Exhaust mass flow ($\dot{m}_{exhaust}$)
- Dilution air mass flow ($\dot{m}_{dilution}$)
- Chimney mass flow ($\dot{m}_{chimney}$)

The current approach is to use Equation 4.26 and4.28 to determine the exfiltration mass flow ($\dot{m}_{exfiltration}$) and combustion chamber mass flow ($\dot{m}_{chamber}$), respectively.

The exhaust mass flow comparison with the waste heat recovery device are presented in Figure 5.1, 5.2, 5.3 and without the waste heat recovery device are presented in Figure 5.4, 5.5, and 5.6.

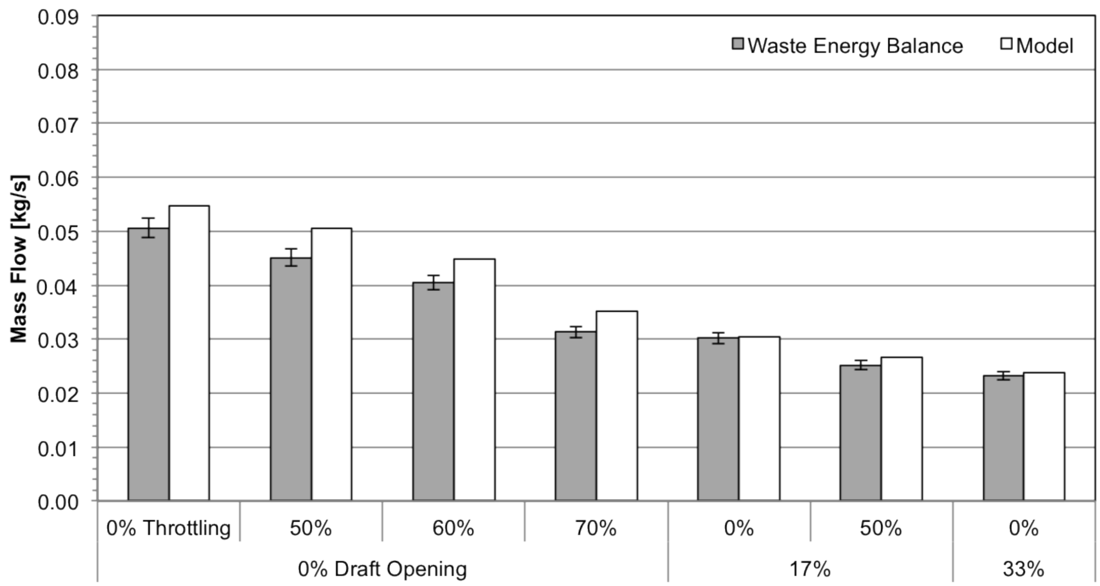

Figure 5.1: Experimental and computational exhaust mass flow comparison for oven temperature of 300°F with TEG POWER system

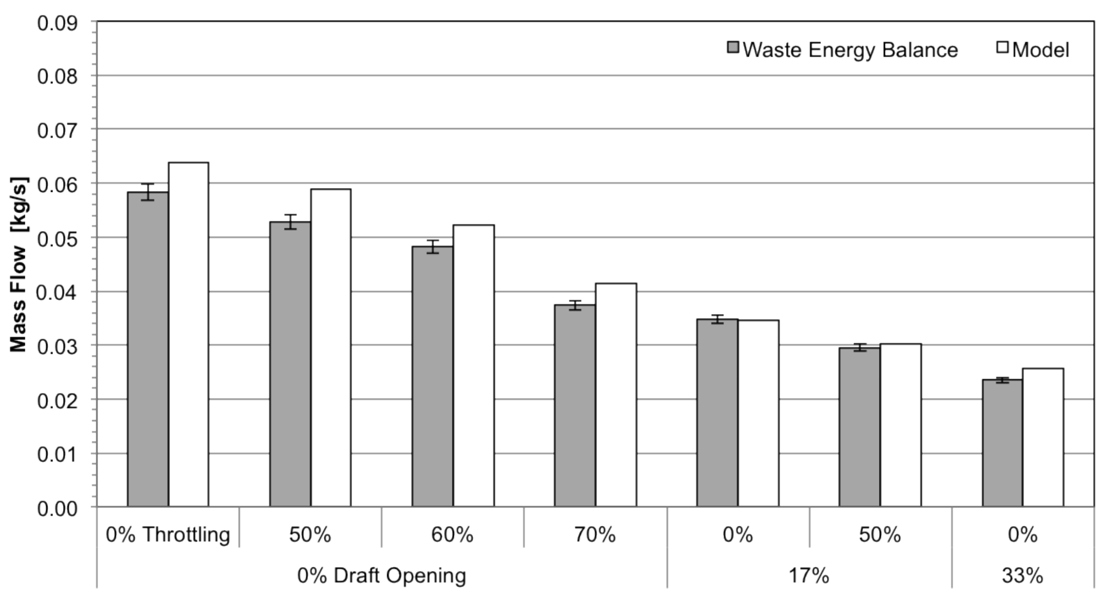

Figure 5.2: Experimental and computational exhaust mass flow comparison for oven temperature of 500°F with TEG POWER system

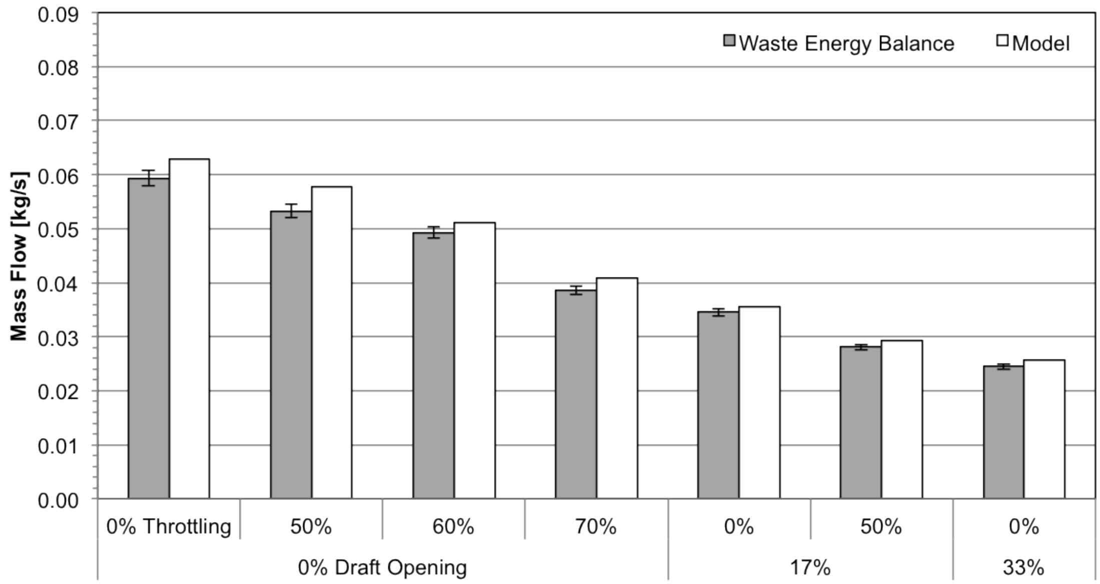

Figure 5.3: Experimental and computational exhaust mass flow comparison for oven temperature of 600°F with TEG POWER system

The comparison shows good agreement between the experimental and computational exhaust mass flow results. The maximum measured relative error was found to over-estimate the measured exhaust mass flow by 12.3% without the application of dilution air and 9.4% with the application of dilution air. On average, the prediction with the application of dilution air over-predicted within 4%, which lies within the uncertainty of the experimental measurements. The prediction without the application of dilution air was found to over-predict by 9% on average, which does not lie within the measurement uncertainty. In the case of no dilution air, the over-prediction is linked to the infiltration of air into the chimney as discussed; which was not applied to the computational model due to minimal information on the exact entry point(s) into the chimney. The effects of infiltration is also seen in the chimney temperature comparison and will be discussed further in Section 5.1.2.

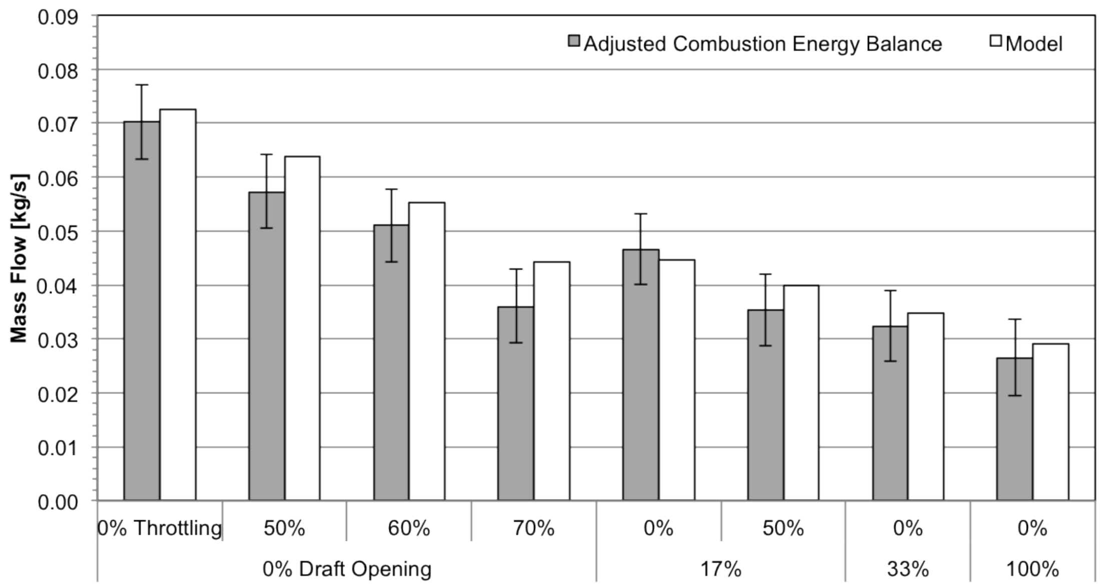

Figure 5.4: Experimental and computational exhaust mass flow comparison for oven temperature of 300°F without TEG POWER system

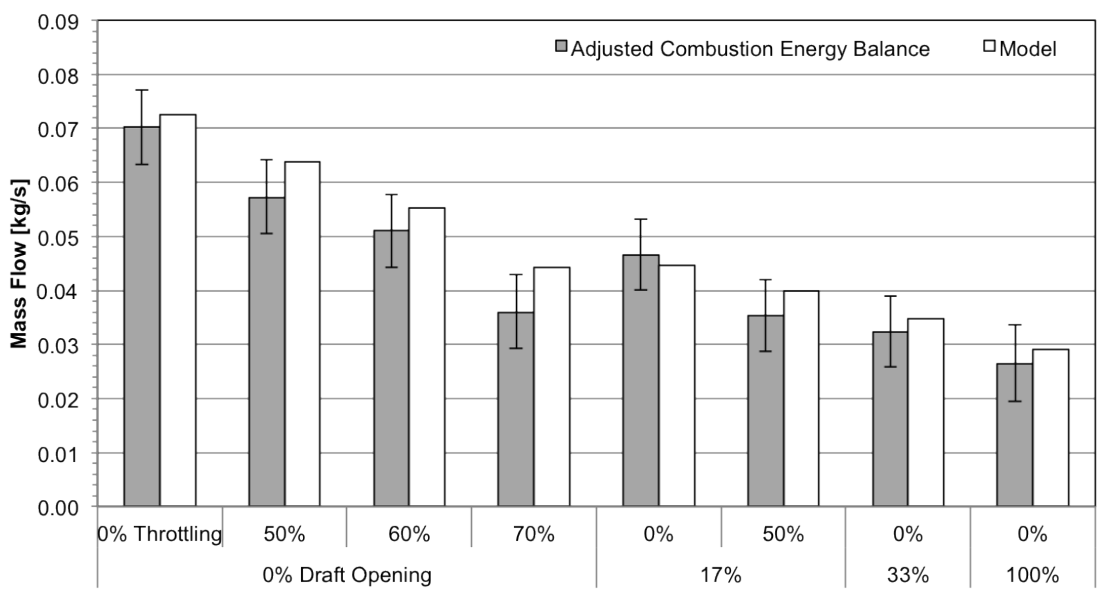

Figure 5.5: Experimental and computational exhaust mass flow comparison for oven temperature of 500°F without TEG POWER system

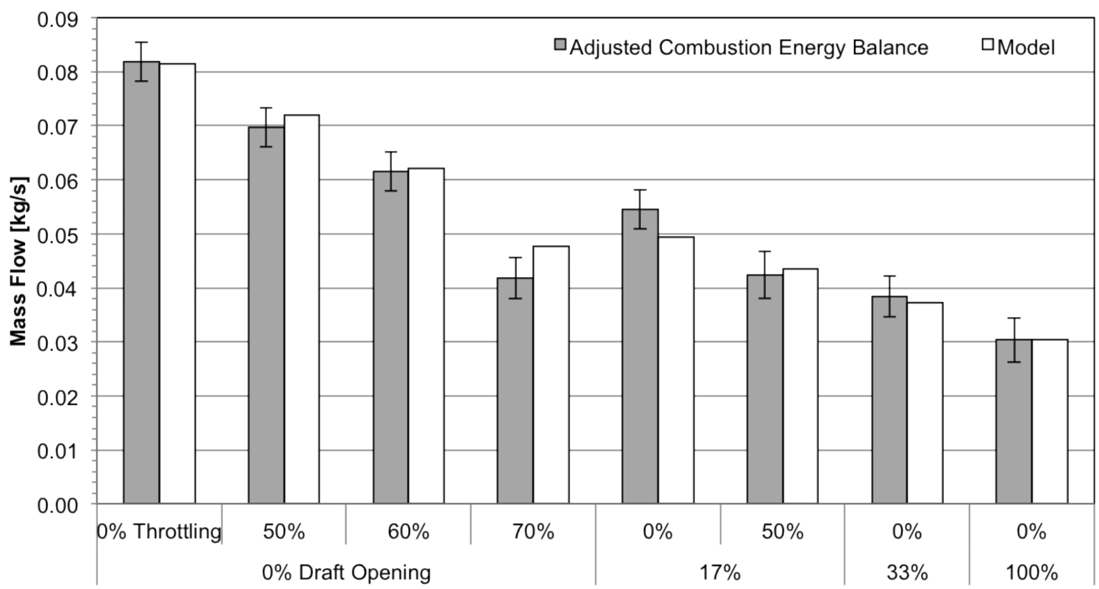

Figure 5.6: Experimental and computational exhaust mass flow comparison for oven temperature of 600°F without TEG POWER system

The comparison shows good agreement between experimental and computational exhaust mass flow results. The maximum relative error was found to over-estimate the measured exhaust mass flow by 22.7% without the application of dilution air and 13.9% with the application of dilution air. On average, the relative errors are 7% and 6%, respectively, and are within the uncertainty of the experimental measurements. The effects of infiltration into the chimney is lost in the uncertainty of experimental measurements, but are present in the chimney temperature comparison in Section 5.1.2.

The dilution and chimney mass flow comparison are presented in Figure 5.7, 5.8, and 5.9.

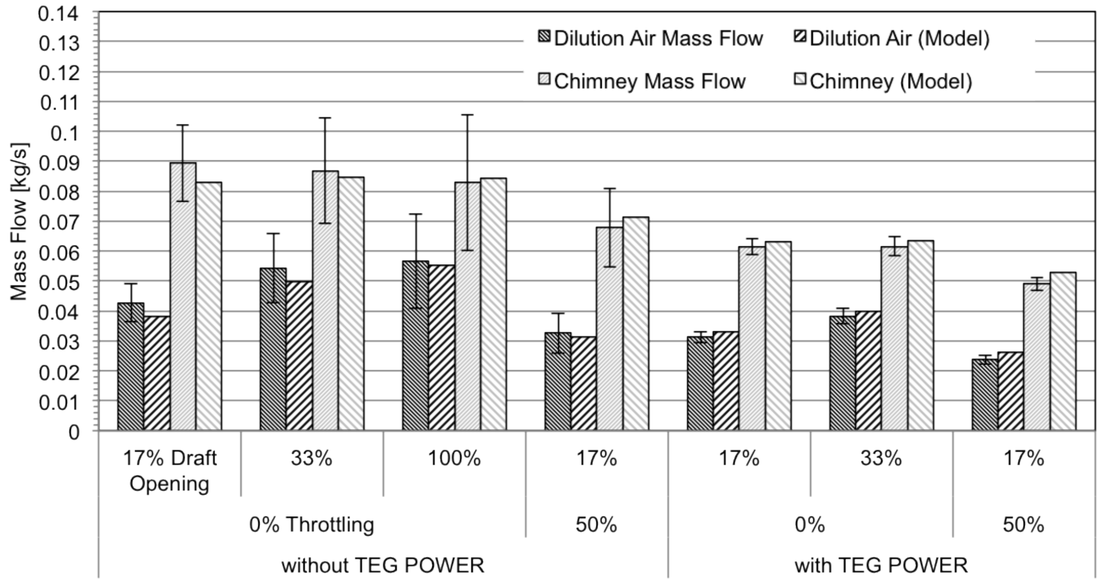

Figure 5.7: Experimental and computational dilution air and chimney mass flow comparison for oven temperature of 300°F

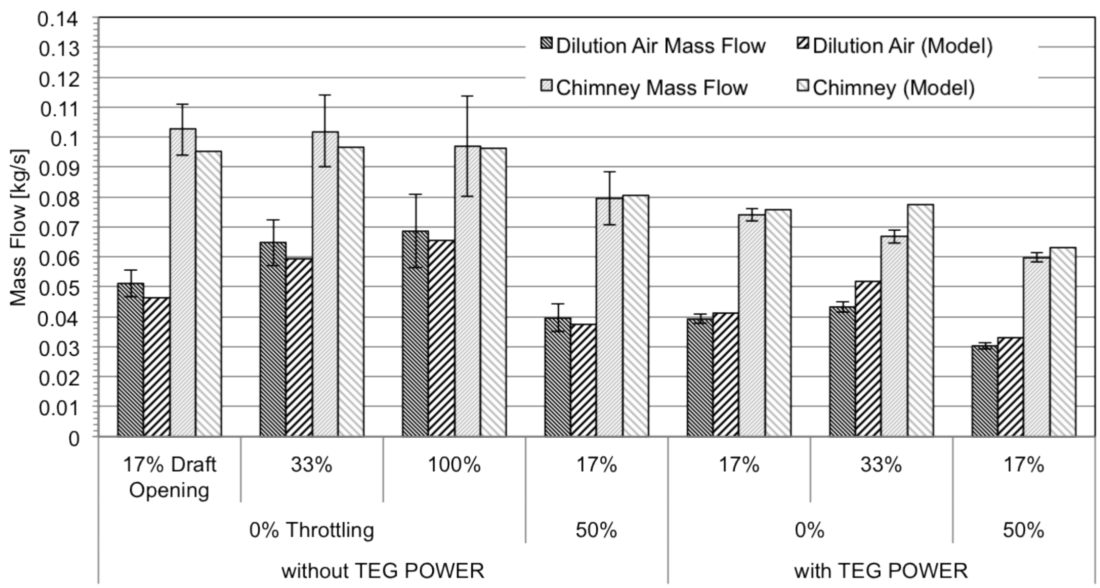

Figure 5.8: Experimental and computational dilution air and chimney mass flow comparison for oven temperature of 500°F

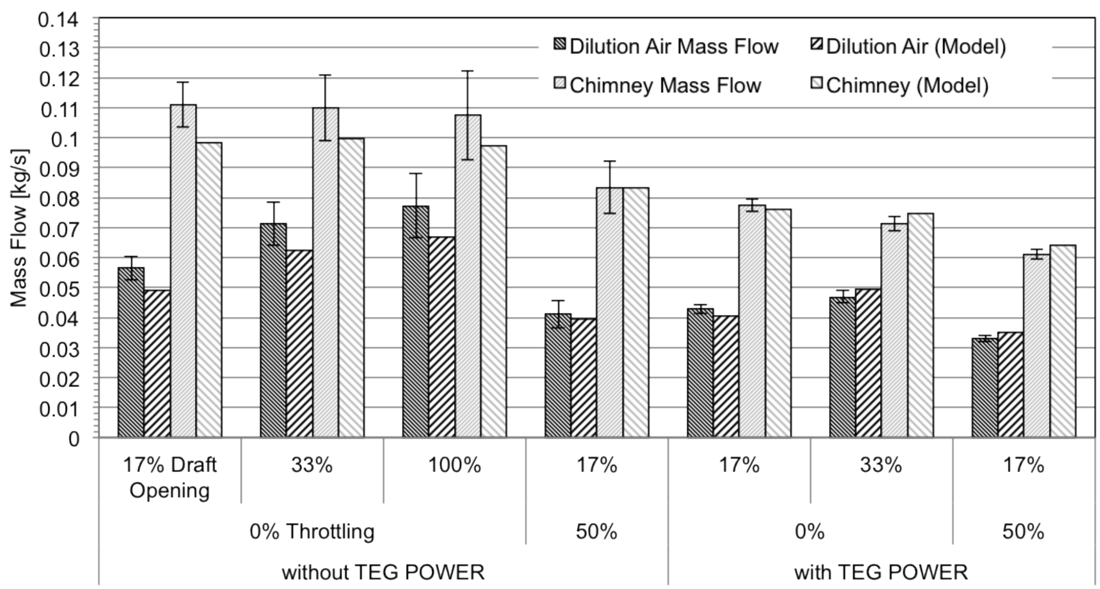

Figure 5.9: Experimental and computational dilution air and chimney mass flow comparison for oven temperature of 600°F

The comparison shows good agreement between experimental and computational dilution and chimney flow results. The maximum relative error of the dilution mass flow was found to under-predict by 13.3% without TEG POWER and 19.4% with TEG POWER. On average, the relative error was found to be 8%, which is within the uncertainty without TEG POWER. The maximum relative error of the chimney mass flow was found to under-predict by 11.5% without TEG POWER and over-predict by 15.7% with TEG POWER. On average the relative error was found to be 5.5%, which is within the uncertainty without TEG POWER.

A potential exception to this statement are the predicted values at 600°F without TEG POWER. The 600°F case is not unique, as the other lower oven temperature tests exhibit an under-prediction, but the 600°F case does exaggerate the error with a minimum of 9%. This is linked to the uncertainty of the dilution air and exhaust temperature inputs into the energy balance methodology imposed onto the draft hood. As the exhaust and the dilution air temperature difference widens (as with the 600°F cases) and the draft opening increases, the uncertainties of the temperature measurements contributes more to the uncertainty of the calculated measurement. This is illustrated by the large uncertainties on the dilution and chimney mass flows without TEG POWER. Except for the 17% draft opening, the remaining draft opening tests are within the measured uncertainty.

Overall, the ability to predict the respective mass flows to within 10% gives confidence that the model is able to interpolate between the test cases. The next step is to compare the temperature values.

5.1.2 Exhaust Temperature Comparison

This section will compare experimental and computational flue gas temperature results, along with a discussion of any discrepancies. The temperature comparison will focus on three temperatures:

- Oven Outlet Temperature (T_{ex} or $T_{HX,in}$)
- TEG POWER Outlet Temperature ($T_{HX,out}$)
- Chimney Temperature ($T_{chimney}$)

The flue gas temperature comparison with the waste heat recovery device are presented in Figure 5.10, 5.11, and 5.12 and without the waste heat recovery device are presented in Figure 5.13, 5.14, and 5.15.

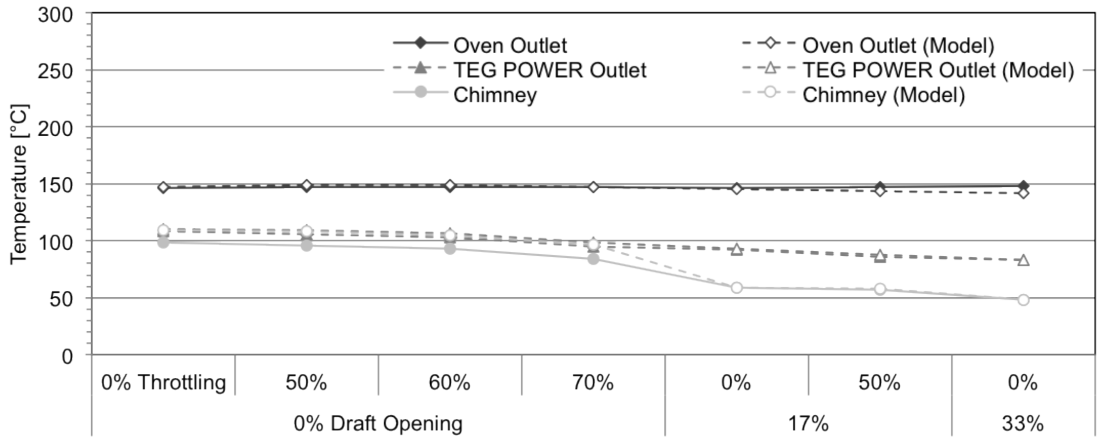

Figure 5.10: Experimental and computational flue gas temperatures comparison for oven temperature of 300°F with TEG POWER system

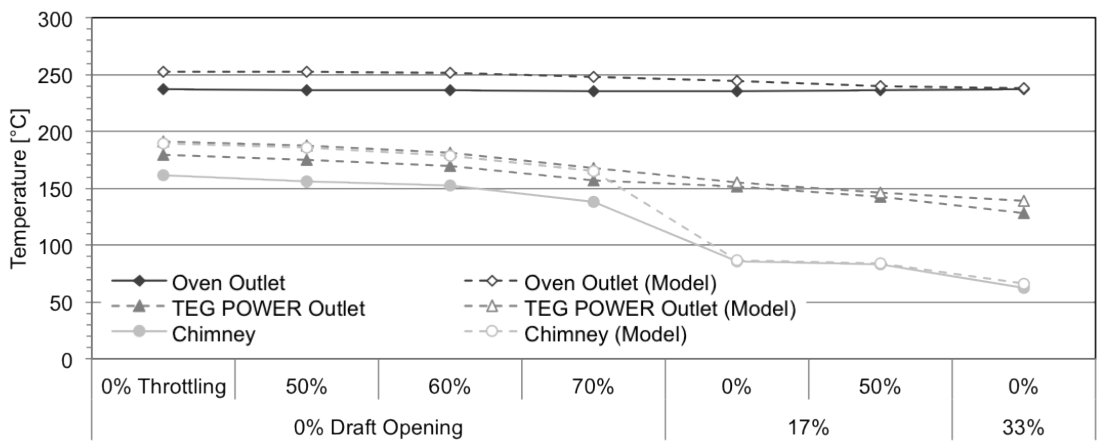

Figure 5.11: Experimental and computational flue gas temperatures comparison for oven temperature of 500°F with TEG POWER system

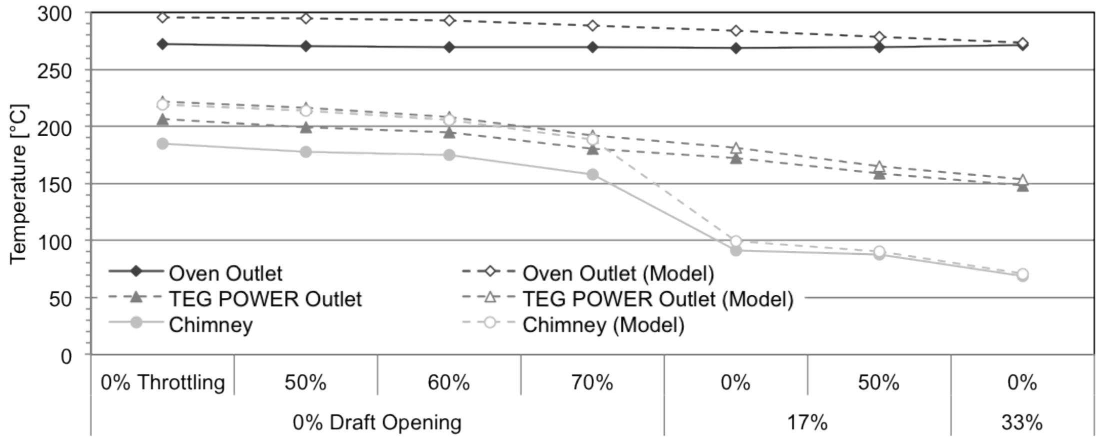

Figure 5.12: Experimental and computational flue gas temperatures comparison for oven temperature of 600°F with TEG POWER system

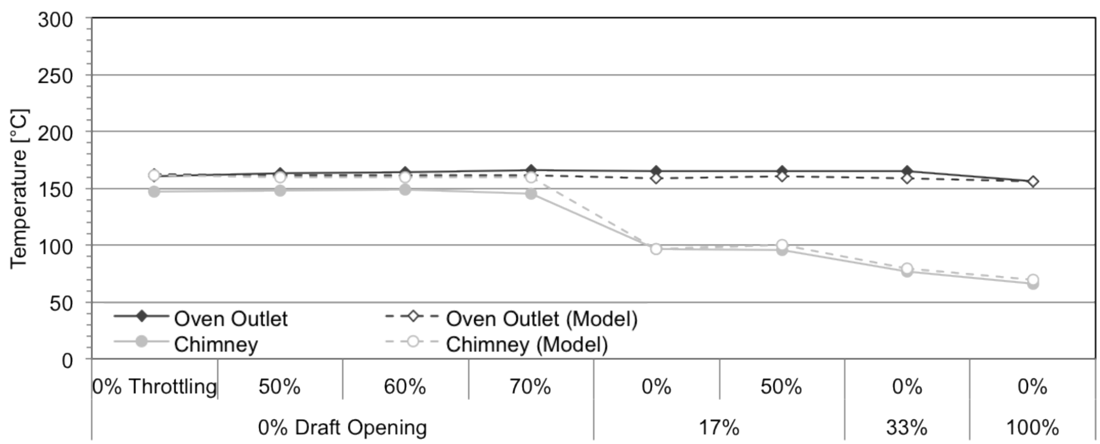

Figure 5.13: Experimental and computational flue gas temperatures comparison for oven temperature of 300°F without TEG POWER system

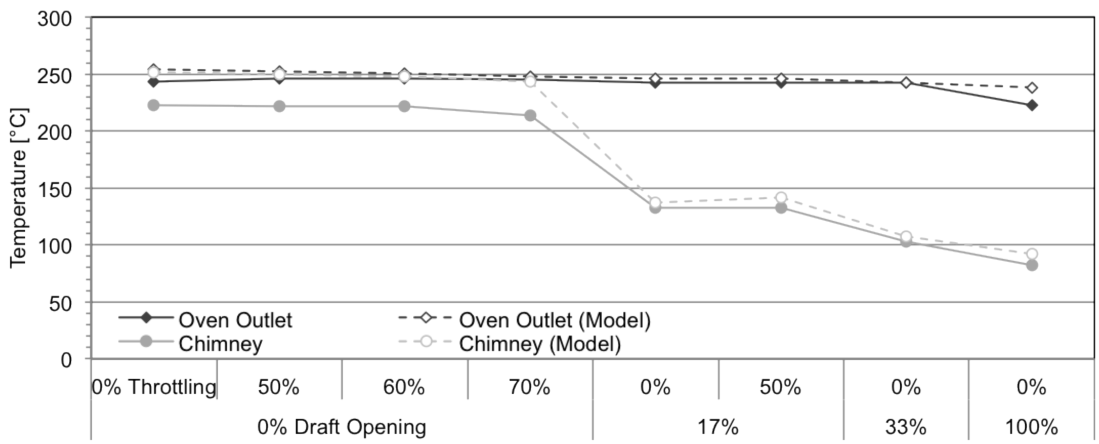

Figure 5.14: Experimental and computational flue gas temperatures comparison for oven temperature of 500°F without TEG POWER system

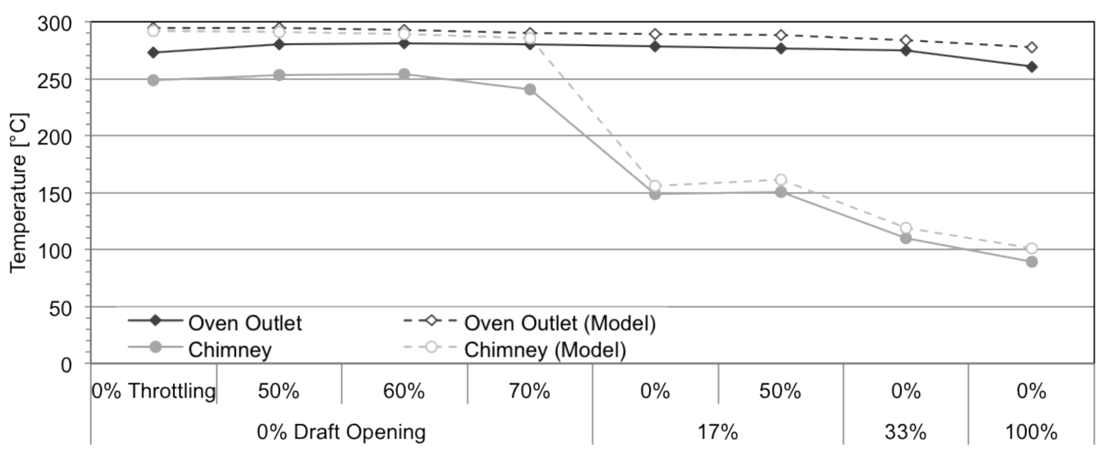

Figure 5.15: Experimental and computational flue gas temperatures comparison for oven temperature of 600°F without TEG POWER system

The comparison across all tests show good agreement to within 7%, except for the chimney temperature during the no dilution air test cases. This large error is caused by infiltration of room temperature air into the chimney, which was not incorporated into the computational model. The next step is to compare draft pressures, in particular the chimney draft pressure, to further identify the effect of infiltration.

5.1.3 Draft Pressure Comparison

This section will compare experimental and computational draft pressure results, along with a discussion of any discrepancies. The draft pressure comparison will focus on three pressures:

- Oven Outlet Draft Pressure (P_{ex} or $P_{HX,inlet}$)
- TEG POWER Outlet Draft Pressure ($P_{HX,outlet}$)
- Chimney Draft Pressure ($P_{chimney}$)

The draft pressure comparison with the waste heat recovery device are presented in Figure 5.16, 5.17, and 5.18 and without the waste heat recovery device are presented in Figure 5.19, 5.20, and 5.21.

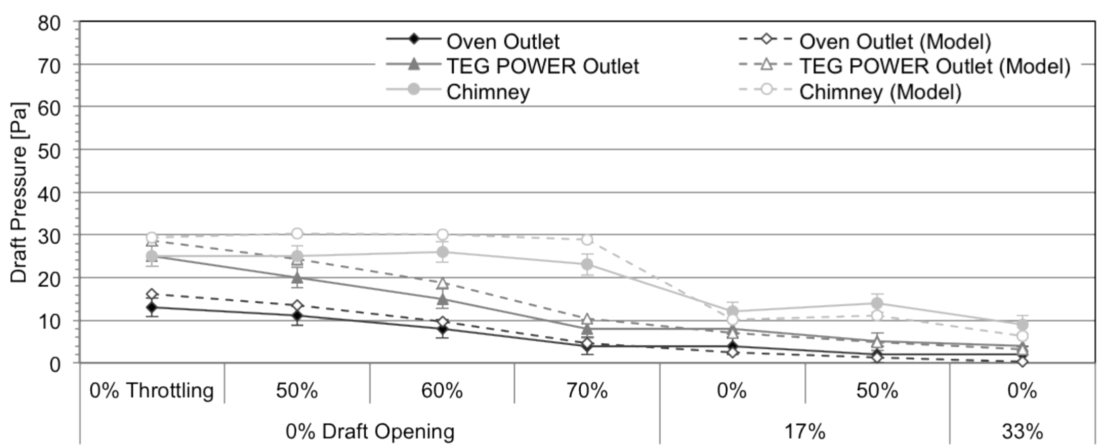

Figure 5.16: Experimental and computational draft pressure comparison for oven temperature of 300°F with TEG POWER system

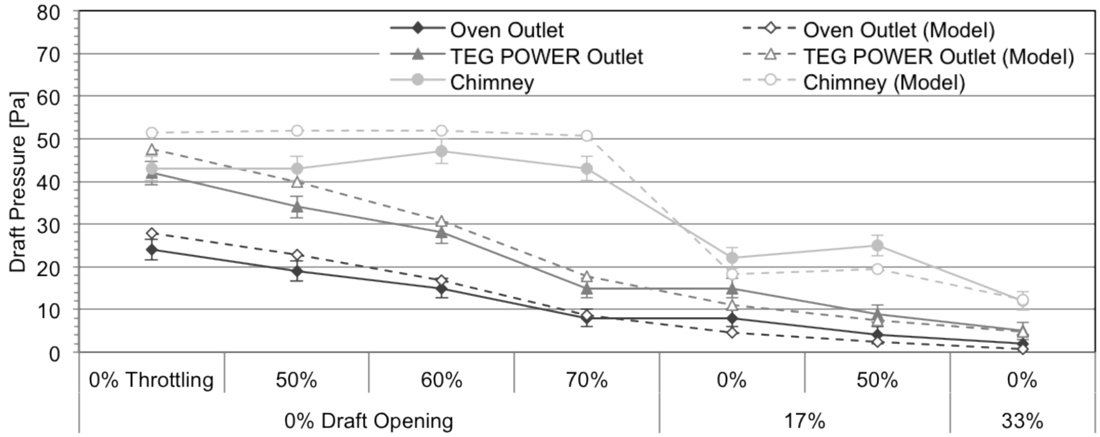

Figure 5.17: Experimental and computational draft pressure comparison for oven temperature of 500°F with TEG POWER system

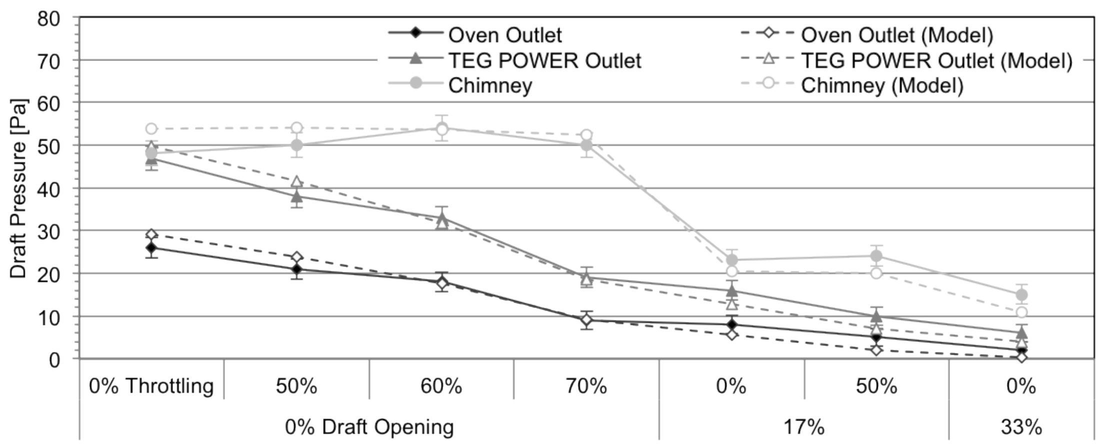

Figure 5.18: Experimental and computational draft pressure comparison for oven temperature of 600°F with TEG POWER system

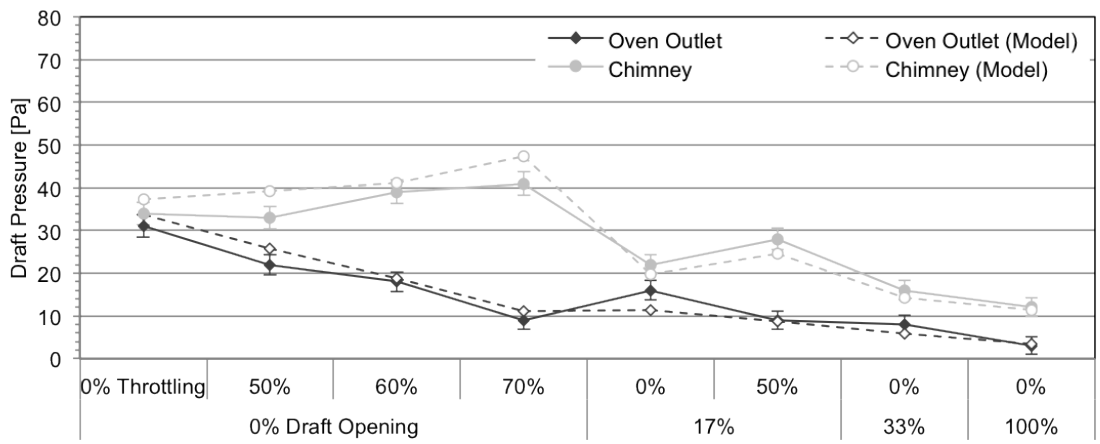

Figure 5.19: Experimental and computational draft pressure comparison for oven temperature of 300°F without TEG POWER system

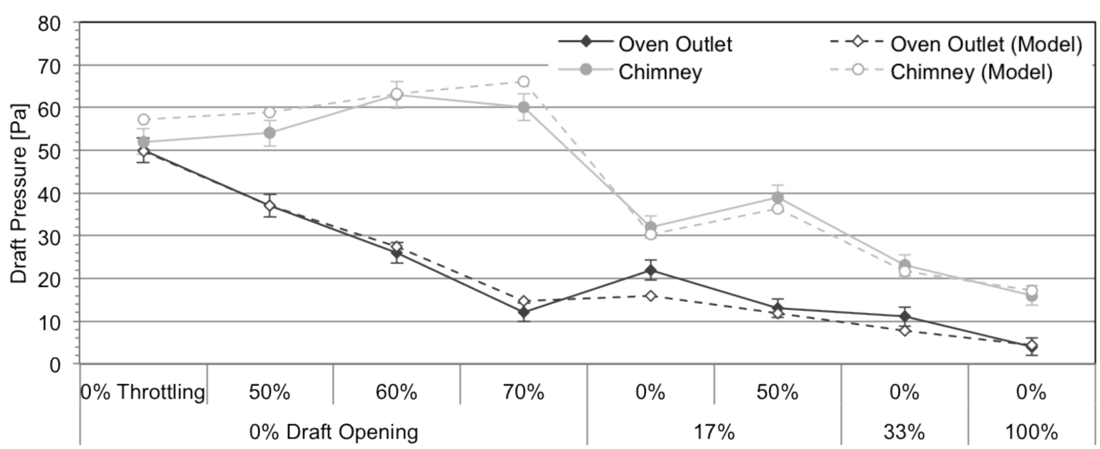

Figure 5.20: Experimental and computational draft pressure comparison for oven temperature of 500°F without TEG POWER system

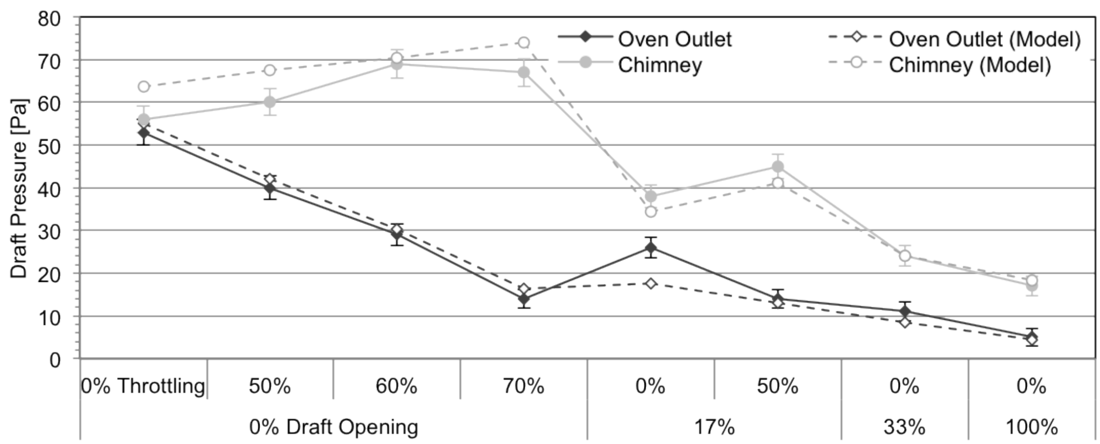

Figure 5.21: Experimental and computational draft pressure comparison for oven temperature of 600°F without TEG POWER system

The comparison across all tests show good agreement as the relative error is within the uncertainty of the pressure measurements, except for the chimney draft pressure during the no dilution air test cases and the oven outlet draft pressure during the 17% draft opening test without the TEG POWER device. During the no dilution air tests, the 20% discrepancies are caused by infiltration of room temperature air into the chimney, which was not incorporated into the computational model. The later error during the dilution air test at 17% draft opening is due to the uncertainty of the empirical loss coefficient relationship used within the computational model for the draft hood. At this flow condition, the predicted loss coefficient of exhaust gases entering the draft hood (mixing chamber) is under-predicted. If this loss coefficient makes up a large portion of the overall exhaust network loss coefficient, this under-prediction will be exaggerated. This assumption is tested by comparing to the case with the TEG POWER system, as the heat exchanger plays a dominant role in the over loss coefficient of the exhaust network. In this case, the presence of the heat exchanger and the associated pressure drop causes the under-prediction to become less pronounced.

5.1.4 Model Comparison Review

The comparison of between the experimental and numerical results provided confidence in the ability of the model to predict mass flow, temperature, and pressure throughout the exhaust system at various operating conditions. With the ability to predict with a 10% certainty, the model can be used to investigate the effects of the exhaust control and heat recovery devices on the performance of the appliance.

5.2 Proposed Exhaust Control and Heat Recovery Design Technique

The exhaust control and heat recovery devices play an important role in increasing the efficiency of an appliance. The method that each of these devices play in that role is different and must be considered when adhering to operational processes and safety requirements. This section will discuss the individual implications of these devices on the exhaust network within the framework of the safety and operation requirements. Once the individual advantages and disadvantages of these devices are discussed, a case study will be conducted with a set of constraints specific to this study with the objective to minimize fuel consumption and to calculate the maximum recoverable heat with these conditions.

5.2.1 Effect of Exhaust Control and Heat Recovery Devices on Exhaust Network Performance

This section will provide more detail on the exhaust control devices by discussing their direct and indirect effects on the exhaust flow. The exhaust control devices are grouped into three categories:

- Waste Heat Recovery
- Dilution Air Induction
- Exhaust Throttling

A waste heat recovery device is an indirect heat exchanger and is typically located at the hottest section of the exhaust flue. It directly affects the temperature of the exhaust gases by transferring the heat to a secondary fluid and cooling the exhaust gases. This leads to a reduction in buoyancy effects to drive the exhaust flow. It also directly acts as a semi-variable flow restriction due to the exhaust flow deceleration during the cooling process and the frictional effects of the heat exchanging surfaces. Waste heat recovery devices are typically not a controlling device, but by varying the amount of heat, the exhaust flow can be indirectly controlled.

A dilution air induction device is a direct heat exchanger and is typically a draft hood. A draft hood is a specialized device used to isolate the appliance from changes in the chimney draft condition due to wind and building pressure changes. The operating principle is to mix cool air with the exhaust air to reduce the chimney temperature. In relation to the draft hood, the mixing ratio is based on the geometry, but the mixing ratio can be controlled using exhaust throttling devices.

A exhaust throttling device is a controllable flow obstruction or valve. Though it is available in various forms, the basic principle is to develop an adjustable pressure drop to directly control the exhaust flow. The position of the throttling device will produce different effects when used in conjunction with a dilution air induction device (draft hood) depending whether it is upstream or downstream. If the throttle is placed downstream of the draft hood, the throttling valve will control the induction of dilution air and the exhaust through the appliance without largely affecting the mixing ratio between the flows and thus maintaining a consistent chimney temperature. If the throttle is placed on the dilution air duct or the exhaust duct, each flow can be controlled independently and the mixing ratio can be adjusted to control the chimney temperature.

Depending the design constraints of the exhaust network, a combination of techniques will need to be employed to safely obtain a specified objective. This is complicated by the inter-dependencies between the devices.

5.2.2 TEG POWER Case Study

This section proposes a systematic method of identifying the proper combination of control devices to achieve a desired objective within the specified constraints. The steps of the method are:

1. Specify the objective(s) and specify their importance
2. Dictate the scope of the design
3. Identify the exhaust network constraints
4. Investigate the positioning of the control devices by:

(a) Fully open dilution air and varying the amount of throttling until the objective(s) and constraint(s) are satisfied;

(b) If not satisfied, systematically increase the amount of throttling while decreasing dilution air between each reduction until satisfied.

This iterative process was performed manually, but can be adapted into an optimization algorithm.

A case study was performed using the aforementioned method to identify the position of the throttling valve in an effort to minimize natural gas consumption. The success was dependent on the ability to maintain appliance isolation from changes in chimney draft conditions, while minimizing natural gas consumption across the appliance operating range with the inclusion of a waste heat recovery (TEG POWER) system.

The first step is to specify the objective(s) and constraint(s) within the scope of the design.

1. Objective(s)
- Minimize natural gas flow to 7 L/min at lowest operating condition; and
- Minimize intake of dilution air

2. Scope
- Appliance operating range of 300°F (148°C) to 600°F (315°C); and
- Exterior temperature fluctuations between -20 to 30°C; and
- With waste heat recovery (TEG POWER); and
- Maximum room depressurization of 3 Pa

3. Constraint(s)
- Maintain appliance mass flow to within $\pm 5\%$; and
- Keep above the safe chimney temperature operating limit of 40°C

It should be noted that these requirements are specific to the exhaust network and the appliance used in this study. The first two requirements are general to all exhaust networks and are presented in Section 2.3, but can vary based on municipal by-laws or engineering practices. The third requirement is specific to the appliance, as testing has revealed that the burners do not operate normally below the specified natural gas flow. This is due to the operating principle of the barrel burner design. The burners require a minimum pressure and flow of natural gas to premix the air and fuel with a venturi nozzle before entering the burner barrel. Below the minimum flow, the pressure and air to fuel ratio is too low and does not allow for continuous combustion.

To isolate the appliance from changes in draft condition by solely using the passive intake of dilution air involves understanding the mechanism driving the isolation. The mechanism will be explained using a pressure profile presented in Figure 5.22, which was developed using the test facility design without heat recovery operating with 100% dilution air found in Figure 4.5.

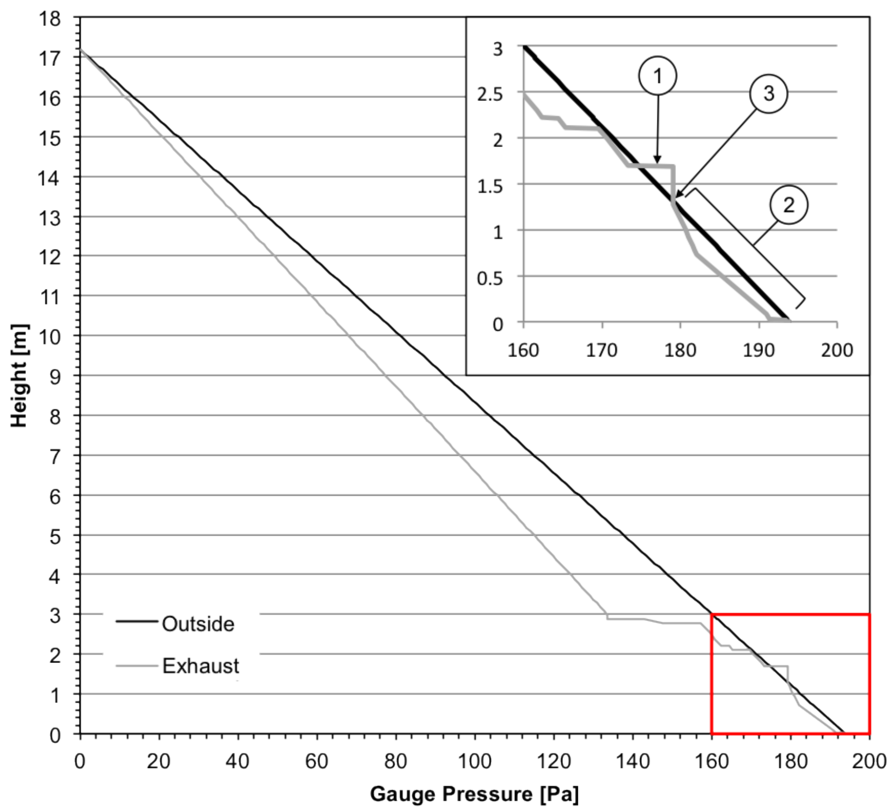

Figure 5.22: Pressure within the exhaust network with a normally operating draft hood [(1) Draft Hood, (2) Appliance, and (3) Draft Hood Draft Pressure]

As explained in Section 2.2.1, any exhaust network with a draft hood will have a near zero available draft pressure at the base of the chimney. This characteristic is highlighted with annotation (3) in Figure 5.22 just as the exhaust pressure line crosses the exterior pressure line. It should be noted that there still exists a small pressure differential between the dilution air inlet and the draft hood to drive the dilution air into the draft hood. This small pressure differential in relation to the larger pressure differential between the combustion air inlet and the draft hood pressure (highlighted with the annotation (2) in Figure 5.22) produces the ability to isolate the appliance. A change in exterior conditions is felt by the exhaust network as a higher (colder temperature) and lower (hotter temperature) pressures at the inlets relative to baseline exterior conditions. The increase (or decrease) in pressure will have higher relative effect on the smaller pressure differential driving the dilution air than the larger pressure differential driving flow through the appliance. Thus the increase (or decrease) in the chimney mass flow will be predominantly supplied by dilution air at a near zero available draft condition.

With the addition (or reduction) in the amount of dilution air with fluctuating exterior conditions, the temperature driving the chimney will decrease (or increase). The inclusion of larger amounts of dilution air aids in dampening out the magnitude of mass flow increases (or decreases) due to changes in exterior conditions.

To maintain isolation, the draft hood must only be kept at a near zero draft pressure. To maintain the near zero draft pressure, a throttling valve can be placed downstream of the draft hood to control the total mass flow and flow blockages will be placed to control the ratio between the dilution air and exhaust entering the draft hood. As the total mass flow decreases, the ratio was adjusted to maintain the exhaust mass flow by limiting the intake of dilution air. Figure 5.23 and 5.24 present the minimization of natural gas consumption and reduction of dilution air.

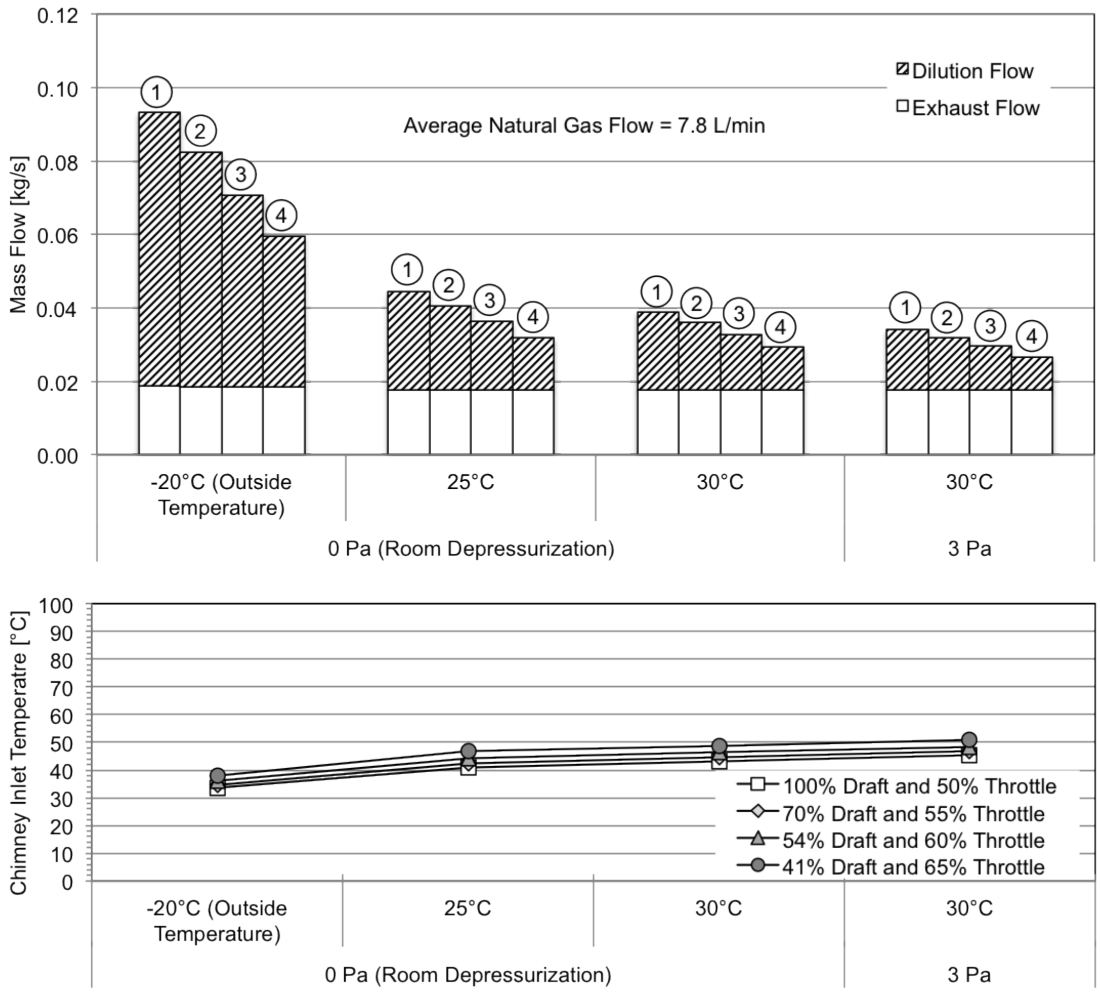

Figure 5.23: Mass flow through the exhaust network and chimney temperature at various exterior conditions at an oven temperature of 300°F [(1) 100% Dilution Air and 50% Throttling, (2) 70% Dilution Air and 55% Throttling, (3) 54% Dilution Air and 60% Throttling, (4) 41% Dilution Air and 65% Throttling]

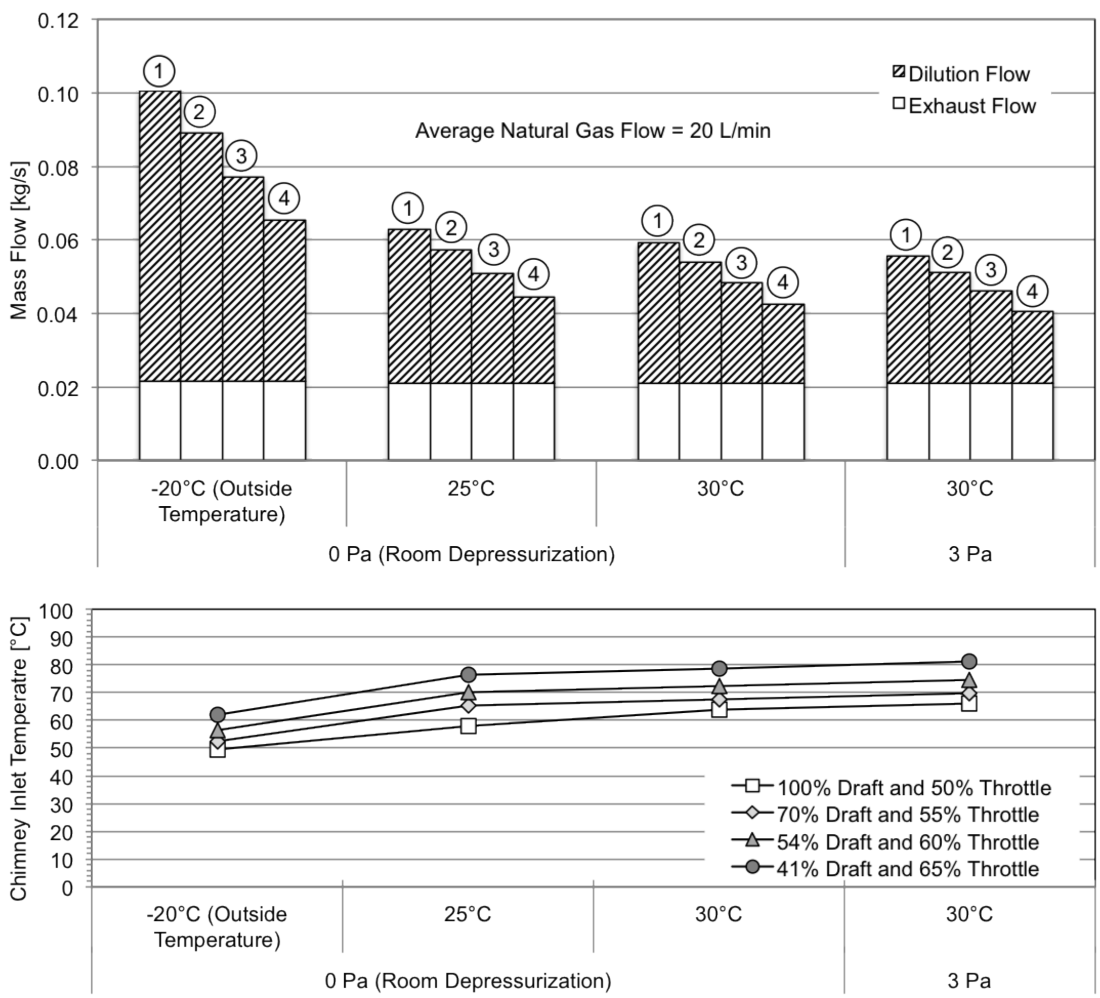

Figure 5.24: Mass flow through the exhaust network and chimney temperature at various exterior conditions at an oven temperature of 600°F [(1) 100% Dilution Air and 50% Throttling, (2) 70% Dilution Air and 55% Throttling, (3) 54% Dilution Air and 60% Throttling, (4) 41% Dilution Air and 65% Throttling]

Figure 5.23 and 5.24 demonstrate that the exhaust network is over-sized for the application, as the chimney mass flow was substantially reduced by inducing a large pressure drop via a throttling valve. This reduction in chimney mass flow in turn required the reduction of dilution air to maintain the appliance mass flow. During the process, the isolation from exterior conditions were also maintained by allowing enough dilution air to make up for the fluctuations in the chimney mass flow. A limit to the reduction of dilution air, while maintaining isolation, was found to occur when the back pressure generated by the chimney throttling valve causes exhaust gases to spill from the draft hood inlet. This limit was found at a 65% throttle position and 41% dilution air inlet area opening.

The chimney temperature was found to usually be over 40°C, with the exception of the -20°C case at a 300°F oven temperature. In this case, the temperature is very close to the constraint and could be further refined with the implementation of an optimization technique.

In addition to reducing the intake of dilution air, the throttling was also able to reduce the natural gas flow at 300 and 600°F. The consumption rates are presented and compared to an appliance operating solely with a draft hood in Table 5.1.The advantage of the TEG POWER system over the baseline appliance using only a draft hood is the ability to capture waste heat. The amount of heat being captured using 15°C coolant is also presented in Table 5.1, along with a conversion to equivalent natural gas flow rate.

Therefore, the implementation of the exhaust control and TEG POWER system lead to a reduction in natural gas consumption of 4.7 L/min and 9.4 L/min at oven temperatures of 300 and 600°F, respectively.

Table 5.1: Baseline comparison against TEG POWER

Oven Temperature	**300F (148C)**		**600F (315C)**	
Reduction in	**Natural Gas**	**Dilution Air**	**Natural Gas**	**Dilution Air**
Draft Hood	9.5 L/min	0.054 kg/s	23.0 L/min	0.075 kg/s
TEG POWER	7.8 L/min	0.014 kg/s	20.0 L/min	0.024 kg/s
Natural Gas Equivalency	1.7 L/min	1.1 L/min	3.0 L/min	1.4 L/min
Recovered Heat [W]	1060		2736	
Natural Gas Equivalency	1.9 L/min		5.0 L/min	
Total Natural Gas	4.7 L/min		9.4 L/min	

Chapter 6

Conclusion and Future Work Recommendations

6.1 Conclusions

The objective of this study was to develop a one-dimensional computational model to investigate the intimately coupled effects of waste heat recovery and exhaust flow control on the flow dynamics of naturally ventilated exhaust streams. The motivation was to establish a better understanding of waste heat recovery from naturally ventilated exhaust streams and develop a design methodology for waste heat recovery systems, including the exhaust control methods. By expanding the current understanding and developing a specific design methodology, the current challenges of waste heat recovery from naturally ventilated exhaust streams will be better understood and allow access to this under-valued source of energy.

The current understanding of exhaust system design and the associated techniques focus on selecting the appropriate exhaust network capacity to adequately vent the selected appliance(s). This approach utilizes the "worst-case" design methodology and is unable to predict the potential impact of a waste heat recovery system. A building ventilation modeling technique based on a nodel network methodology using mass and energy conservation fundamentals was adapted for exhaust flows to address the shortcomings of the current exhaust system design techniques.

As part of the development of the computational model, the predictions of mass flow, temperature, and pressure through the exhaust network needed to be validated against experimental results. The current temperature and pressure measurement techniques have been well-established, but the traditional mass flow measurement techniques were unable to provide accurate results in low velocity flows. Thus prompting the investigation of an energy balance approach on the appliance that was subsequently compared against a secondary energy balance of the waste heat recovery device. To validate the waste heat recovery energy balance, the pressure loss and heat transfer coefficient of the heat recovery device were calculated based on the measured exhaust flows and were shown to agree against well-established empirical correlations.

The validation of the combustion energy balance approach involved the development of a relationship between the exfiltration of exhaust gases from the appliance door and the draft pressure at the appliance outlet. Applying a large draft pressure to draw the exhaust gases into the chimney and minimize the amount of exfiltration, the appliance and waste heat recovery energy balance agreed to within 5%, thus validating the exhaust mass flow calculated via the combustion energy balance approach. Sequentially reducing the draft pressure to induce more exfiltration, a power law relationship between the exhaust exfiltration and the draft pressure at the appliance exhaust outlet was developed. Which allows the exhaust mass flow to be measured without the secondary waste heat energy balance and solely with the exfiltration subtracted from the combustion energy balance approach. The energy balance approach was further extended to the draft hood to measure the dilution and chimney mass flows. The energy balance technique established an accurate and economical method to measure exhaust flows using easily obtainable measurements.

Using the energy balance approach, the computational model was validated across a range of operating conditions. The conditions were conducted with and without waste heat recovery at different oven set point temperatures and varying degrees of dilution air and exhaust throttling. The model was found to predict mass flows, temperatures, and pressures throughout the exhaust network to within a $\pm 10\%$ error. Beyond the reasonable prediction error, the model is able to predict the effects of waste heat recovery and exhaust control methods.

The effect of waste heat recovery and different flow control techniques, dilution air and throttling, were investigated with an emphasis on the performance of the exhaust network and appliance. Waste heat recovery reduces the buoyancy effects and increases the overall pressure drop of the exhaust network. These cumulative effects will reduce mass flow and may require a re-designed exhaust control system based on the applicable performance and safety requirements. Dilution air was found to reduce the buoyancy effects within the exhaust network, but decrease the overall exhaust network pressure drop. These effects allow the chimney to operate at a lower temperature and dampen changes in the chimney mass flow during fluctuations in exterior conditions. In addition, the dilution air provides an alternate source of mass entering the exhaust network, thus limiting the exhaust mass flow through the appliance. The alternate method is exhaust gas throttling, which simply controls the exhaust flow by applying a controllable pressure drop without affecting chimney exhaust temperature. Unlike dilution air, throttling has the advantage to be performed anywhere in the network since it has no affect on temperature. The application of the exhaust control techniques with and without waste heat recovery is highly dependent on the objective and the constraints placed on the exhaust network design.

A case study was presented with the objective to minimize natural gas consumption and reduce the intake of dilution air. The case study provided a means to identify an exhaust control approach to accomplish the objectives within a set of constraints without conducting experimental testing. Relative to a typical exhaust system that has a nominal natural gas consumption of 9.5 and 23 L/min, the inclusion of a waste heat recovery device and exhaust controls showed the potential to reduce natural gas consumption by up to 18% (1.7 L/min) and 12% (3 L/min) at 300 and 600°F, respectively. The control techniques reduced the intake of dilution air by up to 70%, while maintaining the appliance operational stability during fluctuations in exterior conditions. The waste heat recovery device captured 1.0 and 2.7 kW of thermal energy, or a natural gas equivalent of 1.9 and 5 L/min, at 300 and 600°F respectively. With the implementation of the TEG POWER system in a typical pizza restaurants, a reduction of 8187 cubic meters of natural gas consumption and 14 metric tonnes of CO_2 could be achieved. An alternative comparison is the reduction of natural gas is comparable to three average Canadian households. The computational exhaust model provides a means of investigating the potential impact of waste heat recovery systems and exhaust control schemes to better utilization of combustible fuels.

6.2 Future Work Recommendations

This research was focused on developing a steady-state, one-dimensional computational model to investigate the effects of waste heat recovery and exhaust control techniques on the performance of a naturally ventilated exhaust network. This section will outline areas of focus to extend the functionality and accuracy of the computational model.

The model is well adapted to predict the level of depressurization needed to reverse the exhaust flow through an exhaust network. To utilize this functionality, the next step is to better characterize the associated loss coefficients of a draft hood across various flow conditions, such as a flow reversal through the dilution air intake, via a computational analysis and comparison to empirical correlations. Then the exhaust model results should be validated against experimental results using a testing facility which can safety handle a flow reversal.

The model is also well adapted to predict exfiltration from the interpretation that the oven door is a secondary output from the appliance, as oppose to the primary output from the exhaust network, due to a localized high pressure region within the appliance near the door. Further discretization of the appliance, to capture the localized high pressure regions, and an investigation of the appliance door loss coefficient will allow the prediction of exfiltration via fundamental flow principles.

The model is also well adapted to predict the effects of wind and multi-appliance exhaust networks, but will also require the development of experimental test to validate the predictions calculated from the computational model. The prediction of exfiltration, flow reversal due to room depressurization and wind effects would provide a useful tool in identifying problematic pressure conditions and implement appropriate standard operating procedures for appliances.

The database of exhaust duct components is limited and should be expanded to include more components, such as combining and diverging ducts, manifolds, and valves. This will allow the model to be more adaptable in predicting the performance of other exhaust networks.

The use of the computational model to investigate the proposed case study using TEG POWER was cumbersome due to the manual iterations. A future step would be to incorporate the model into an optimization algorithm. This would allow the model to become useful to a wider user set and allow for faster analysis and implementation of waste heat recovery systems and exhaust control schemes.

Beyond the steady-state model, an extension into the time domain would allow an investigation of time dependent effects such as cooking and condensation. This would require an extensive alteration to the solution algorithm along with the addition of thermal capacitance terms and accounting of the various chemical species forming during combustion and cooking. Due to these extensive changes, it is recommended to experimentally investigate the effects of cooking on the exhaust mass flow and how often the appliance is cycled leading condensation to become a critical issue. If these effects are found to be critical to the continued performance of the appliance and exhaust network components, then it is recommended to extend the solution algorithm into the time domain.

Appendices

Appendix A

Uncertainty Analysis

A.1 Uncertainty in Temperature Measurements

The uncertainty of the temperature measurement has been divided into three categories: calibrated thermocouples, non-calibrated thermocouples, and RTDs. However, the total uncertainty for any temperature measurement will be estimated by:

$$\delta T = \sqrt{\sum_{i=1}^{n} (\delta_i)^2} \tag{A.1}$$

where δ_i represents the uncertainty association, which will vary based on the measurement and outlined on the following sections.

A.1.1 Calibrated Thermocouples

The uncertainty of a calibrated thermocouple is underlined by the uncertainties of the calibration device, the temperature gradients in the water bath, along with the uncertainties associated with the data acquisition system. Drnovsek *et al.* (1998) outlined a methodology to estimate the calibration uncertainty.

The calibration facility was comprised of a platinum resistance thermometer (Omega DP251) submersed in a circulating water bath (Thermo Electron RTE10). The inlet and outlet coolant water thermocouples were calibrated by placing them in the water bath. The extension wires and the data acquisition system (National Instrument 9213) were used during the calibration, which allows the uncertainties related to the extension length, wire connections, linearity, zero-offset to be incorporated into the calibration curve uncertainty. Therefore, the uncertainties of calibrated temperature measurements are:

- δ_1: The uncertainty related to the reference temperature (RTD)
- δ_2: The uncertainty related to the drift of the reference temperature (RTD)
- δ_3: The uncertainty related to the reference temperature measurement device
- δ_4: The uncertainty related to the water bath
- δ_5: The uncertainty related to the data acquisition system
- δ_6: The uncertainty related to the calibration curve
- δ_7: The uncertainty related to the reproducibility of the measurements

A.1.1.1 Uncertainty related to the reference temperature (RTD)

The uncertainty for the reference temperature (Omega DP251) is $\pm 0.01^{\circ}$C, as stated by the manufacturer.

A.1.1.2 Uncertainty related to the drift of the reference temperature

Documentation of the RTD probe does not include uncertainty of the annual drift. Therefore, the annual drift recommended by Drnovsek *et al.* (1998) of ±0.0075°C/year was used and based on 2 years. The uncertainty related to the drift of the reference temperature is ±0.0715°C.

A.1.1.3 Uncertainty related to the water bath

The uncertainty of the water bath was measured monitoring the bath at various locations. An uncertainty of ±0.02°C was found using the reference temperature RTD.

A.1.1.4 Uncertainty related to the data acquisition system

The uncertainty of the data acquisition system is ±0.01°C, as stated by the manufacturer.

A.1.1.5 Uncertainty related to the calibration curve

The calibration data was fitted with linear, second-order, third-order, and fourth-order polynomial fitted curves. The best fit was found to be a second-order polynomial with a maximum uncertainty observed to be less than ±0.1°C.

A.1.1.6 Uncertainty related to the reproducibility of the measurements

The reproducibility uncertainty was estimated to be twice the standard deviation over 100 readings, which relates to a 95% confidence level. The uncertainty was estimated to be less than ±0.03°C.

Using equation A.1, the uncertainty for the water inlet and outlet T-type thermocouples are presented in Table A.1.

Table A.1: Uncertainty breakdown of the water inlet and outlet thermocouples

Uncertainty Type	Water Inlet	Water Outlet
	°C	°C
RTD Bias	0.010	0.010
RTD Drift	0.015	0.015
Water Bath Bias	0.020	0.020
DAQ Bias	0.010	0.010
Calibration Error	0.090	0.075
Repeatability Error	0.028	0.027
Total Uncertainty	**±0.10**	**±0.10**

A.1.2 Non-Calibrated Thermocouples

The less important temperature measurements were recorded using non-calibrated T-type and E-type thermocouples. The uncertainty related to non-calibrated thermocouples is based on uncertainties of zero offset, linearity, hysteresis, and associated extension wires and connectors. The non-calibrated T-type thermocouples used in the experimental facility include the surface temperature measurements of the TEGs, the chimney temperature, and the natural gas temperature. The E-type thermocouple is used to measure the oven temperature. Therefore, the uncertainties of non-calibrated temperature measurements are:

- δ_1: The uncertainty related to the non-calibrated thermocouple

- δ_2: The uncertainty related to the data acquisition system

A.1.2.1 Uncertainty related to the non-calibrated thermocouple

The uncertainty of a non-calibrated T-type thermocouple is ±1.0°C, as stated by the manufacturer. The uncertainty of a non-calibrated E-type thermocouple is ±1.7°C, as stated by the manufacturer.

A.1.2.2 Uncertainty related to the data acquisition system

The uncertainty of the data acquisition system is ±0.01°C, as stated by the manufacturer.

Using equation A.1, the uncertainty for the non-calibrated T-type and E-type thermocouples are presented in Table A.2.

Table A.2: Uncertainty breakdown of the non-calibrated thermocouples

Uncertainty Type	T-Type	E-Type
	°C	°C
Non-Calibrated Thermocouple Error	1.0	1.7
DAQ Bias	0.01	0.01
Total Uncertainty	**±1.0**	**±1.7**

A.1.3 Resistance Thermometer Detectors (RTDs)

The inlet and outlet of the exhaust (hot) heat exchanger was measured with three 100ohm platinum RTDs at each location. The uncertainty of an RTD is based in the temperature range and class. In this case, the RTDs used were Class B at temperatures between 100-300°C. The uncertainties of Class B RTD temperature measurements are:

- δ_1: The uncertainty related to 100ohm platinum RTDs Class B
- δ_2: The uncertainty related to the data acquisition system

A.1.3.1 Uncertainty related to RTDs

The manufacturer data did not elaborate on the accuracy of the RTDs, therefore IEC 751 specifications for Platinum Resistance Thermometers, which uses the DIN 43760 requirements for accuracy, will be referenced. According to IEC 60751, the Class B RTDs have the following permissible uncertainties:

Table A.3: Uncertainty vs Temperature relation of 100ohm Platinum RTD Class B

Temperature Range	50°C-150°C	150°C-250°C	250°C-350°C
	°C	°C	°C
Class B Platinum RTD Error	±0.8	±1.3	±1.8

A.1.3.2 Uncertainty related to the data acquisition system

According to manufacturer specifications, the uncertainty related to the data acquisition system is based on the temperature range outlined in Table A.4.

Table A.4: Uncertainty vs Temperature relation of data acquisition system

Temperature Range	50°C-150°C	150°C-250°C	250°C-350°C
	°C	°C	°C
DAQ Bias	±0.5	±1.0	±1.0

Using equation A.1, the uncertainty for the 100ohm platinum RTDs Class B are presented in Table A.5.

Table A.5: Uncertainty breakdown of the 100ohm platinum RTDs Class B

Temperature Range	100°C	200°C	300°C
	°C	°C	°C
DAQ Bias	0.8	1.3	1.8
DAQ Bias	0.5	1.0	1.0
DAQ Bias	**±0.94**	**±1.64**	**±2.06**

A.2 Uncertainty in Flow Rate Measurements

The uncertainty of the flow rate measurements has been divided into two categories: thermal dispersion volumetric flow meter and corilis mass flow meter. However, the total uncertainty for any flow meter measurement will be estimated by:

$$\delta\dot{V} = \delta\dot{m} = \sqrt{\sum_{i=1}^{n}(\delta_i)^2} \tag{A.2}$$

where δ_i represents the uncertainty association, which will vary based on the measurement and outlined on the following sections.

A.2.1 Thermal Dispersion Volumetric Flow Meter

The natural gas volumetric flow rate was measured using a McMillian 50D-13 thermal dispersion flow meter. The manufacturer provided information pertaining to the flow meters accuracy, repeatability, temperature and pressure sensitivity. It was also noted by the manufacturer that these uncertainties are only applicable from 10-100% of the rate flow. Therefore, the uncertainties of the volumetric flow rate measurements are:

- δ_1: The uncertainty related thermal dispersion volumetric flow meter
- δ_2: The uncertainty related to repeatability of the flow meter
- δ_3: The uncertainty related to temperature sensitivity from calibration temperature
- δ_4: The uncertainty related to pressure sensitivity from calibration pressure

A.2.1.1 Uncertainty related thermal dispersion volumetric flow meter

The uncertainty, as stated by the manufacturer, of the 0 to 100L/min volumetric flow meter is $\pm 1.5\%$ of the full scale. This corresponds to an uncertainty of ± 1.5L/min.

A.2.1.2 Uncertainty related to repeatability of the flow meter

The repeatability of the flow meter is $\pm 0.25\%$ of the full scale, or ± 0.25L/min, as stated by the manufacturer.

A.2.1.3 Uncertainty related to temperature sensitivity

The uncertainty related to the difference between the calibration and process temperature is $\pm 0.15\%$ per °C, or ± 0.15L/min per °C, as stated by the manufacturer.

It was observed that the maximum temperature difference is 5°C. The maximum temperature sensitivity uncertainty is ±0.75L/min.

A.2.1.4 Uncertainty related to pressure sensitivity

The uncertainty related to the difference between the calibration and process pressure is ±0.02% per psi, or ±0.02L/min per psi, as stated by the manufacturer. It was observed that the maximum temperature difference was less than 1 psi. Therefore the pressure sensitivity uncertainty is small.

Using equation A.2, the uncertainty for the thermal dispersion volumetric flow meter is presented in Table A.6.

Table A.6: Uncertainty breakdown of the thermal dispersion flow meter

Uncertainty Type	**L/min**
Thermal Dispersion Flow Meter Error	1.5
Repeatability Error	0.25
Temperature Sensitivity	0.75
Pressure Sensitivity	-
Total Uncertainty	**±1.7**

A.2.2 Coriolis Mass Flow Meter

The coolant water mass flow rate was measured using a Endress+Hauser Promass 80E coriolis mass flow meter. The manufacturer provided information pertaining to the flow meters accuracy, repeatability, temperature and pressure sensitivity. It should be noted that the manufacturer that the temperature and pressure sensitivity has no considerable effect on the readings. Therefore, the uncertainties of the volumetric flow rate measurements are:

- δ_1: The uncertainty related coriolis mass flow meter
- δ_2: The uncertainty related to repeatability of the flow meter

A.2.2.1 Uncertainty related coriolis mass flow meter

The accuracy of the mass flow meter for liquids, as stated by the manufacturers, is ±0.25% of the reading.

A.2.2.2 Uncertainty related to repeatability of the flow meter

The repeatability of the flow meter, as stated by the manufacturer, is ±0.10% of the reading.

Using equation A.2, the uncertainty for the thermal dispersion volumetric flow meter is presented in Table A.7.

Table A.7: Uncertainty breakdown of the Coriolis mass flow meter

Uncertainty Type	**% of reading (kg/s)**
Coriolis Mass Flow Meter Error	0.25
Repeatability Error	0.1
Total Uncertainty	**±0.27**

A.3 Uncertainty in Combustion Analysis Measurements

The combustion analysis was conducted using an E-Instrument E8500. The uncertainty of the combustion analysis measurements has been divided into the individual sensors, which include:

- Oxygen (O2) sensor
- Carbon monoxide (CO) sensor
- Carbon dioxide (CO2) sensor
- Hydrocarbon (CxHy) sensor
- Nitric oxide (NO) sensor
- Nitrogen dioxide (NO2) sensor
- Sulfur dioxide (SO2) sensor

However, the total uncertainty for any chemical measurement will be estimated by:

$$\text{Concentration Uncertainty} = \sqrt{\sum_{i=1}^{n} (\delta_i)^2} \tag{A.3}$$

where i represents the uncertainty association, which are:

- δ_1: The uncertainty related resolution of reading
- δ_2: The uncertainty related to accuracy of the reading

A.3.0.3 Uncertainty related resolution of reading

The uncertainties due to the resolution of the sensors in the combustion analyzer, as stated by the manufacturer, are found in Table A.8.

Table A.8: Uncertainty associated to the resolution error

Chemical	O_2	CO	CO_2	C_xH_y	NO	NO_2	SO_2
	%	%	%	%	ppm	pmm	pmm
Resolution Error	0.05	0.005	0.05	0.005	0.5	0.5	0.5

A.3.0.4 Uncertainty related to accuracy of the reading

The uncertainties due to the accuracy of the sensors in combustion analyzer, as stated by the manufacturer, are found in Table A9.

Table A.9: Uncertainty associated to the sensor accuracy error

Chemical	O_2	CO	CO_2	C_xH_y	NO	NO_2	SO_2
	%	% of rdg	% of rdg	% of rdg	% of rdg	% of rdg	% of rdg
Resolution Error	0.1	4	3	3	4	4	4

Using equation A.3, the uncertainty for the combustion analysis must be calculated on an individual test basis.

Appendix B

Heat Losses

B.1 Oven

The overall heat transfer coefficient of the oven was estimated through a transient analysis of the temperature profiles during oven cool down experiments collected by Hirmiz (2014). The process began by bringing the oven to a steady state temperature setpoint of 600°F (315°C), at which point the oven was subsequently sealed and turned off to allow it to cool to room temperature ($T_{air,db}$). Throughout the process, the oven temperature (T_{oven}) was recorded and the room temperature was maintained at 25°C.

Using the identical process described above, an uninsulated and insulated case were investigated. The uninsulated case involved no modification to the oven other than sealing the oven doors to limit heat loss via mass transfer. The insulated case involved wrapping the entire oven with 2-inches (5cm) of fiberglass insulation with an aluminum foil covering except for the combustion air intake at the bottom of the oven. The doors were once again sealed to limit mass transfer.

Investigating the temperature profiles, it was discovered that the throttling valve used to seal the oven from the exhaust system had a small leak. This allowed a minute amount of exhaust gases to transport thermal energy out of the oven and must be accounted for to adequately discern the overall heat transfer coefficient.

The analysis was completed based an energy balance of a lumped system, which is represented with an ordinary differential equation.

$$\left(mc_p\frac{dT}{dt}\right)_{oven} = (\dot{m}c_p)_{air}(T_{oven} - T_{air,db}) + (UA)_{oven}(T_{oven} - T_{air,db}) \tag{B.1}$$

where

m_{oven} is the mass of the cordierite baking stone inside the oven [kg]

$c_{p,oven}$ is the heat capacity of the cordierite baking stone [J/kg K]

$\dot{m}_{air}$ is the air infiltration mass flow [kg/s]

$c_{p,air}$ is the heat capacity of the outside air [J/kg K]

$(UA)_{oven}$ is the overall heat transfer coefficient of the oven [W/K]

Using the solution of the differential equation found below and a least-squared regression technique, the infiltration ($\dot{m}_{air}$) and overall heat transfer coefficient (UA_{oven}) can be estimated by fitting the analytical solution to the experimental data.

$$\frac{T_{oven} - T_{air,db}}{T_{oven,setpoint} - T_{air,db}} = \exp\left[-\frac{(\dot{m}c_p)_{air} + (UA)_{oven}}{(mc_p)_{oven}}\right] \tag{B.2}$$

The regression analysis is based on the minimization of the sum of squares (S_r) value of the analytical solution for the insulated and uninsulated cases, where the infiltration is assumed to have remained constant. Investigating the insulated case, the insensitivity of the solution towards variation in the heat transfer coefficient, based on the properties of the insulation, found that the infiltration was the dominant mode of heat loss. Based on this case, the mass transfer through the oven was estimated. Using the calculated value for infiltration, the uninsulated case was used to estimate the overall heat transfer coefficient. The known parameters and results of the regression technique are found in Table B.1.

Table B.1: Parameters of the cooling profile regression analysis

Parameter	**Units**	**Uninsulated**	**Insulated**
Known			
m_{oven}	kg	85	
$c_{p,oven}$	J/kg K	1460	
$c_{p,air}$	J/kg K	1007	
Results			
UA_{oven}	W/K	3.71	0.2
$\dot{m}_{air}$	kg/s	0.0051	
R^2		0.99954	0.9989

The fit of the regression analysis is represented by the R^2 value found in Table B.1. In addition, the fit of the model is illustrated in relation to the experimental data in Figure B.1.

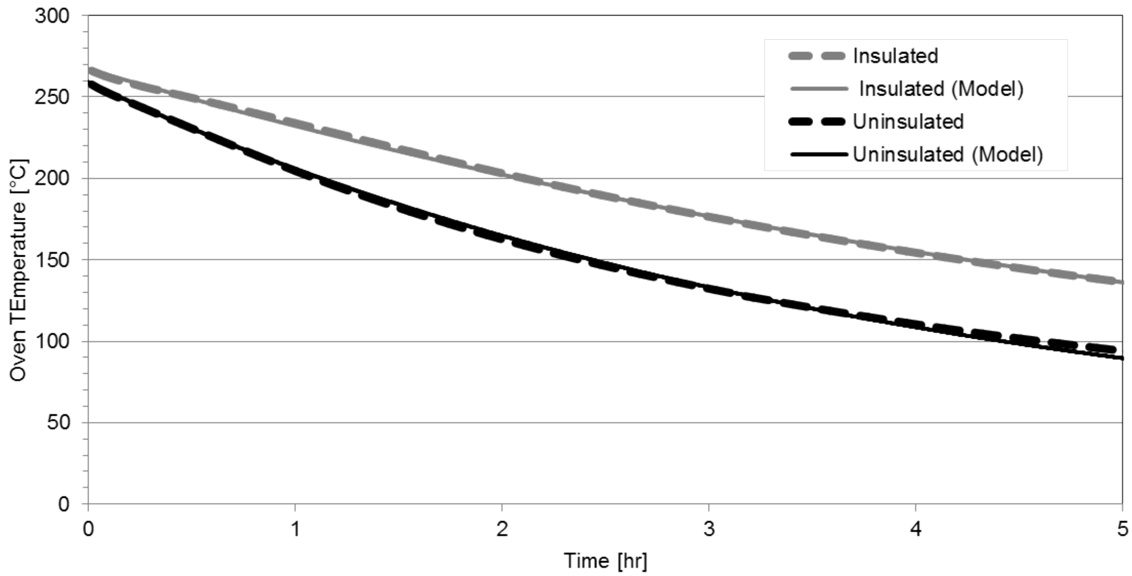

Figure B.1: Regression Analysis of Oven Cooling

Based on observations, the regression analysis was only preformed between a start time slightly after the oven was turned off and ended once the temperature of the oven reached 150°C; which presented in Figure B.1.

B.2 Draft Hood

The thermal losses ($Q_{loss,hood}$) were estimated using a heat transfer coefficient (UA) based purely on conductive heat transfer through the insulation; as the insulation encapsulating the draft hood and the exhaust duct leading to the chimney temperature measurement location was observed to be the dominant heat transfer resistance. The cases without dilution air were used as a comparison tool to access the validity of the thermal loss estimates. The temperature potential was predicted using a logarithmic temperature difference ($LMTD$) between the exhaust gases and the surroundings.

$$Q_{loss,hood} = UA \times LMTD \tag{B.3}$$

The application of the combustion energy balance technique requires the estimation of the thermal effects within the draft hood and the ductwork between the temperature measurement locations.

To estimate the thermal effects, the heat losses were quantified by imposing an energy balance between the appliance's exhaust outlet and the chimney thermocouple for test scenarios that were not introducing dilution air. It found that the heat losses were four times larger than an estimation using analytical formulations. After an investigation of the analytical estimation, it was determined that any meaningful adjustments of the limiting heat transfer coefficient (mineral wool insulation) would not reproduce the measured heat losses. This suggests that a portion of the thermal effects is caused by infiltration via the duct connections.

Using an energy balance, the infiltration air can be modeled as dilution air entering a mixing chamber. The chimney draft pressure will dictate the amount of infiltration entering, therefore a no dilution air experiment showing a similar chimney draft condition as a the worst dilution air case was identified. The worst case showed an infiltration intake of 0.0036 kg/s or 7% increase in the smallest chimney mass flow. Along with affecting the chimney mass flows, the loss coefficient of the throttling valve may be affected depending on the location of infiltration. Evaluating the worst case, it was found that the loss coefficient will decrease by a maximum of 13% with the inclusion of infiltration. In the case of no dilution air scenarios, the infiltration was incorporated into the chimney mass flow ($\dot{m}_{chimney}$) and, in the case of dilution air scenarios, the infiltration was simply added to the dilution air mass flow ($\dot{m}_{dilution}$) and ultimately finds itself in the chimney mass flow. The worst case effect of infiltration on the mass flow measurements are incorporated, but are not expected to effect the accuracy of the measurements as the change is within the $\pm15\%$ confidence interval.

Appendix C

Pressure Loss Coefficients

C.1 Waste Heat Recovery Device

This section will provide a general approach, and accompanying assumptions, to quantify the exhaust flow pressure loss across the waste heat recovery device. The approach can be applied to a wide variety of heat exchanger designs, but for convenience, a pin fin heat exchanger will be depicted and used throughout the analysis. The approach requires the following assumptions to be made:

- Flow is steady and turbulent
- Body forces caused by gravity, magnetic, electrical, and other fields are negligible
- Fluid density is only dependent on temperature and is treated as a constant.
- Frictional effects are averaged and considered constant across a component.

The pressure drop through a heat exchanger can be attributed to two major components: the core of the heat exchanger and the entrance/exit manifolds distributing the flow into the heat exchanger. The core of the heat exchanger contributes to the pressure drop by acting as a flow resistance and influencing the fluid momentum through the addition/removal of thermal energy. The entrance/exit manifolds provide additional pressure changes through contractions or expansions leading to momentum and viscous dissipation effects. Therefore, the total pressure drop can be inferred by dividing the heat exchanger into three sections, as illustrated in Figure C.1.

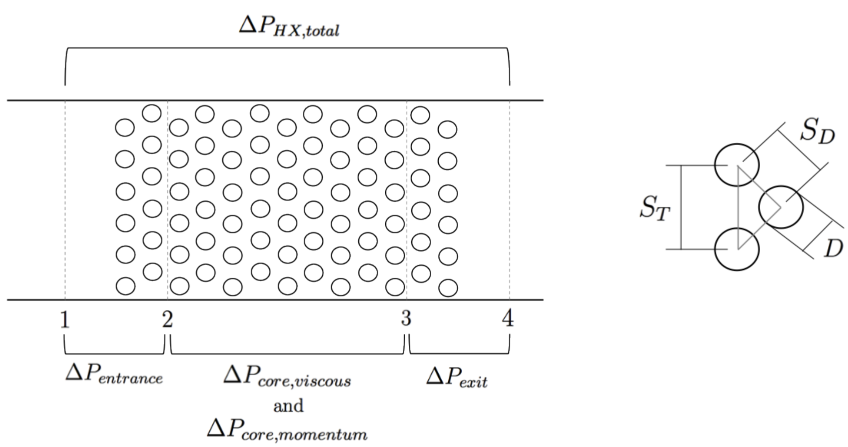

Figure C.1: Illustration of the waste heat recovery device divided to isolate the contribution to pressure drop effects from the respective components

As outlined by Kays and London (1954), the pressure drop contribution of each respective component can be summed together to form the total pressure drop across the heat exchanger.

$$\Delta P_{HX,total} = \Delta P_{entrance} + \Delta P_{core,momentum} + \Delta P_{core,viscous} + \Delta P_{exit} \tag{C.1}$$

Entrance Pressure Drop

The entrance pressure drop is attributed to a flow acceleration due to a contraction in flow area and to the energy dissipation caused by a sudden contraction. Applying the conservation of mechanical energy across the entrance (1-2) and assuming that the fluid density across the entrance section is constant.

$$P_1 + \frac{\rho_{inlet} V_1^2}{2} = P_2 + \frac{\rho_{inlet} V_2^2}{2} + K_{entrance} \frac{\rho_{inlet} V_2^2}{2} \tag{C.2}$$

Using the conservation of mass, the velocity can transformed via an area ratio (σ) and the pressure drop across the entrance can be represented by:

$$\Delta P_{entrance} = P_1 - P_2 = \frac{\dot{m}_{exhaust}^2}{2\rho_{inlet} A_{HX}^2} \left(1 - \sigma_{inlet} + K_{entrance}\right) \tag{C.3}$$

The area ratio is based on the contraction from the frontal flow area of the inlet duct (A_{inlet}) to the minimum flow area of the heat exchanger (A_{HX}).

$$\sigma_{inlet} = \frac{A_{HX}}{A_{inlet}} \approx \frac{2(S_D - D)}{S_T}$$

The entrance loss coefficient ($K_{entrance}$) is dependent on the heat exchanger design and geometry, along with the accompanying flow conditions. Referencing the data presented by Kays and London (1954), the loss coefficient can be represented by:

$$K_{entrance} = 0.53 - 0.4018\sigma_{inlet}$$

The area ratio (σ) and the loss coefficient (K) presented are tailored specifically for a staggered pin fin geometry and do not apply to other geometries.

Core Pressure Drop

The core pressure drop is a combination of a flow deceleration due to the cooling effects and the energy dissipation due to turbulent wakes and friction across the heat exchanger pins. The combination of the two effects requires the pressure drop across the core (2-3) to be divided into two parts:

$$P_2 - P_3 = (P_2 - P_3)_{momentum} + (P_2 - P_3)_{viscous} \tag{C.4}$$

The deceleration is captured using the conservation of momentum across the heat exchanger core without the frictional effects.

$$(P_2 - P_3)_{momentum} A_{HX} = \dot{m}_{exhaust} (V_3 - V_2) \tag{C.5}$$

Rearranging to provide a common factor with Equation C.3, the pressure effects due to a change in momentum is:

$$\Delta P_{core,momentum} = (P_2 - P_3)_{momentum} = \frac{\dot{m}^2_{exhaust}}{2\rho_{inlet} A^2_{HX}} \left(\frac{\rho_{inlet}}{\rho_{outlet}} - 1 \right) \tag{C.6}$$

On the other hand, the conservation of mechanical energy can be applied across the heat exchanger at a constant mean density (ρ_{HX}) to calculate the pressure drop due to frictional effects

$$\Delta P_{core,viscous} = (P_2 - P_3)_{viscous} = \frac{\dot{m}_{exhaust}^2}{2\rho_{inlet} A_{HX}^2} K_{HX} \left(\frac{\rho_{inlet}}{\rho_{HX}} \right) \tag{C.7}$$

The mean density within the heat exchanger (ρ_{HX}) is calculated based on the mean logarithmic temperature difference. As an ideal gas, the mean exhaust density can be calculated by:

$$\rho_{HX} = \frac{2}{\dfrac{1}{\rho_{inlet}} + \dfrac{1}{\rho_{outlet}}} \tag{C.8}$$

Exit Pressure Drop

The exit pressure drop is attributed to an expansion in flow area causing both a pressure recovery due to a flow deceleration and a pressure drop due to a sudden expansion. In a similar technique to the entrance pressure drop, the conservation of mass and energy across the exit (3-4) is used to calculate the exit pressure drop.

$$\Delta P_{exit} = P_3 - P_4 = \frac{\dot{m}_{exhaust}^2}{2\rho_{inlet} A_{HX}^2} (\sigma_{outlet} - 1 + K_{exit}) \left(\frac{\rho_{inlet}}{\rho_{outlet}} \right) \tag{C.9}$$

where

$$\sigma_{outlet} = \frac{A_{HX}}{A_{outlet}} \approx \frac{2(S_D - D)}{S_T}$$

$$K_{exit} = 1.064\sigma_{outlet}^2 - 2.156\sigma_{outlet} + 1.005$$

Total Pressure Drop

The total pressure drop can be calculated by substituting the terms into Equation C.1 and simplifying to:

$$\Delta P_{HX,total} = \frac{\dot{m}^2_{exhaust}}{2\rho_{inlet}A^2_{HX}} \left[\left(K_{entrance} + 1 - \sigma^2_{inlet}\right) + 2\left(\frac{\rho_{inlet}}{\rho_{outlet}} - 1\right) \right.$$
$$\left. + K_{HX}\left(\frac{\rho_{inlet}}{\rho_{HX}}\right) + \left(\sigma^2_{outlet} - 1 + K_{exit}\right)\left(\frac{\rho_{inlet}}{\rho_{outlet}}\right) \right] \quad \text{(C.10)}$$

However the total pressure drop with flow through a tube bank or wire mesh typically integrate the entrance and exit loss coefficients into the core loss coefficient to simplify the total pressure drop equation to:

$$\Delta P_{HX,total} = \frac{\dot{m}^2_{exhaust}}{2\rho A^2_{HX}} \left[\left(1 + \sigma^2_{inlet}\right)\left(\frac{\rho_{inlet}}{\rho_{outlet}} - 1\right) + K_{HX}\left(\frac{\rho_{inlet}}{\rho_{HX}}\right) \right] \quad \text{(C.11)}$$

Bibliography

Andersen, K. T. (2003). Theory for natural ventilation by thermal buoyancy in one zone with uniform temperature. *Building and Environment*, **38**(11), 1281–1289.

Beale, S. (1993). *Fluid Flow and Heat Transfer in Tubes Banks*. Ph.D. thesis, Univeristy of London.

CESAR (2010). Sankey Diagram of Canada's Energy Systems. [Online] http://www.cesarnet.ca/visualization/sankey-diagrams-canadas-energy-systems?scope=Quebec&year=2010&modifier=none&hide=exp&scalevalue=0.17647594672753303#chart-form [Accessed: 4 May 2014].

Chase, M. W. J. (1998). *NIST-JANAF Thermochemical Tables, 4th Edition*. American Institute of Physics, New York.

CSA (2010). Natural gas and propane installation code. Standard B149.1-10, Canadian Standards Association International, Mississauga, ON.

Drnovsek, J., Pusnik, I., and Bojkovski, J. (1998). Reduction of uncertainties in temperature calibrations by comparison. *Measurement Science and Technology*, **9**(11), 1907.

Emswiler, J. (1926). The neutral zone in ventilation. *ASHVE Transactions*, **32**, 59–72.

Energy Efficiency and Renewable Energy (2004). Waste heat reduction and recovery for improving furnace efficiency, productivity and emissions perfomance. Technical report, U.S. Department of Energy.

Figliola, R. and Beasley, D. (2010). *Theory and Design for Mechanical Measurements*. Wiley.

Glanville, P., Brand, L., and Scott, S. (2011). Simulation and experimental investigation of condensation in residential venting. *ASHRAE Transaction*, **117**, 95–103.

Hirmiz, R. (2014). Oven cooldown temperaute profiles under various conditions.

IEC (2008). Industrial platinum resistance thermometer sensor. Standard IEC 60751:2008, International Electrotechnical Commission, Geneva, Switzerland.

Johnson, M.-H., Zhai, Z. J., and Krarti, M. (2012). Performance evaluation of network airflow models for natural ventilation. *HVAC&R Research*, **18**(3), 349–365.

Kakaç, S., Shah, R., Bergles, A., and Division, N. A. T. O. S. A. (1983). *Low Reynolds Number Flow Heat Exchangers: Advanced Study Institute Book*. Advanced study institute book. Hemisphere Publishing Corporation.

Kays, W. and London, A. (1954). *Compact Heat Exchangers*. McGraw-Hill series in mechanical engineering. McGraw-Hill.

Kuehn, T., Gerstler, W., Ortiz, H., Sandberg, A., Tjandra, H., Vidhani, J., and

Pui, D. (2001). Effects of air velocity on grease deposition in exhaust ductwork. *ASHRAE Research Project RP-1033 Final Report*.

Li, Z. (2007). *Characteristics of Buoyancy Driven Natural Ventilation through Horizontal Openings*. Ph.D. thesis, Aalborg University: Department of Civil Engineering.

McMaster University (2014). Mcmaster weather station: Current weather conditions. [Online] http://geomedia.mcmaster.ca/muws/index.php [Accessed: 16 June, 2014].

National Energy Board (2014). Canadas energy future: Energy supply and demand projections to 2035. Technical Report NE2-12/2013E-PDF, Government of Canada, Calgary, AB.

NFPA/AGA (2014). Standard for ventilation control and fire protection of commercial cooking operations. Standard NFPA 96, National Fire Protection Association, Quincy, MA and American Gas Association, Washington, DC.

NFPA/AGA (2015). National fuel gas code. Standard NFPA 54/ANSI Z223.1, National Fire Protection Association, Quincy, MA and American Gas Association, Washington, DC.

Owen, M. (2008a). *ASHRAE Handbook - Fundamentals (SI).* American Society of Heating, Refrigeration and Air-Conditioning Engineers, Atlanta, Georgia.

Owen, M. (2008b). *ASHRAE Handbook - HVAC Systems and Equipment (SI).* American Society of Heating, Refrigeration and Air-Conditioning Engineers, Atlanta, Georgia.

Parish, O. O. and Putnam, T. W. (1977). Equations for the determination of humidity from dewpoint and psychrometric data. NASA TN D-8401, National Aeronautics and Space Administration.

Rapp, V. H., Pastor-Perez, A., Singer, B. C., and Wray, C. P. (2012). Assessment of literature related to combustion appliance venting systems. Technical Report LBNL-5798E, Ernest Orlando Lawrence Berkeley National Laboratory, San Francisco, CA.

Rapp, V. H., Pastor-Perez, A., Singer, B. C., and Wray, C. P. (2013). Predicting backdrafting and spillage for natural-draft gas combustion appliances: A validation of vent-ii. *HVAC&R Research*, **19**(3), 295–306.

Rutz, A., Fischer, R., and Paul, D. (1992). *Presentation of the VENT-II solution methodology*. Gas Research Institute.

Sherman, M. (1991). Single-zone stack-dominated infiltration modeling. pages 297–314, Ottawa, ON. Proceedings of the 12th IEA Conference of the Air Infiltration and Ventilation Centre.

Statistics Canada (2011). Households and the environment: Energy use. [Online] http://www.statcan.gc.ca/pub/11-526-s/11-526-s2013002-eng.htm?contentType=application%2Fpdf [Accessed: 27 August, 2016].

Stone, R. (1971). A practical general chimney design method. *ASHRAE Transactions*, **77(1)**, 91–100.

Union Gas (2014). Chemical composition of natural gas. [Online] https://www.

uniongas.com/about-us/about-natural-gas/chemical-composition-of-natural-gas [Accessed: 4 May, 2014].

Versteeg, H. and Malalasekera, W. (2007). *An Introduction to Computational Fluid Dynamics: The Finite Volume Method*. Pearson Education Limited, 2 edition.

Wexler, A. (1976). Vapor pressure formulation for water in range 0 to 100 C. A revision. *Journal of Research of the National Bureau of Standards Section A: Physics and Chemistry*, **80A**, 775–785.

Zukauskas, A. and Ulinskas, R. (1985). Efficiency parameters for heat transfer in tube banks. *Heat Transfer Engineering*, **6**(1), 19–25.